Effects of Material Inelasticity on the Design and Performance of Reinforced Concrete Link Beams Subjected to Gravity Loading

A thesis submitted by

Ferris F. Masri

In partial fulfillment of the requirements for the degree of

Master of Science

in

Civil and Environmental Engineering

Tufts University

August 2017

Adviser:

Daniel A. Kuchma, PhD

Abstract

For the determination of sectional design forces in concrete structures, it is nearly always assumed that structural concrete is a linear elastic material. However, structural concrete is highly inelastic, in which the stiffness may be only a small fraction of the uncracked elastic stiffness. Codes-of-Practice provide largely empirical provisions that focus on ensuring that structural members have adequate strength, and provide little guidance to determine the performance of the structure under service loadings or overloads. Recent advancements in reinforced concrete nonlinear models and high-speed computing power provide the design engineer with the necessary tools to make a more realistic, performance-based, and optimum design. In this thesis, a case study is made of the design of six link beams of a high-rise structure that is subjected to gravity loading. An iterative design procedure is proposed and developed using VecTor2 (Vecchio et al. 2013), a specialized nonlinear finite element analysis software. VecTor2 employs constitutive relationships from various nonlinear models, including the Modified Compression Field Theory (Vecchio and Collins 1986), which defines the response of a two-dimensional continuum structure undergoing membrane action. In order to explore and validate the degree of nonlinearity in the response, a single link beam model is constructed using VecTor2 as well. The response of the single link beam model is then used to inform the iterative design procedure.

Dedication

To my Mother and Father

Acknowledgments

I sincerely thank my advisor and committee chair, Dr. Daniel Kuchma for his invaluable guidance and support throughout the course of this research. This work would not have been possible without his input and support.

I would also like to sincerely thank Dr. Masoud Sanayei and Dr. Po-Shang Chen for serving on my thesis committee. Thanks also to the department faculty and staff for making my time at Tufts University a great and memorable experience.

I would also like to thank my friends at Tufts University and elsewhere for their constant support and encouragement. Last but not least, I would like to show my gratitude towards my parents and sisters for making this unforgettable journey at Tufts University possible, and for their constant support, prayers, and encouragement.

Table of Contents

List of Tables

List of Figures

PART I

Chapter 1: Introduction

1.1 Background

One shortcoming of general structural engineering design practice is that we determine the distribution of design force values (i.e. Shear, Moment, Axial Loads, Torsion, etc.) with the assumption that structural concrete is a linear elastic material. In reality, structural concrete is highly inelastic and its stiffness may be only a small fraction of the uncracked elastic stiffness. For example, the flexural stiffness of a lightly reinforced beam may be as little as 10% of the uncracked flexural stiffness. The effect of this is that the actual distribution of design force values may be considerably different than those assumed, and the relative values of these demands will change with the magnitude of the loading that the structure is designed to resist.

Another shortcoming of typical design practice is that empirical code provisions do not provide sufficient guidance for completing a performance-based design. Such building code provisions, such as those of the American Concrete Institute (ACI318-14), focus on the Ultimate Limit Strength (ULS) of the structural member. Little provisions are presented on the state of the member's components under service loads or overloading. For instance, the state of stress of the reinforcement or the crack spacing/width, and other valuable information are not possible to predict with empirical code provisions. However,

with the availability of powerful computational tools, the effects of inelasticity can be predicted for any structural member on a global and local level.

Over the past 60 years (*fib* Practitioners' Guide 2008) [20], great progress has been made in the development of computational tools that can predict the full inelastic response of structural concrete. These tools are able to account for the major factors influencing the stiffness and strength of concrete structures including compression softening, tension stiffening, bond degradation, and other effects. For the majority of applications, these tools can now predict stiffness and strength of concrete structures to within about plus/minus 20%, which is much better than current codes-of-practice for most aspects of a design.

1.2 Objective

The objective of this thesis work was to determine when it would be necessary to consider the inelastic response of reinforced concrete structures, and to propose a design procedure based on a presented case study that illustrates how the use of a state-of-the-art computational tool can improve the design and performance of concrete structures relative to standard practice that uses linear elastic analyses coupled with building code provisions.

1.3 Description of Thesis

This report presents a specific case study on the inelastic response of a typical reinforced concrete high-rise building. The core of the building is linked to a buttressed "wing" by stocky link beams, as shown in Figure 1.1. A specialized open-source software called VecTor2 was used to perform nonlinear finite element analyses for a typical gravity loading case. Two-dimensional plane-stress membrane elements were used. The steel reinforcing was smeared over the elements. The Modified Compression Field Theory (MCFT) proposed by Vecchio and Collins (1986)[21] is the basis of the inelastic material model employed by VecTor2. It employs a smeared rotating crack approach, that will be explained in Chapter 2 of this report. The finite element model of the structure used in the study is shown in Figure 1.1.

Chapter 2 of this report reviews the related literature and presents nonlinear models for the response of reinforced concrete under several types of loading. Chapter 3 introduces the case study and analyze of the structure in Figure 1.1 using the traditional method of practice and following the ACI 318-14 building code provisions. Chapter 4 investigates and discusses the single link beam model nonlinear response in order to understand the degree of nonlinearity that is expected, and informs the necessity for performing a nonlinear analysis on the full structure. Chapter 5 develops and presents an iterative method of nonlinear design for the structure in Figure 1.1. Chapter 5 also describes how the link beams were reinforced based on the initial linear elastic analysis from

Chapter 3, and an optimization via iterative trial-and-error nonlinear analyses, until demands converge. Chapter 6 concludes the thesis and lists the findings.

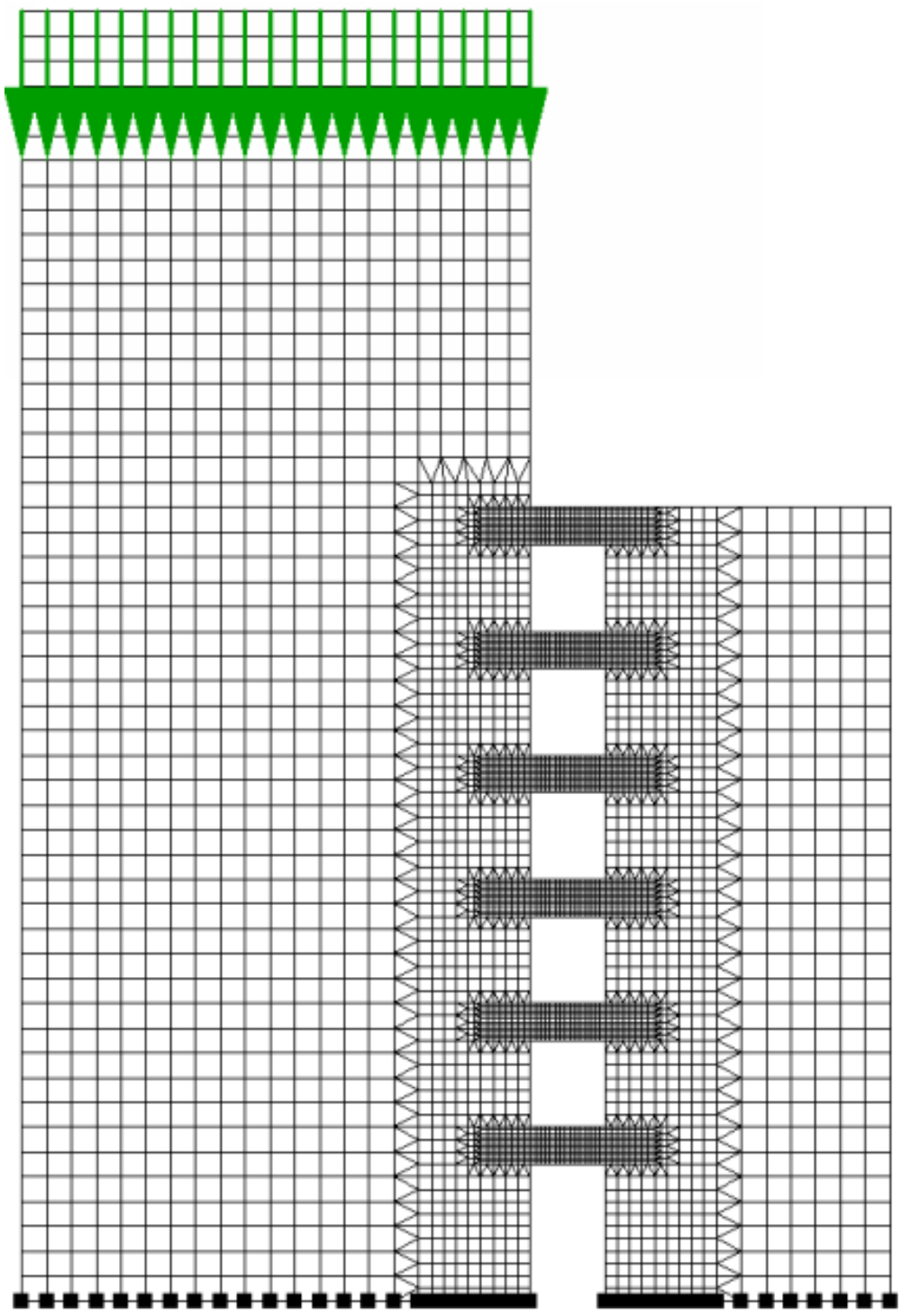

Figure 1.1: Finite element model of the structure used for this case study, showing the link beams, the fixed bottom restraints, and the gravity loading on the core.

Chapter 2: Literature Review

2.1 Nonlinear Finite Element Analysis

Finite element analysis procedures for reinforced concrete have seen major advancements in the last 60 years (*fib* Practitioners' Guide 2008) [20]. These advancements were made possible by improved method of physical testing and measurement that in turn made possible the development of non-linear constitutive relationships and complete behavioural models for the response of crack concrete structures. The simultaneous and exponential growth in personal computing power has enabled Nonlinear Finite Element Analysis (NLFEA) to be a powerful tool available not only in the realm of research, but for practicing design engineers as well. Figure 2.1.1 shows data compiled by Bentz that demonstrates the clear exponential growth of computing speed around the turn of the millennia. The figure shows the time required to conduct a nonlinear shear analysis of a prestressed T-beam using a layered beam element algorithm procedure.

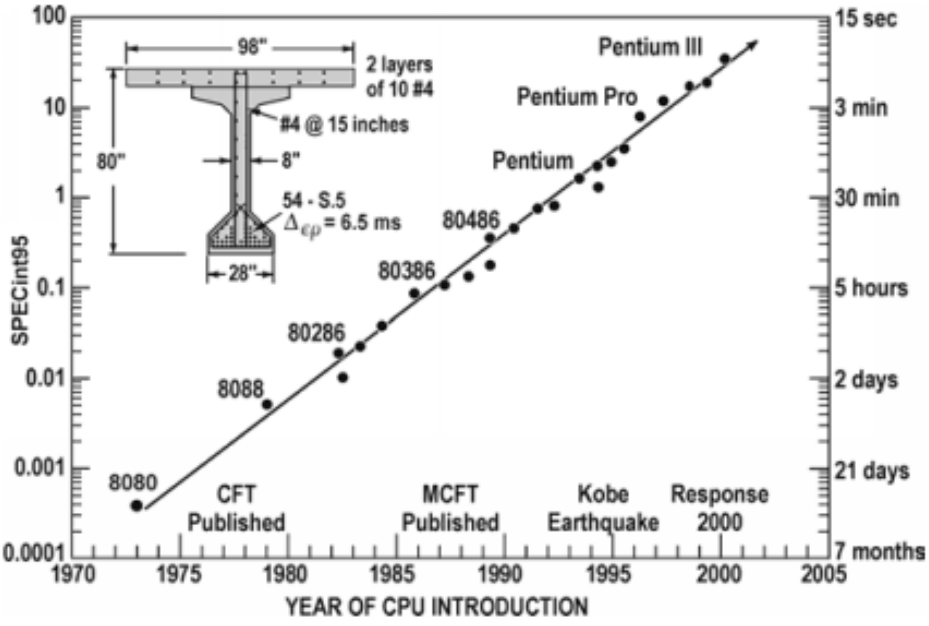

Figure 2.1.1: Rapid increase in computing power. [20]

One of the most beneficial advantages of NLFEA procedures is that they provide performance based predictions such as service level loads or overloads, contrary to current design procedures dictated by empirical code provisions that are focused on ultimate strength. Also, and as noted in the *fib* Practitioners' Guide (2008) noted in reference 20, conventional analysis and design calculations are largely inadequate in providing accurate load capacity assessments of indeterminate structures.

NLFEA procedures are used for structural retrofitting and forensics engineering applications. In addition to geometric and material nonlinearities, NLFEA programs may also consider temperature effects on material behaviors, time-dependent effects, and other influencing factors. A major limitation in their

use, however, is the requirement for specialized experience. NLFEA procedures for reinforced concrete can be a part of a general-purpose NLFEA software package or a more specialized software built solely for reinforced concrete problems. For the general-purpose packages and the majority of specialized packages, the user must specify or assume many inelastic material and behavioral model parameters specific to the structure being examined. The usability issue lies not only with the volume of parameters that need to be defined, but also with choosing the correct material behavior theory. As will be discussed later, there are many different theories regarding the behavior of reinforced concrete. The initial assumptions that define those theories dictate the nature of the constative model development and the test data analysis procedure. However, the NLFEA software package used for the case study presented in this report mitigates this issue by providing reasonable and informed default parameter values.

It is important to note that experimental results in and of themselves are subject to large variations, scatter, and error. Exact test conditions may be extremely difficult to repeat, especially if repeated by a different laboratory. However, current NLFEA procedures provide a significant degree of confidence with their response predictions. Despite the ability to accurately model the nonlinear response of reinforced concrete, it is incumbent upon the users of NLFEA procedures to be aware of several potential dangers and issues.

There exists a very diverse number of theoretical and behavioral approaches for NLFEA modeling of reinforced concrete. Models may be built on

nonlinear elasticity, plasticity, fracture mechanics, damage continuum mechanics, endochronic theory, and other hybrid formulations. Cracking can be modelled discretely or using smeared crack approaches. Smeared cracks can be either fully rotating cracked models, fixed crack models, multiple non-orthogonal crack models, or hybrid crack models. Some modeling approaches emphasize classical mechanics procedures, while others focus more heavily on empirical data and phenomenological models.

Reinforced concrete behaves in a linear elastic manner until cracking or compressive stresses exceed approximately 50% of its compressive stress capacity. After cracking, the effects of its extreme composite and non-orthotropic nature comes to light. Post-cracking behavior is dominated by nonlinear or second-order influences. Depending on the specific details of the structural body in question, its strength, ductility, deflection, and failure modes will most likely be significantly affected by mechanisms that include compression softening, tension stiffening, tension softening, shear slip along cracks, reinforcement bond slip, and many more that will be explained in the subsequent sections of this chapter.

Reinforced concrete behavioral models depend on the particular theoretical approach assumptions. Constitutive relationships from one theoretical or behavioral approach cannot be transplanted to, or combined with, a model utilizing another theoretical approach without very careful consideration. During the development of a particular behavioral model, the initial assumed mechanical

material models and analysis assumptions should, in general, be carried along the entire development process. For instance, a behavioral model that was developed based on the assumption of a rotating crack formulation for compression softening cannot be implemented into, or combined with, a behavioral model that was developed based on a fixed crack formulation, even though both behavioral models may be independently used to predict nonlinear reinforced concrete response. This produces a wide variety of behavioral models for the same phenomenon. For instance, there exists over 20 models for crack widths. The accuracy of each of these models depends on their area of application, and there is no consensus by the academic research community as to how to select which is best.

Due to the vast diversity in the mentioned theoretical approaches, behavioral models, and their incompatibility, NLFEA analysis of reinforced concrete structures require a certain amount of experience and expertise to apply them successfully. Furthermore, decisions must be made regarding mesh layout, element type, how to represent and model reinforcement (discrete or smeared), boundary conditions, loading method, convergence criteria, and more. The decisions made can have a very significant effect on the response predicted by the analysis.

Another area where user experience is required is post processing. Unlike typical plane-section analysis, NLFEA predicts very detailed performance as derived from data that can be too overwhelming to interpret without a powerful

post-processing software. Predicted data can include stresses and strains at each integration point of each element, with respect to local and principal axes, nodal displacements, sectional forces at each integration point, reinforcement stresses and strains, stiffness matrices and their coefficients, crack widths and crack orientations, and more. Even with a powerful post-processor, the user must be aware and informed on how to interpret the predicted data.

It is imperative to note the reality that reinforced concrete behavior remains poorly understood. Otherwise, there would not be such a diverse approach to modeling and analysis. With that in mind, NLFEA must be performed with a reasonable degree of caution and skepticism. The analyst should preferably choose behavioral models that have been validated and calibrated against benchmark tests that involved specimens subjected to similar loading and boundary conditions as the structure being modelled by the NLFEA program. As mentioned earlier, since physical lab tests can have inherent errors in and of themselves, it is preferred that the analyst predicts the nonlinear reinforced concrete response based on more than one model in order to observe and interpret the differences. Validation can also be done by running NLFEA predictions on a known problem.

It should also be noted, however, that the diversity in analysis procedures available provides more value than a disadvantage. Since the behavioral models are very specific to a certain structural condition, modeling that specific condition and predicting its desired response would be much more accurate than a general

behavioral model approach. The 2008 Practitioners' Guide to Finite Element Modeling of Reinforced Concrete Structures published by the International Federation of Structural Concrete (*fib*) refers to the need to establish databases for benchmark tests to use for validation. This would provide a wide variety of specific structural conditions to be used as a base for selecting the appropriate behavioral model in the NLFEA program used.

The *fib* guide (2008) also encourages the development of accurate and user friendly NLFEA programs that apply the behavioral models in the interface's background; invisible to the user. Such programs are in the early stages of maturity, including VecTor2, which is the one used for the case study presented in this report. A detailed explanation of VecTor2 will be presented later in this report.

2.2 Response of Reinforced Concrete in Compression

Reinforced concrete in compression experiences linear elastic behavior for about one-half of the compressive stress capacity as shown in Figure 2.2.1. This figure also shows a bilinear relationship for the tensile response of reinforced concrete. This will be discussed in section 2.3 of this report. The majority of the compressive response of reinforced concrete is nonlinear and can be quite brittle. While the nonlinearity is an inherent property, the degree of brittleness increases with increasing compressive stress capacity and it is mitigated by the use of confinement reinforcement.

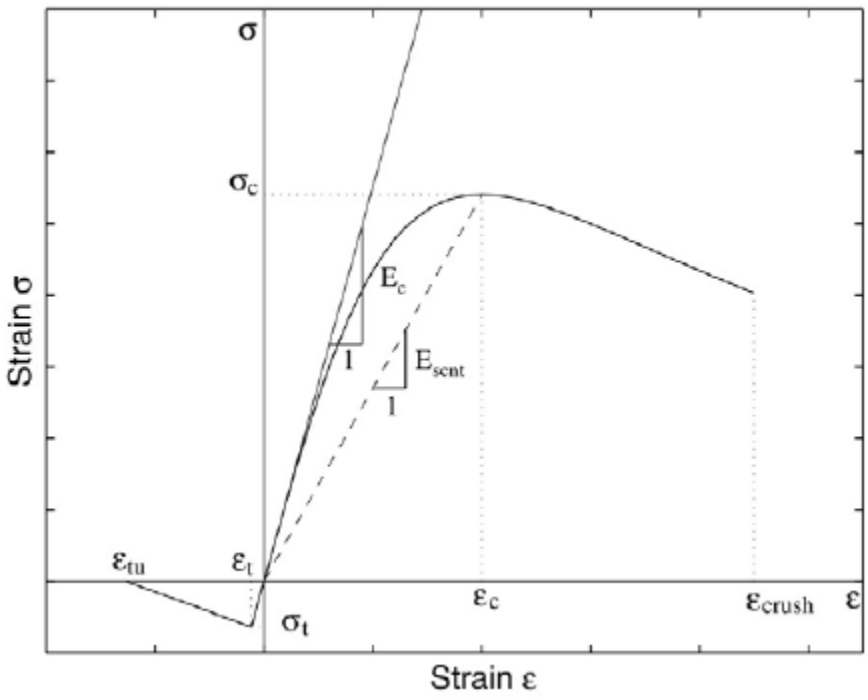

Figure 2.2.1: Reinforced concrete stress-strain response in tension and compression.

Structural concrete can be confined in compression by placement of transverse reinforcement. Unconfined concrete uniaxial cylinder compressive strength is significantly lower than that of confined concrete. However, the main benefit of confinement is not only in increasing the cylinder compressive strength; confinement adds a considerable amount of ductility, which makes it a fundamental characteristic for seismic, blast, or impact design and detailing. Figure 2.2.2 shows a typical stress-strain model that illustrates the behavior of confined and unconfined concrete via test data from a circular column with transverse reinforcement. The strain in the confinement reinforcement is roughly

equal to the axial strain multiplied by Poisson's ratio. Thereby, the development of confining stress increases more rapidly at higher axial stress levels due to the greater internal fracturing causing dilation effects in the concrete, which in turn engage the transverse reinforcing in resisting that effect.

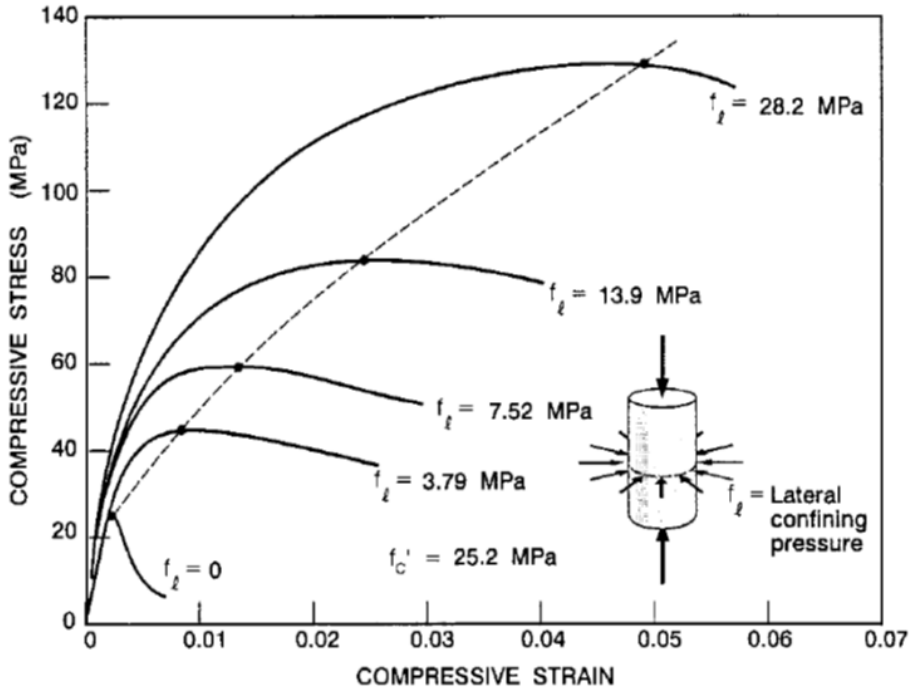

Figure 2.2.2: Confined vs. unconfined reinforced concrete stress-strain response.

The aforementioned basic discussion about confined versus unconfined concrete is the typical scope covered by standard design practice. If the concrete is subjected to transverse stress and straining, a significant inelastic phenomenon is observed that is seldom captured in empirical code provisions and typical design practice. This phenomenon is known as compression softening.

Compression softening describes the reduction of compressive strength of concrete due to principal tensile strains acting transverse to the principal tensile stresses. The results of shear panel tests performed by Vecchio and Collins (1986) highlight the importance of compressive strength reduction due to the compression softening effect. These tests resulted in the Modified Compression Field Theory (MCFT), which is discussed in greater detail in section 2.5 of this report. In order to mechanically describe compression softening, a constitutive model was developed by the MCFT, shown below:

$$f_{c2} = \frac{f'_c[(2(\varepsilon_{c2}/\varepsilon'_c)) - (\varepsilon_{c2}/\varepsilon'_c)^2]}{0.8 - 0.34(\varepsilon_{c1}/\varepsilon'_c)} \qquad \text{(E 2-1)}\ [22]$$

Where, f_{c2} is the principal compressive stress of the concrete, f'_c is the cylinder compressive strength of the concrete, and the strain value subscripts for, ε, carry the same definitions. The subscript 1 denotes principal tension. As evident in the constitutive relation in equation 2-1, when the principal tensile strain of the concrete is increased, it can significantly reduce the principal compressive stress, thereby softening the concrete. Figure 2.2.3 shows a graphic of this effect. The numerator portion of equation 2-1 is known as the Hognestad (1951) compression model[22], which describes the compressive stress-strain relationship as a parabola symmetric about the strain corresponding to compressive peak stress. This model along with many others will be discussed in section 2.6 of this. Figure 2.2.4 shows an even more informative representation of the compressive stress-strain

relationship defined by equation 2-1. The symmetric parabola of the Hognestad relationship is shown along the principal compressive strain axis, ε_2, and the degree of compression softening is shown along the principal tensile strain axis, ε_1. The 3-dimensional "shell" provides a visual representation of the degree of compression softening that can occur.

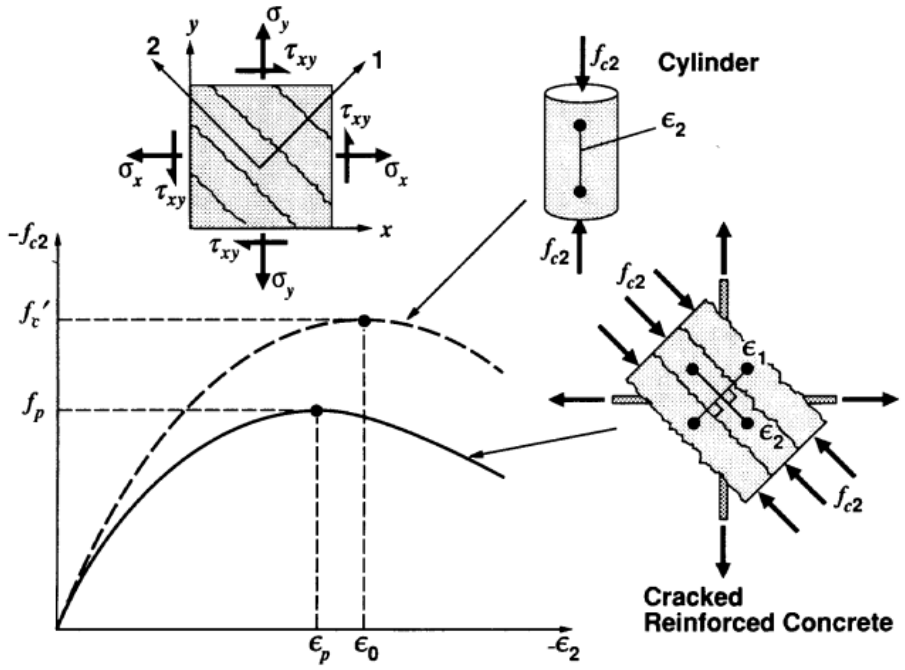

Figure 2.2.3: Average stress-strain relationship for cracked reinforced concrete in compression. (Vecchio et al. 1986) [21]

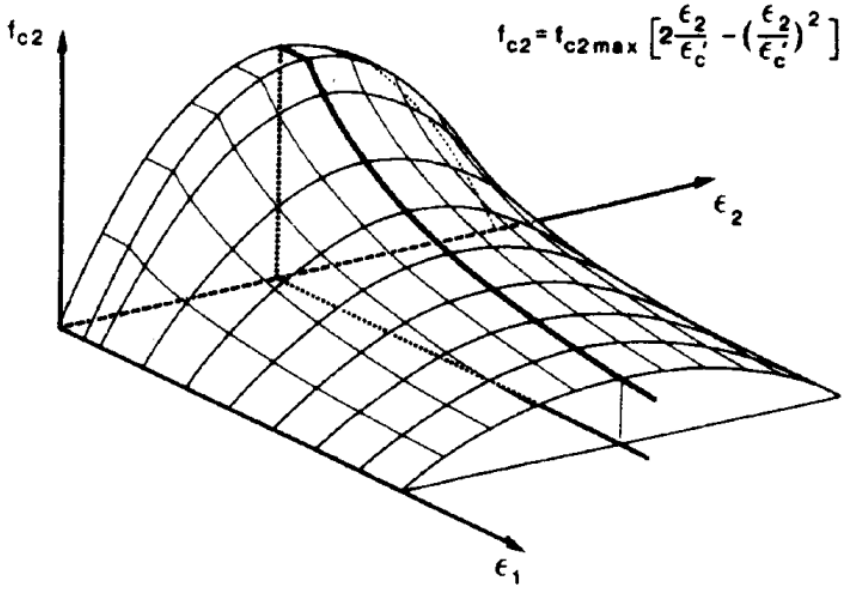

Figure 2.2.4: Three-dimensional representation of compressive stress strain relationship, including compression softening. (Vecchio et al. 1986) [21]

Noguchi (1991) [19] and others [19] have also observed that the softening effect may be more pronounced with high-strength concrete, possible due to the formation of smooth fracture planes, which would result in an earlier onset of local compression stability failure or in earlier crack-slip failure.

Another phenomenon observed with post-cracking behavior of reinforced concrete in compression is crack rotation. Depending on the diagonal compressive strut in the member, the principal tensile stresses will orient cracks at a certain angle. After the initial principal tensile crack, the stiffness of the concrete is altered in an orthotropic fashion. This changes the distribution of internal forces and load path, which in turn modifies the principal axis orientation and can cause new cracks to form at a different angle and earlier cracks to close. This effect

progresses with every concrete stiffness alteration, thus creating a rotating crack path. As the crack rotates and forms in a new orientation, internal equilibrium and compatibility might close an earlier crack. However, Vecchio and Collins (1993) [22] have shown that the principal tensile strain was the single most important factor in dictating the degree of softening that was observed. Under typical monotonic loading conditions, the load path, crack rotation, crack orientation relative to the reinforcement, and the reinforcing bar type appeared to have negligible influence on the degree of compression softening that occur. However, as Noguchi [19] and others [19] have observed, concrete strength has some influence in that higher strength concrete experiences slightly more softening.

2.3 Response of Reinforced Concrete in Tension

In empirical code provisions and typical reinforced concrete design, the tensile stiffness of the concrete is completely neglected. Since the typical tensile strength of concrete is under 10% of the cylinder compressive strength and flexural cracks must be present before the flexural steel can be engaged, the steel reinforcing alone is expected to provide tensile resistance. However, the reality is that tensile stresses do exist between the cracks and in the concrete still anchored around the steel reinforcing bars. Vecchio and Collins [21] defined tension stiffening in the MCFT by the following relationship and Figure 2.3.1. Prior to cracking, when $\varepsilon_1 \leq \varepsilon_{cr}$, the relationship is linear elastic and described by:

$$f_{c1} = E_c \varepsilon_1 \qquad \text{(E 2-2)}\ [21]$$

Where E_c is the concrete modulus of elasticity, and ε_{cr} is the average cracking strain.

The relationship suggested after cracking, when $\varepsilon_1 > \varepsilon_{cr}$, the tension stiffening relationship is nonlinear and described by:

$$f_{c1} = \frac{f_{cr}}{1+\sqrt{200\varepsilon_1}} \qquad \text{(E 2-3)}\ [21]$$

Where f_{cr} is the average cracking stress of the concrete.

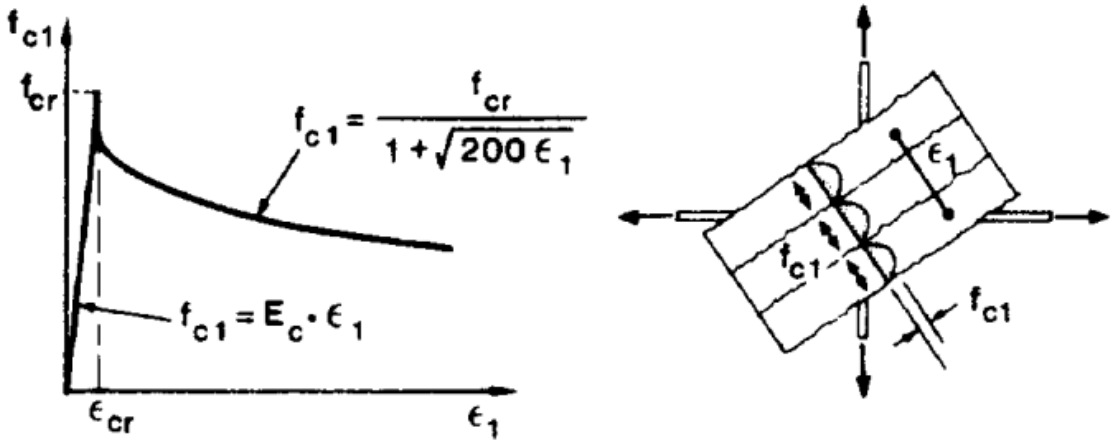

Figure 2.3.1: Average stress-strain relationship for cracked reinforced concrete in tension. (Vecchio et al. 1986) [21]

Concrete is brittle in tension, and its response can be characterized into uncracked and cracked response, as shown in the bilinear relationship in Figure

2.2.1. Prior to cracking, the response is assumed to be linear-elastic. After cracking in reinforced concrete structures, the concrete tensile stresses diminish virtually to zero at the free surface of cracks. However, concrete does not crack suddenly and completely. It undergoes progressive micro-cracking due to inherent strain softening. Further, due to bond action with the reinforcement, average concrete tensile stresses continue to exist in the concrete between the cracks in the locality of the reinforcement. Immediately after first cracking, f_{cr}, the intact concrete between adjacent primary cracks carries considerable tensile force due to the bond between the steel and the concrete. Cracks widen with additional tensile straining, the bond action degrades near the cracks, and the average concrete tensile stresses gradually diminish to zero. While these average concrete tensile stresses must be less than the cracking strength of concrete to guard against additional cracking, they act over a relatively large tributary area of the reinforcement. This results in the stiffness of the reinforced concrete in tension to be considerably greater than that of the reinforcement alone, which is based on a fully cracked section. This phenomenon is known as tension stiffening. [21]

Tension stiffening is important to modeling the load-deformation behavior, particularly in the context of nonlinear finite element analysis. If tension stiffening is neglected, the concrete tensile stress reduces immediately to zero upon cracking and the tensile stress must be redistributed entirely to the reinforcement. The discontinuity in the stiffness may manifest as an unrealistic abrupt abnormality in the load-deformation response due to unexpected stress

concentrations and impose difficulties to the solution convergence for lightly reinforced structures.

Another important nonlinear phenomenon in reinforced concrete is known as tension softening. Tension softening refers to the presence of post-cracking tensile stresses in plain concrete. Under increased tensile straining, the tensile stresses gradually diminish to zero. This phenomenon due to the fact that concrete is not perfectly brittle. Rather, as described by fracture mechanics approaches, the formation of a localized crack requires energy. As the fracture process progresses and the crack widens, concrete in the vicinity of the crack is gradually relieved of stress, and the dissipated energy propagates the crack tip.

Tension softening is significant in several ways to the analysis of reinforced concrete structures, particularly those having lightly reinforced regions. The tension softening response may be important to modeling the stress redistribution and localized damage of lightly reinforced structures experiencing brittle failure modes. By including a descending post-cracking stress-strain portion for plain concrete, it is possible to more accurately determine the load-deformation response and ductility of the member.

Moreover, tension softening may mitigate inaccuracies associated with the coarseness of a finite element mesh. In the case of 2-dimensional continuum membrane elements, as will be discussed in subsequent section, the elements invariably include both cracked and uncracked concrete due to their finite size. Accounting for the post-cracking tensile stress in cracked elements represents to

some extent the stiffness contribution of uncracked concrete, and prevents unwarranted stress concentrations in adjacent uncracked elements.

2.4 Response of Reinforced Concrete Membrane Elements

For the majority of large-scale structures, including high-rise buildings, off-shore oil platforms, and nuclear power plants, the loads are primarily carried through in-plane stresses or membrane action. These in-plane stresses can be modeled and represented by an array of rectangular membrane elements that carry only in-plane share and axial stresses. In other words, membrane elements are considered to have no bending stiffness. If the response of a membrane under shear and normal stresses can be predicted, then the response of an assembly of membrane elements, known as a 2D continuum, can be predicted as well.

If the state of strain of a reinforced concrete element is known, finding the resulting stresses and forces is straight forward. Constitutive relationships are used to go from a state of strain to a state of stress, and equilibrium equations are used to go from a state of stress to determine the force(s) on a section. However, if the force is given while the stresses and strains are not, predicting the response requires more parameters.

2.5 The Modified Compression Field Theory

The power of 2D continuum analysis is captured in the application of the Modified Compression Field Theory (MCFT). In the 1980s, Vecchio and Collins

conducted 30 tests at the University of Toronto on reinforced concrete panels. [21] In order for the panels to act as membrane elements, they were tested under a variety of well-defined uniform biaxial stresses and pure shear.

The MCFT includes experimentally derived constitutive relationships for reinforcement and concrete, based on average stresses and strains in the concrete and at cracks. The MCFT provides a description on how average tensile stresses in the concrete are transmitted across cracks, which is a stress transfer that is not captured in traditional reinforced concrete constitutive relationships or in the Compression Field Theory (CFT). Figure 2.5.1[21] presents a summary of the relationships used in the modified compression field theory, where the variables *f*, *v*, are normal and shear stresses, respectively. The subscripts 1 and 2 denote principal tensile and principal compressive directions, respectively.

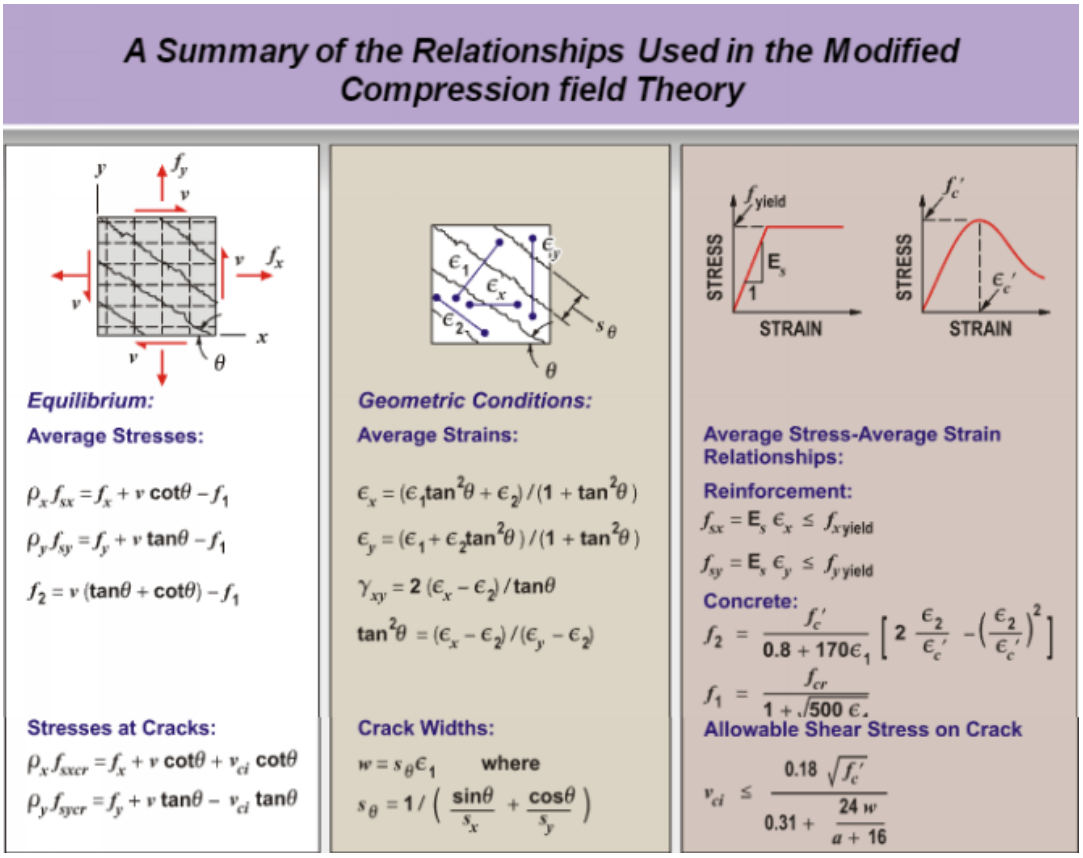

Figure 2.5.1: Summary of the Modified Compression Field Theory relationships. [21]

The equilibrium relationships of the MCFT are defined based on analysis of a membrane element that is orthogonally reinforced with transverse and longitudinal steel, as presented in Figure 2.5.2 It can be shown that a static equilibrium analysis of the membrane free body diagrams shown in Figure 2.5.2 would produce the equations shown in the "Equilibrium" of Figure 2.5.1. The equilibrium relationships amount in three equations, which are not enough for the parameters usually considered. Therefore, there must be a methodology to relating

stress equilibrium equations with the strains of the membrane element. This is achieved through constructing compatibility relationships.

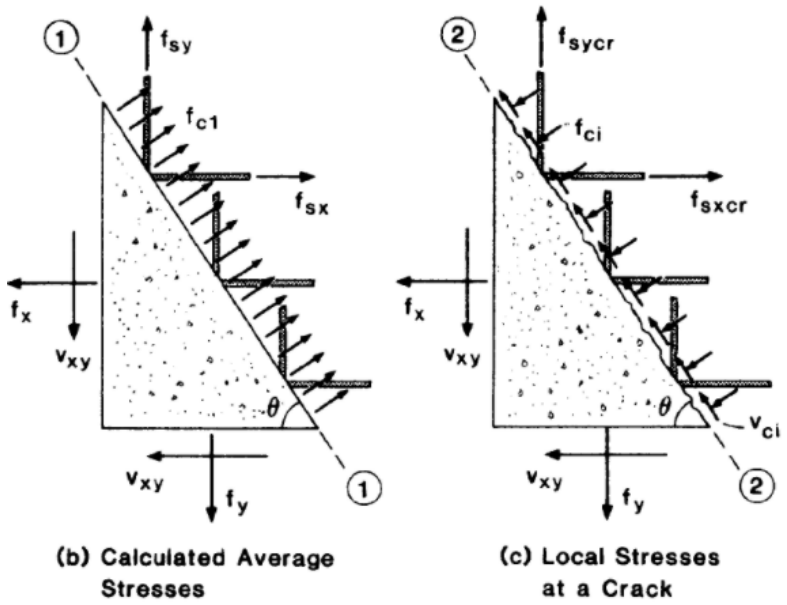

Figure 2.5.2: Comparison of local stresses at a crack with calculated average stresses. (Vecchio et al. 1986) [21]

Compatibility equations in the MCFT are derived based on the assumptions that a perfect bond exists between the steel and concrete before cracking, and that the angle of inclination, θ, for principal stresses and principal strains is equal for both the steel and concrete. It can be shown that a Mohr's Circle can be constructed based on the aforementioned assumptions, as shown in Figure 2.5.3, which elegantly summarizes the "Geometric Conditions" section of Figure 2.5.1. However, compatibility and equilibrium relationships alone do not describe material specific behaviors, and more importantly cannot be related to

each other. Constitutive relationships that are based on empirically verified equations for stress-strain behavior of specific materials, such as the reinforced concrete panel tests, provide a relationship between the equilibrium and compatibility relationships. The third section in Figure 2.5.1 presents the constitutive relationships that were derived from the MCFT. These relationships were discussed in sections 2.2 and 2.3 of this report.

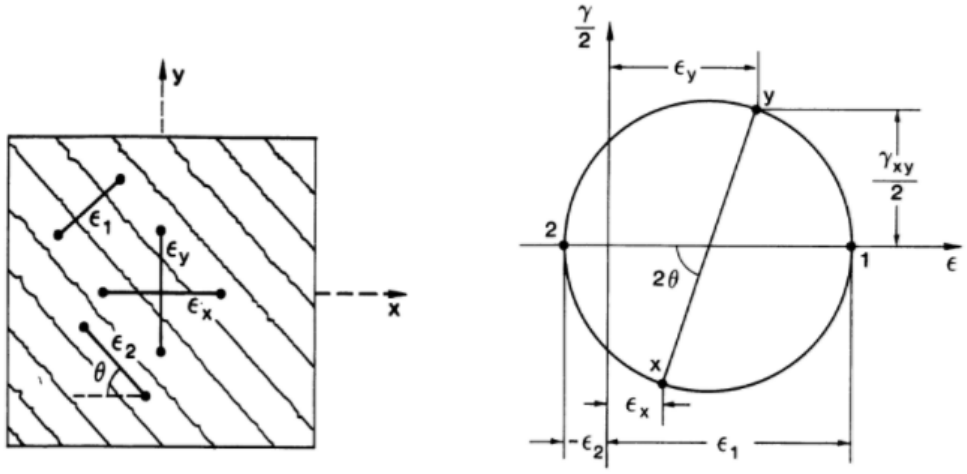

Figure 2.5.3: Average strains in cracked element and Mohr's Circle for average strains. (Vecchio et al. 1986) [21]

2.6 VecTor2

VecTor2 is an open source NLFEA program that is specialized for reinforced concrete. [22] VecTor2 is the NLFEA program used for the case study presented in this report. The program was developed and enhanced by Professor

Frank Vecchio, Wong, Trommels, [22] and others at the University of Toronto to predict the response of two-dimensional continuum reinforced concrete structures. The 2D continuum is represented by membrane elements that are subjected to in-plane normal and shear stresses, and analyzed using principles of the Modified Compression Field Theory (MCFT), as was explained in the previous sections of this chapter. VecTor2 has the ability to predict the nonlinear response of reinforced concrete under monotonic, cyclic, and reverse cyclic loading. Nonlinear response relationships in addition to those of the MCFT include, compression softening, tension stiffening, tension softening, and others.

The graphical user interface (GUI) of VecTor2 is called FormWorks. It is the platform used to create the finite element model, select the various nonlinear material models, define boundary conditions and loading criteria, and others. The graphical post-processor of VecTor2 is called Augustus. It is a very powerful graphical tool which helps visualize and interpret the nonlinear results in a much more intuitive fashion. All of the figures that discuss results in Part II of this report were taken from Augustus.

The finite element models constructed for VecTor2 use a relatively fine mesh of low-powered elements. This methodology has advantages of computational efficiency and numerical stability. The element library includes a three-node constant strain triangle, a four-node plane stress rectangular element and a four-node quadrilateral element for modeling concrete with smeared reinforcement; a two-node truss-bar for modeling discrete reinforcement; and a two-node link and a four-node contact element for modeling bond-slip

mechanisms. Since the reinforcement was smeared for the case study presented in this report, the four-node plane stress rectangular element was primarily used in constructing the finite element model. One large disadvantage of VecTor2 is its relatively low node limit of 5200 nodes. As a result, the majority of the finite element model constructed for the case study presented in this report consisted of relatively large elements away from the link beams, which are the focus of the analysis. In order to transfer from a coarse into a relatively fine mesh density of rectangular elements, triangular elements must be used at the transfer location. Therefore, some three-node elements were used in the finite element model construction.

2.6.1 Models for Concrete Materials

The accuracy of VecTor2 results is a function of the concrete constitutive and behavioral models. At each load step, the structural stiffness matrix is determined from the stresses and strains calculated from the constitutive models. The suitability of the results pertaining to a specific analysis is determined by the models included or omitted. Most of the models in VecTor2 include several options and parameters, which may produce a divergence of results. As noted in section 2.1, the user is assumed to have an acceptable amount of experience in order to choose the appropriate models that can predict the vital information being studied. However, as stated previously, the intent of this case study is to discuss the benefits of using the default parameters inherent in VecTor2.

With regard to the constitutive relationships, VecTor2 utilizes Cauchy-type models, [22] which describe the concrete response via nonlinear functions of stress and strain. A Cauchy stress tensor, also known as the "true" stress tensor, includes the reality that a solid material's cross section may change with an induced strain. As noted in the introduction of this report, the relationships describing structural concrete behavior typically involve mechanical properties that were determined from standard specimens under specific stress and strain conditions, rather than being inherent material properties. Given that the combined behavior of aggregates, cement and reinforcement in structural concrete, which can often only be described by empirical relationships, the Cauchy-type nonlinear approach is appropriate in describing realistic behavior.

This section now describes the available constitutive and behavioral models available in VecTor2 that pertain primarily to the response of the concrete material, although many models must be discussed in the context of reinforced concrete.

1. *Linear* [22] – Figure 2.6.1 shows an elastic-plastic response in which the concrete compressive response remains linear until it reaches the peak compressive stress and then acts plastically thereafter.

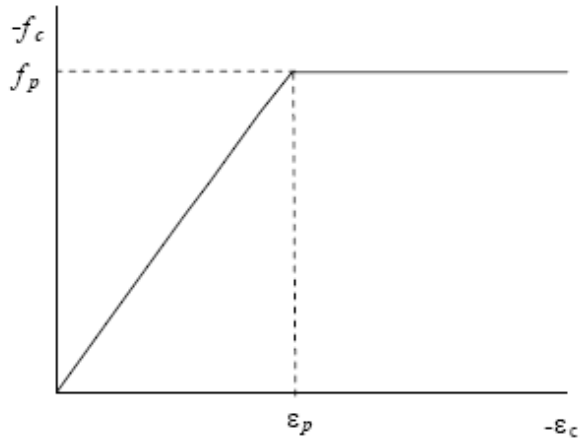

Figure 2.6.1: VecTor2 linear compressive response.

2. *Popovics (1973)* [22] – Figure 2.6.2 shows the compressive response which captures properties associated with different concrete strengths, such as the reduced ductility associated with increased peak compressive stress, and the greater linearity and stiffness associated with higher strength concretes.

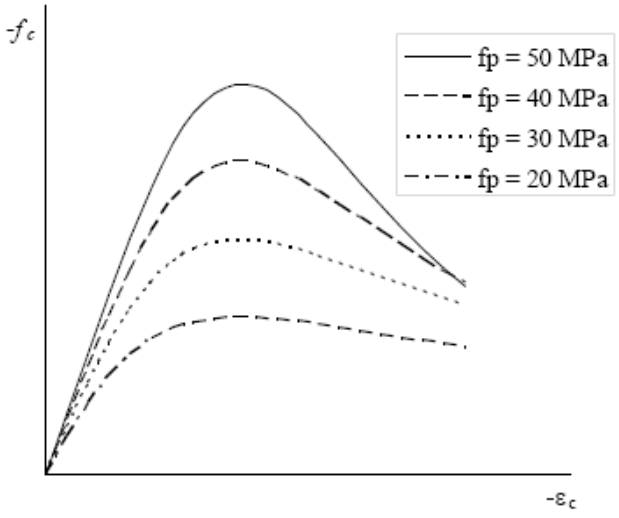

Figure 2.6.2: VecTor2 Popovics compressive response.

3. *Popovics/Mander* [22] – Popovics (1973) [22] was modified to model concrete confined with transverse hoop reinforcement. The form of the curve is the same, however, the initial tangent stiffness is assigned a particular value as described in the VecTor2 user manual (2013) [22].

4. *Hognestad* (1951) [22] – Figure 2.6.3 shows the compressive stress-strain relationship is a parabola symmetric about the strain corresponding to compressive peak stress.

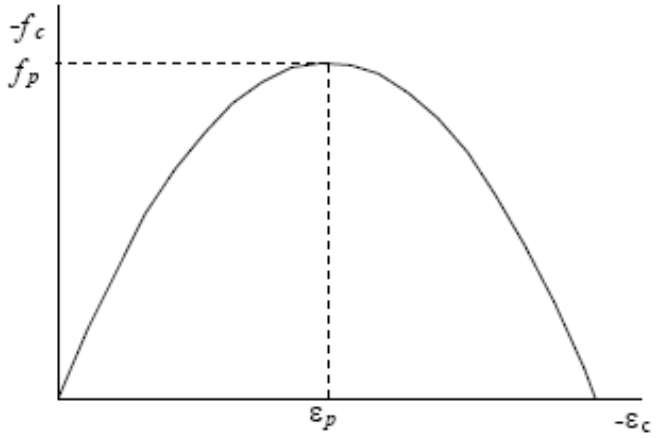

Figure 2.6.3: VecTor2 Hognestad compressive response.

5. *High Strength Popovics (1987)* [22] – As mentioned in the VecTor2 user manual [22], "Experimental studies demonstrate that as the concrete strength increases, the response is linear to a greater percentage of the maximum compressive stress, the strain corresponding to the peak compressive stress increases, and the descending branch of the stress-strain curve declines more steeply. Also, intermediate high

strength concretes exhibit a decreased ultimate compressive strain". The Popovics High Strength relationship shown in Figure 2.6.4 was developed to capture these phenomena.

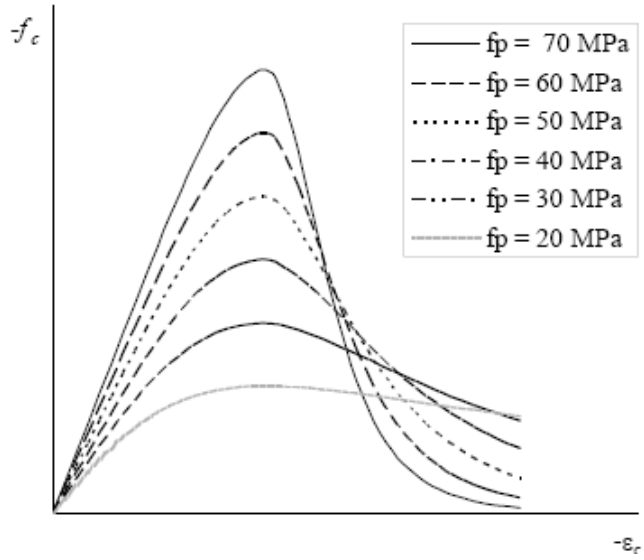

Figure 2.6.4: VecTor2 Popovics (High Strength) compressive response.

6. *Hoshikuma et al. (1997)* [22] – Figure 2.6.5 shows a pre-peak concrete compressive relationship that was developed to reconcile an inconsistency in the Hognestad parabolic relationship. Experimental studies showed that peak values of stress and corresponding strain are dependent upon the amount of hoop reinforcement, but the initial stiffness is not. However, because the initial stiffness used in the Hognestad response is a function of the peak compressive stress and strain, it is implicitly a function of the amount of hoop reinforcement, an inconsistency.

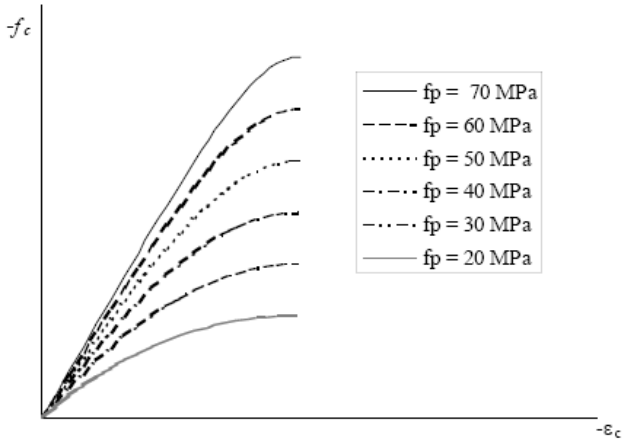

Figure 2.6.5: VecTor2 Hoshikuma et al. pre-peak compressive response.

7. *Hoshikuma et al. (1997)* [22] – Figure 2.6.6 shows a linear post-peak concrete compressive response formulated to model concrete confined with transverse hoop reinforcement. In this model, the deterioration rate is a function of the volumetric ratio and yield stress of the hoop reinforcement as well as the concrete cylinder strength.

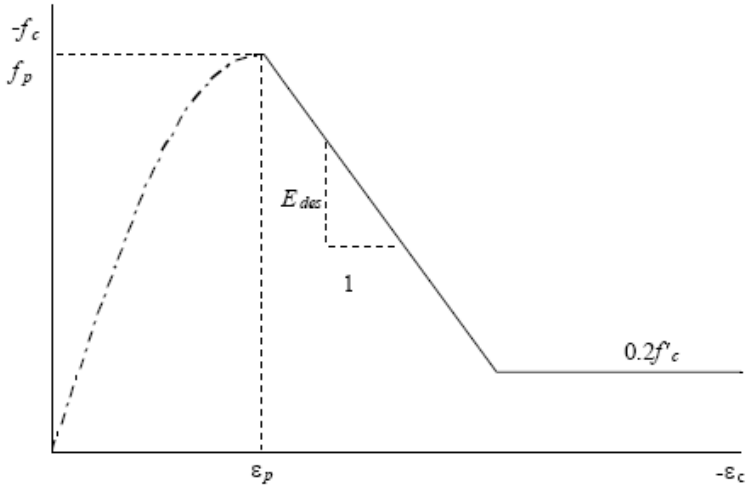

Figure 2.6.6: VecTor2 Hoshikuma et al. post-peak compressive response.

8. *Modified Park-Kent (1982)* [22] – Figure 2.6.7 shows a linear decreasing post-peak concrete compressive response formulated to model transverse hoop confined concrete by accounting for the enhancement of concrete strength and ductility. The descending slope is a function of the concrete cylinder strength, concrete compressive strain corresponding to the cylinder strength and principal stresses acting transversely to the considered direction.

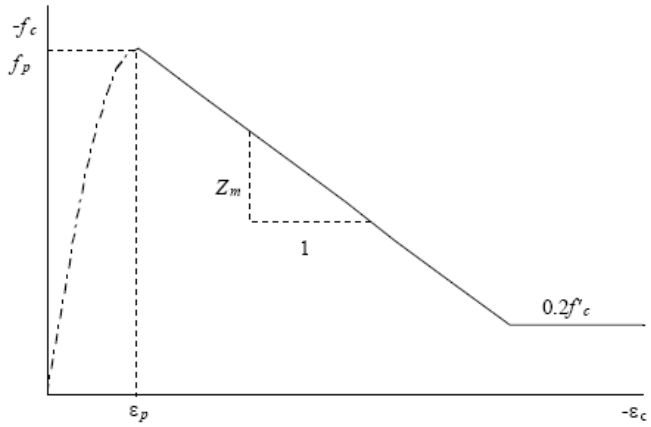

Figure 2.6.7: VecTor2 Modified Park-Kent post-peak compressive response.

9. *Saenz/Spacone (1964)* [22] – Figure 2.6.8 shows a compressive post-peak model that accounts for a more "rapidly descending compression post-peak response" exhibited by confined higher strength concrete. This model proposes that the curve passes through a post-peak control point strain equal to four times the strain corresponding to peak compressive stress.

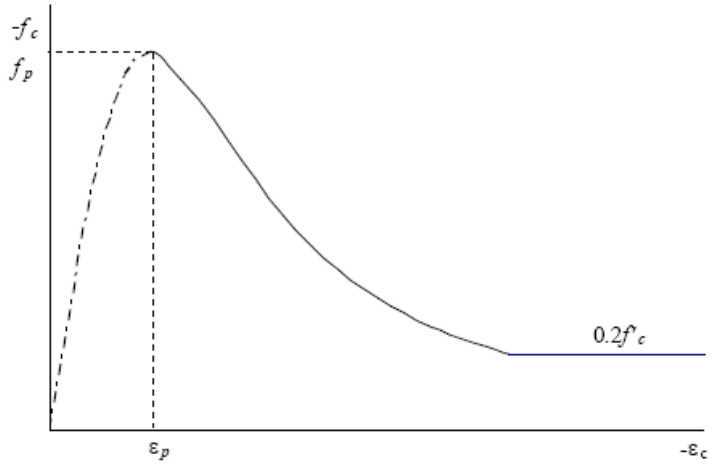

Figure 2.6.8: VecTor2 Saenz/Spacone post-peak compressive response.

In order to account for *compression softening*, a reduction or softening of strength and stiffness due to cracking and tensile straining, VecTor2 contains models used to calculate a "softening parameter, β_d" that ranges between 0 and 1 that are used to modify the compression response curves. According to the VecTor2 user manual, "Depending on how the models calculate and apply β_d, the following compression softening models may be classified into two types: strength and strained softened and strength-only softened models". The following models were developed based on panel and shell element tests at the University of Toronto by Vecchio and Collins (1986):

- *No compression softening* [22] : $\beta_d = 1$ (E 2.6-1)

- *Vecchio 1992-A (e1/e2-Form)* [22]:
  - $\beta_d = \frac{1}{1 + C_s \cdot C_d} \leq 1$ (E 2.6-2)

- Strength-and-strained softened model, originally developed for the Popovics (high strength) compression stress-strain model
- The value of C_s depends on whether or not slip is considered (epoxy coated or galvanized reinforcing bars)
- The value of C_d is a function of the ratio of tensile to compressive principal strains

- *Vecchio 1992-B (e1/e0-Form)* [22]:
  - $$\beta_d = \frac{1}{1 + C_s \cdot C_d} \leq 1 \qquad \text{(E-2.6-3)}$$
  - Strength-only version of Vecchio 1992-A model
  - The value of C_s depends on whether slip is considered
  - The value of C_d is a function of the ratio of the principal tensile strain to compressive strain corresponding to f'c.

- *Vecchio-Collins 1982* [22]:
  - $$\beta_d = \frac{1}{0.85 - 0.27\left(\frac{\varepsilon_{c1}}{\varepsilon_{c2}}\right)} \leq 1 \qquad \text{(E2.6-4)}$$
  - Strength-and-strained softened model, originally developed for the Hognestad Parabola compression stress-strain model

- *Vecchio-Collins 1986* [22]:
  - $$\beta_d = \frac{1}{0.8 - 0.34\left(\frac{\varepsilon_{c1}}{\varepsilon_o}\right)} \leq 1 \qquad \text{(E2.6-5)}$$
  - Strength-only version of Vecchio-Collins (1986)

Before cracking of the concrete, the stress-strain relationship in tension is assumed to be linear elastic and the following relationship between the initial tangent stiffness and the principal tensile strain shown in equation 2-2 is used:

$$f_{c1} = E_c \varepsilon_{c1} \quad for\ 0 < \varepsilon_{c1} < \varepsilon_{cr} \qquad \text{(E 2.6-6)}\ [22]$$

After cracking, VecTor2 has means of accounting for both tension stiffening and tension softening effects. Tension stiffening accounts for the fact that, even after cracking, the stiffness of the reinforced concrete is greater than the stiffness of the reinforcement alone. Tension softening refers to the reduction in tensile stresses in plain concrete after cracking under increased tensile straining. In VecTor2, the average concrete tensile stress due to tension stiffening is denoted $f_{c1}{}^{a}$, and the average concrete tensile stress due to tension softening is denoted, $f_{c1}{}^{b}$. The average concrete tensile stress after cracking has occurred is assumed to be the larger of stresses calculated with regard to either tension stiffening or tension softening as follows:

$$f_{c1} = max\left(f_{c1}{}^{a}, f_{c1}{}^{b}\right) \qquad \text{(E 2.6-7)}\ [22]$$

The following six models in VecTor2 account for *tension stiffening* [22]:

- *No tension stiffening* – post-cracking concrete tensile stress is zero.

$$f_{c1}^{a} = 0 \quad for\ \ 0 < \varepsilon_{cr} < \varepsilon_{c1} \qquad \text{(E 2.6-8)}\ [22]$$

Bentz (1999) – Equation E2.6-9 accounts for bond characteristics with a parameter, *m* that "reflects the ratio of the area of concrete to the bonded surface area of the reinforcement".

$$f_{c1}^{a} = \frac{f_{cr}}{1+\sqrt{3.6m \cdot \varepsilon_{c1}}} \quad for \;\; 0 < \varepsilon_{cr} < \varepsilon_{c1} \qquad \text{(E 2.6-9)}$$

- *Izumo, Maekawa Et Al. (1992)* – The model in Figure 2.6.9 was developed for use with RC panels subjected to in-plane stresses using a smeared crack approach. The exponent, c is a parameter that reflects bond characteristics.

$$f_{c1}^{a} = \begin{cases} f_{cr} & for \;\; 0 < \varepsilon_{cr} < \varepsilon_{c1} < 2\varepsilon_{cr} \\ f_{cr}\left(\dfrac{2\varepsilon_{cr}}{\varepsilon_{c1}}\right)^{c} & for \;\; 0 < 2\varepsilon_{cr} < \varepsilon_{c1} \end{cases} \qquad \text{(E 2.6-10)}$$

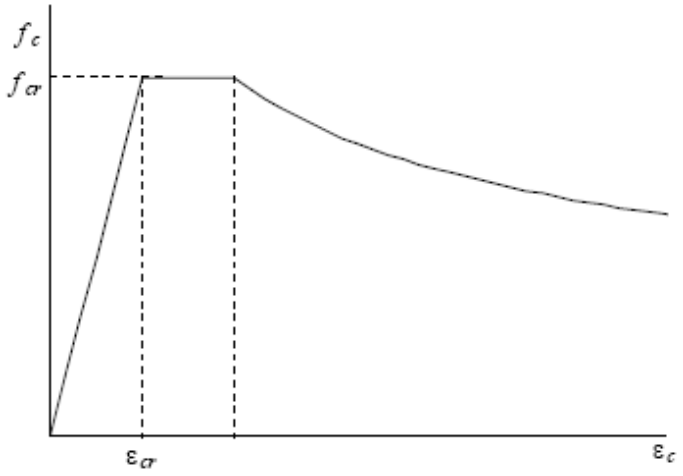

Figure 2.6.9: VecTor2 Izumo, Maekawa, et al. tension stiffening response.

- *Vecchio (1982)*– This model is "more appropriate for smaller scale elements and structures". It was formulated based on welded wire mesh reinforced panel element tests conducted at the University of Toronto.

- *Collins-Mitchell (1987)* – This is a modification of the Vecchio (1982) and is "more appropriate for larger scale elements and structures". It was formulated based on shell elements reinforced with bars tested at the University of Toronto.

$$f_{c1}^{a} = \frac{f_{cr}}{1+\sqrt{200\,\varepsilon_{c1}}} \quad for \;\; 0 < \varepsilon_{cr} < \varepsilon_{c1} \qquad \text{(E 2.6-11)}$$

$$f_{c1}^{a} = \frac{f_{cr}}{1+\sqrt{500\,\varepsilon_{c1}}} \quad for \;\; 0 < \varepsilon_{cr} < \varepsilon_{c1} \qquad \text{(E 2.6-12)}$$

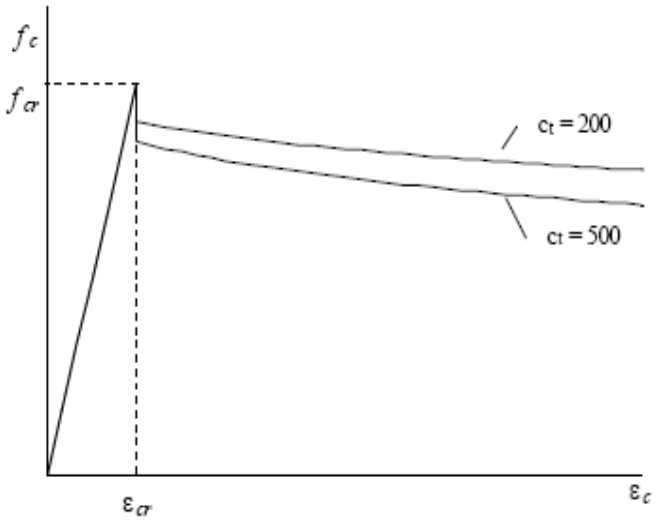

Figure 2.6.10: VecTor2 Vecchio and Collins-Mitchell tension stiffening response.

To account for *tension softening*, the term $f_{c1}{}^{b}$ is taken as the larger of that computed from the "tension softening base curve" or the "residual tensile stress", if included in the model. The following three models are available in VecTor2 to account for tension softening [22]:

- *No tension softening* – post-cracking concrete tensile stress is zero.

$$f_{c1}{}^{b} = 0 \qquad \text{(E 2.6-13)}$$

- *Linear* – The base curve post-cracking stress-strain behavior is linearly decreasing to the strain corresponding to zero stress as shown in figure 2.6.12 below. This figure also shows a residual stress branch.

$$f_{ts,base} = f_{cr}\left[1 - \frac{(\varepsilon_{c1} - \varepsilon_{cr})}{(\varepsilon_{ch} - \varepsilon_{cr})}\right] \geq 0, \quad for\ \varepsilon_{cr} < \varepsilon_{c1} \qquad \text{(E 2.6-14)}$$

Figure 2.6.11: VecTor2 linear tension softening response.

- *Yamamoto (1999) – No residual* – The base curve post-cracking stress strain behavior decreases nonlinearly to the "characteristic stress and strain" and the linearly to the strain corresponding to zero stress as shown in figure 2.6.12 below. This figure also shows a residual stress branch.

$$f_{ts,base} = \begin{cases} \dfrac{f_{cr}}{1+\sqrt{c(\varepsilon_{c1}-\varepsilon_{cr})}} & for\ \varepsilon_{cr} < \varepsilon_{c1} < \varepsilon_{ch} \\ f_{ch}\dfrac{(\varepsilon_{te}-\varepsilon_{c1})}{(\varepsilon_{te}-\varepsilon_{ch})} \geq 0 & for\ \varepsilon_{ch} < \varepsilon_{c1} \end{cases} \qquad \text{(E 2.6-15)}$$

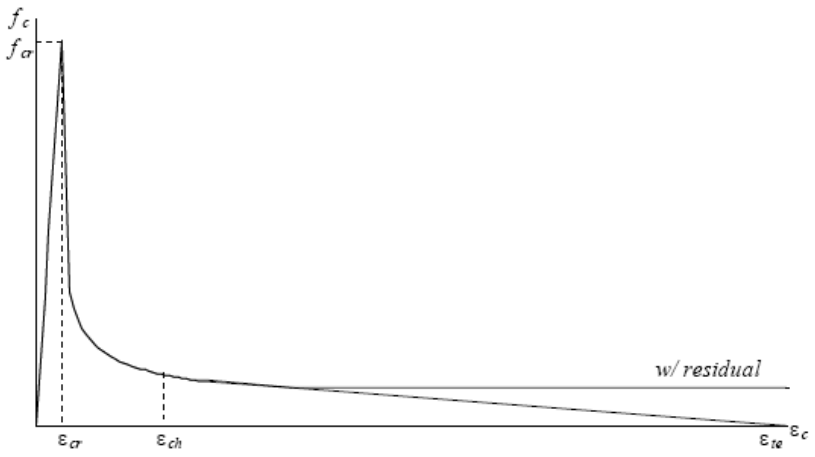

Figure 2.6.12: VecTor2 Yamamoto tension softening response.

To account for *cracking*, VecTor2 has the following four cracking criterion models available [22]:

1. Uniaxial cracking stress – "The cracking strength is taken as the specified uniaxial cracking strength":

$$f_{cr} = f'_t \qquad \text{(E 2.6-16)}$$

2. Mohr-Coulomb (stress) – In this model, "the cracking strength is the principal tensile stress, fc1, of the Mohr's circle tangent to the failure envelope as shown in figure 2.6.13 below. VecTor2 assumes the internal angle of friction is 37°, c is a cohesion parameter, and f_{cru} is the unconfined cracking strength.

$$f_{cr} = f_{cru}\left(1 + \frac{f_{c3}}{f'_c}\right), \qquad 0.20 f_t^{'} \le f_{cr} \le f_t^{'} \qquad \text{(E 2.6-17)}$$

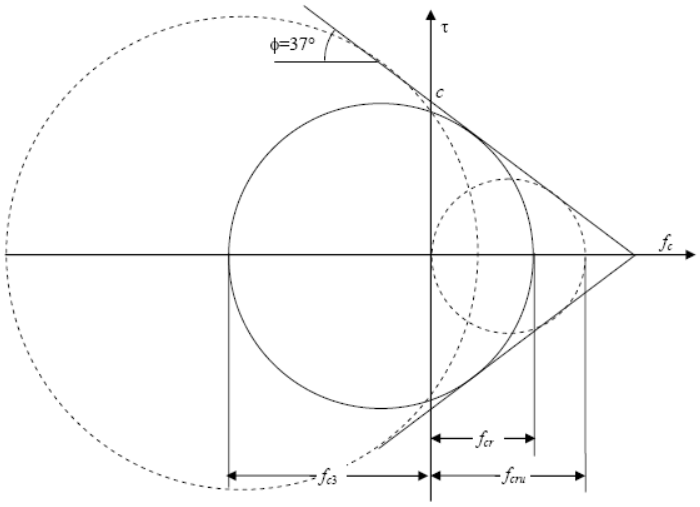

Figure 2.6.13: VecTor2 Mohr-Coulumb (stress) cracking criterion.

3. Mohr-Coulomb (strain) – In this model, the cracking strength can be computed by using the Mohr's circle of strains given the principal concrete strains:

$$f_{cr} = f_{cru}\left(1 - \frac{\varepsilon_{c3}}{\varepsilon_o}\right), \qquad 0.20 f'_t \le f_{cr} \le f'_t \qquad \text{(E 2.6-18)}$$

4. CEB-FIP Model – Based on a relationship developed by Kupfer et al. (1973), the cracking strength is reduced as the biaxial compression is increased:

$$f_{cr} = f_{cru}\left(1 + 0.8\frac{f_{c3}}{f'_c}\right), \qquad 0.20 f_t' \le f_{cr} \le f_t' \qquad \text{(E 2.6-19)}$$

VecTor2 also has the capability to perform a *crack slip* check. As described in the VecTor2 manual: "When element crack slip distortions are not considered, as in the MCFT, it is necessary to check that the local shear stresses, v_{ci}, at a crack do not exceed a maximum shear stress, v^{max}_{ci}, corresponding to sliding shear failure. If this value is found to be exceeded, then the average concrete tensile stresses, f_{ci} must be reduced by the factor v^{max}_{ci}/ v_{ci}, and the stress and strain state of element is reconsidered". In the MCFT, aggregate interlock is what transfers stress at a crack. The local shear stresses at the crack are calculated using the equation below, along with small local compressive stresses across the crack, f_{ci}, from work by Walraven (Vecchio and Collins 1986): Vecchio-Collins 1986 Model.

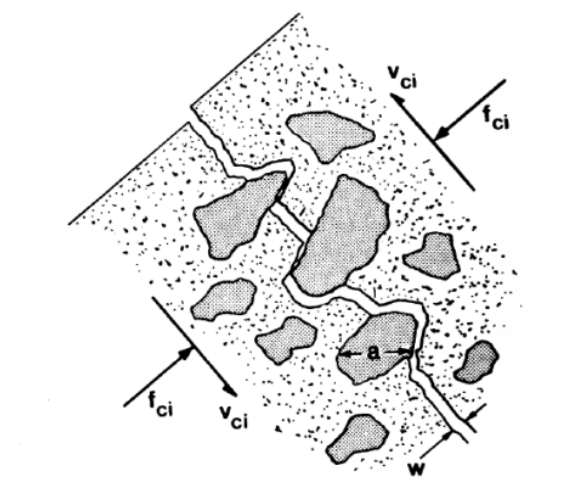

Figure 2.6.14: Shear across a crack via aggregate-interlock (Vecchio et al. 1986) [21]

$$v_{ci} = 0.18v_{ci,max} + 1.64f_{ci} - 0.82\frac{f_{ci}^2}{v_{ci,max}} \qquad \text{(E 2.6-20) [22]}$$

where,

$$v_{ci}^{max} = \frac{\sqrt{f'_c}}{0.3 + 24w/(a+26)} \quad (mm, MPa) \qquad \text{(E 2.6-21) [22]}$$

VecTor2 also has the capability to determine crack width. According to the VecTor2 manual, "rapidly reducing the average compressive stress when the crack limit is exceeded provides more accurate predictions of the load-deformation response." [22]

In addition to the responses previously discussed, VecTor2 is equipped to model tension Splitting, lateral expansion, element shear slip distortion, confinement strength, time-dependent effects such as creep, and dynamic effects.

The specific formulations and criteria are found in the VecTor2 User Manual (2013).

Figure 2.6.15 shows the default models preselected in FormWorks for the VecTor2 analysis. These models will be used to perform the nonlinear analysis on the case study structure presented in this report, with the exception of the effects that will not be considered, such as creep, hysteretic response, and buckling.

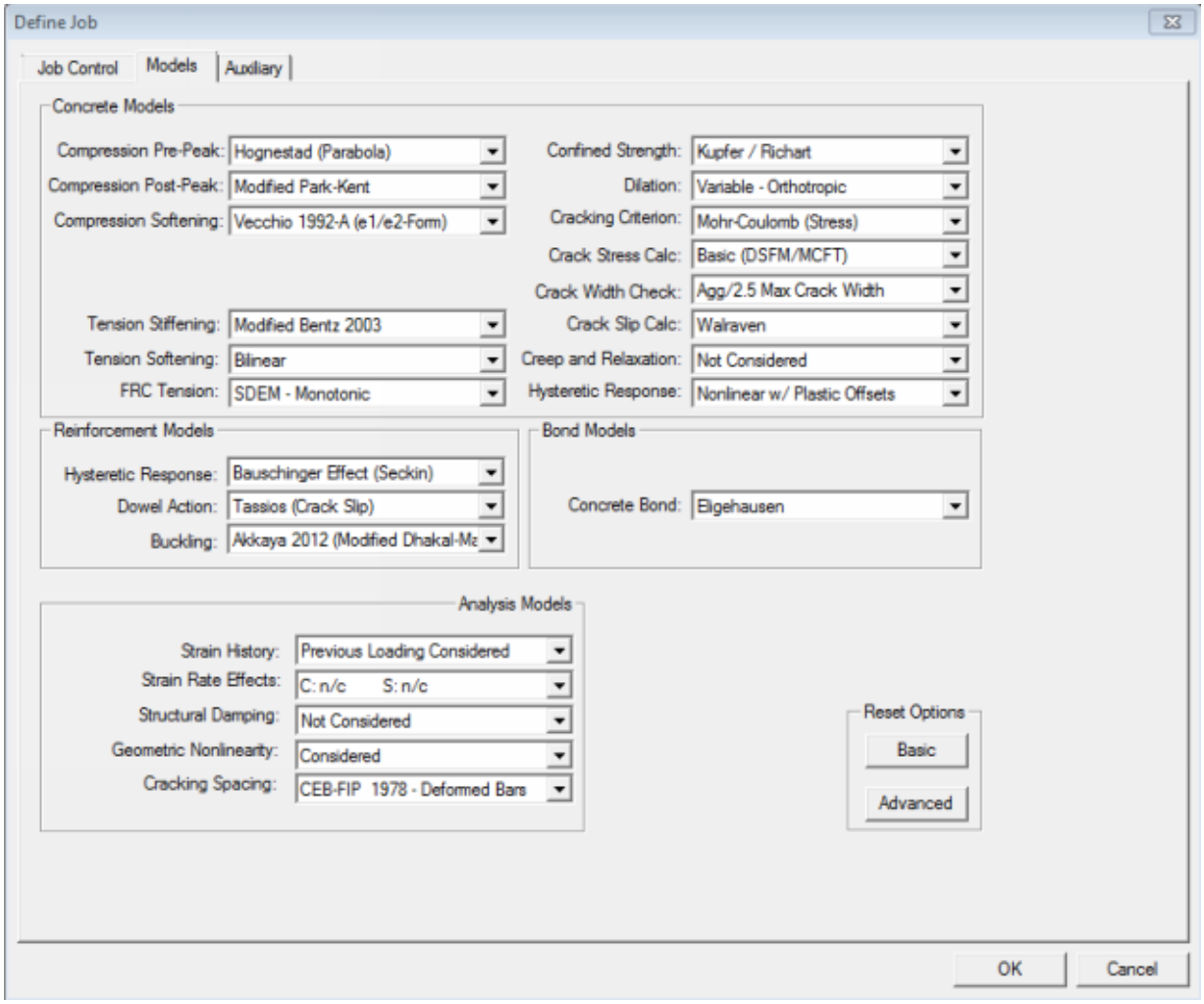

Figure 2.6.15: Snapshot from FormWorks: VecTor2 Default Model Selections.

PART II

Chapter 3: Case Study - Traditional Design and Analysis

This chapter presents a traditional analysis and design for the case study referenced in this report which is gravity links beams that are connecting two structural walls or piers of a high-rise building is discussed. The structure is modeled as being linear elastic, where the nonlinear effects discussed in Chapter 2 are not included, and then is designed for flexure and shear using the building code requirements of ACI 318M-02 [2] (ACI 318M-14 [3] remains virtually unchanged). The specific geometries and loading conditions for this case study are shown in Figure 3.1 and Figure 3.2.

In traditional design, the engineer applies the factored loads to the structure, computes the factored demands using linear elastic methods, and checks that those factored demands (i.e. Shear, Moment, Axial Loads, Torsion, etc.) are within the limits of empirical design provisions. The shear and flexural reinforcement criteria for this case study are provisioned in Chapters 10 and 11 in ACI 318M-02 [2].

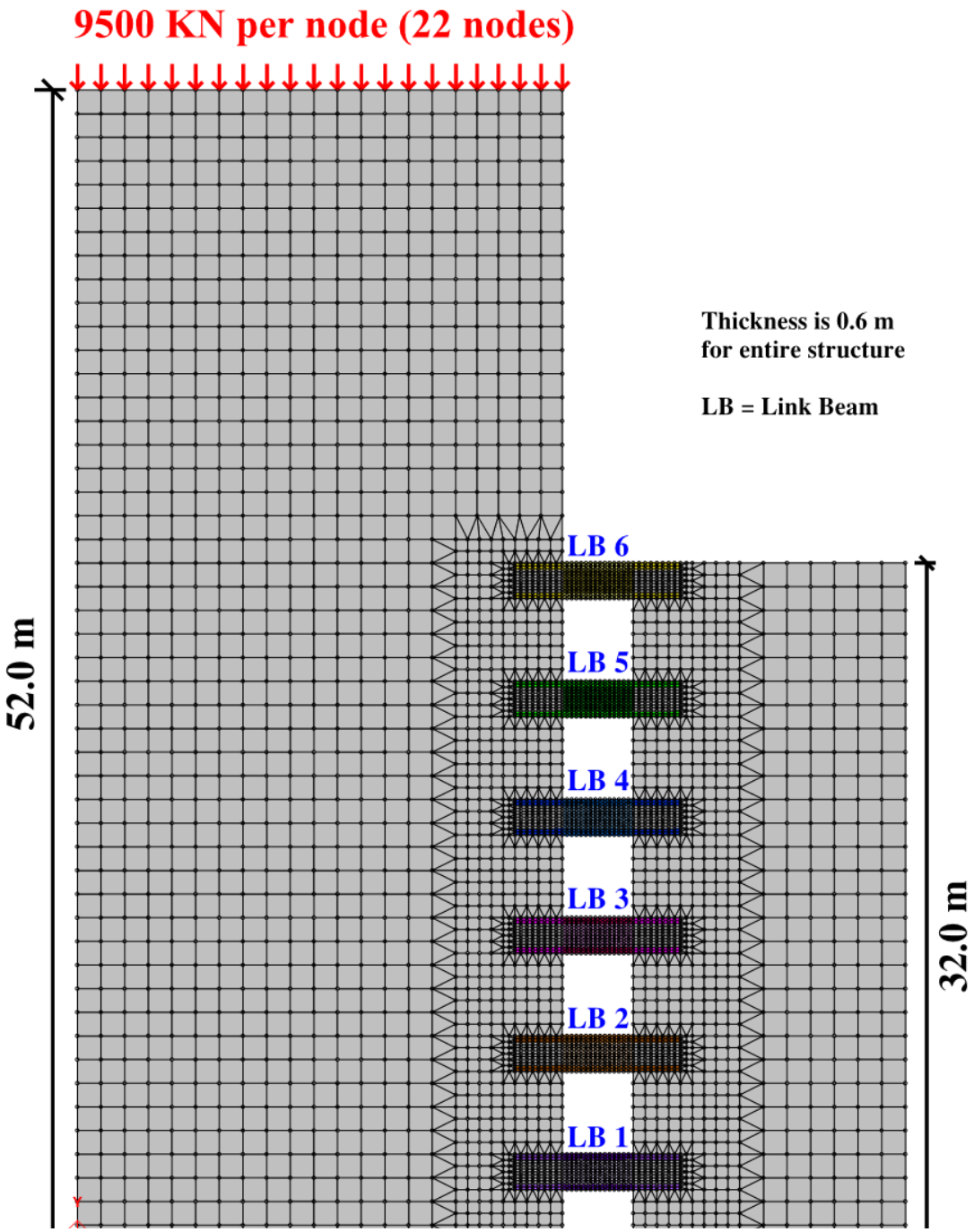

Figure 3.1: Finite element model of high-rise building wall piers showing overall geometry, dimensions, factored load, boundary conditions, and the six link beams.

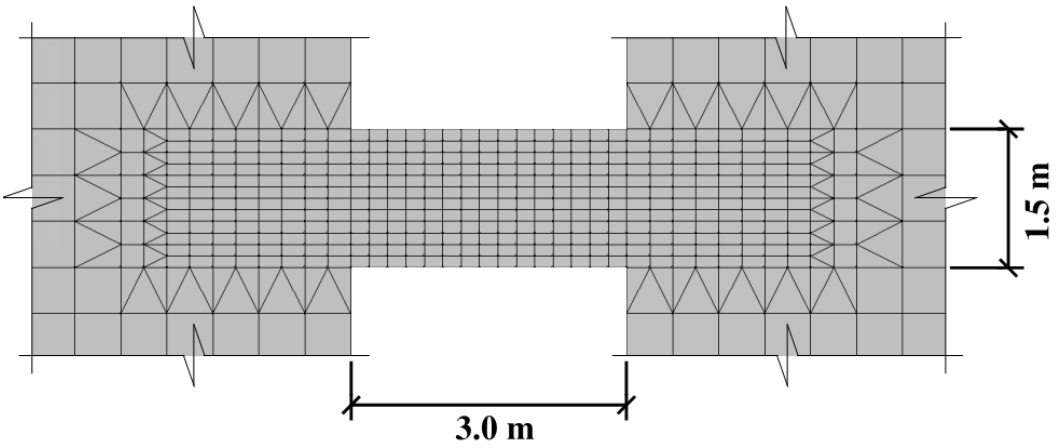

Figure 3.2: Cutout from Figure 3.1, showing overall geometry for one of the link beams.

The applied factored load distributed load in Figure 3.1 is equivalent to a point load of 209 MN. This load was chosen based on typical high-rise (50 stories or more) building gravity loads, and it will be used as the primary factored design gravity load on the full model for the remainder of the chapters in this report, including nonlinear analysis. A concrete design compressive strength of f'_c = 35 MPa will also be constant throughout the case study.

Figures 3.1 and 3.2 show the overall finite element model with clear locations of the mesh density transitions, indicating where triangular elements were used as mentioned in section 2.6. Figure 3.3 presents a snapshot from FormWorks, which shows the number of elements and nodes in the global structure. It is important to note that 4889 is almost 95% of the 5200 node limit, making the finite element mesh very efficient relative to the limitations imposed by VecTor2. [22]

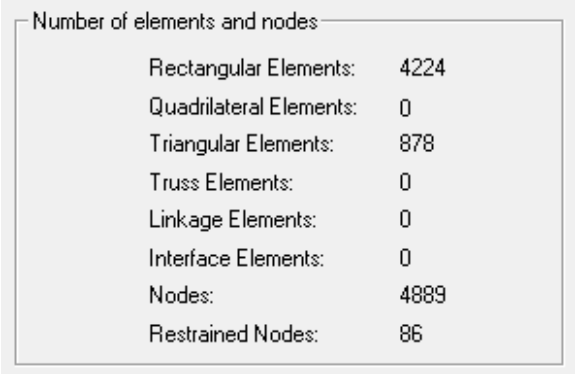

Figure 3.3: Snapshot from FormWorks, showing the number of nodes and elements for the finite element mesh in Figure 3.1.

Tables 3.1 through 3.3 present a summary of the entire traditional linear elastic design process following the ACI318[2, 3] code provisions. V_u and M_u are the factored shear and moment demands obtained from VecTor2, respectively. The point of contra-flexure denotes the location along the span of the link beam where the internal moment approaches zero. The point of contra-flexure is the point of zero curvature along the beam and is also often referred to as the point of inflection. Since the point of contra-flexure is not always at mid-span, the internal moment demands at either ends of the link beam indicate the point's location.

Table 3.1: Factored demands computed by VecTor2 in the six link beams.

*FULL MODEL - LINEAR ELASTIC RESPONSE					
Plain Concrete, Factored Applied Load = 209,000 KN					
Link Beam	Vector2 Factored Demands				
	V_u	Left M_u	Right M_u	Point of Contra-flexure	Axial, N_u
6	4636	7105	-5570	Closer to Right Support	-3175
5	3949	5426	-5359	Closer to Right Support	63
4	2849	3898	-3882	L/2	446
3	2008	2724	-2759	L/2	370
2	1366	1824	-1905	Closer to Left Support	-147
1	861	1124	-1227	Closer to Left Support	-980

All units in KN, m

The factored demands in Table 3.1 appear reasonable since it is expected that the top link beam resists what it has the capacity to resist from the overall shear transferred from the main core, then it would transfer what is left to the succeeding link beams below it. This pattern is apparent all the way until the bottom link beam. Further, since internal moments are a function of internal shear forces, it is expected that lower link beams have lower internal moments demands. In an efficient structure, the point of contra-flexure is preferred to be in the middle since it would provide the lowest internal moment demands, and by extension the least variation in reinforcing amounts. Even when the point of contra-flexure is somewhat skewed in Table 3.1, the variation in moments is not significant, and thereby designing for the higher moment does not appear to be overly inefficient. Further, the link beams in Figure 3.1 are expected to experience negligible axial stresses. A quick spot check on the axial stress demand of link beam 6 (approximately 3.5 MPa) indicates negligible axial stresses relative to the concrete design compressive strength.

Design for Shear:

ACI318M-02 design requirements for shear reinforcement in Chapter 11 of the code prescribe that the factored nominal shear strength or capacity, $\emptyset_v V_n$, must be greater than or equal to the factored shear demand, V_u, where $\emptyset_v$ is the shear strength reduction factor, taken as 0.75.

The nominal shear capacity is provided by the nominal concrete capacity, V_c, and the nominal transverse steel reinforcing capacity, V_s. ACI318M-02[2] provides the following equation:

$$V_n = V_c + V_s \quad \text{(E 3-1)}$$

V_c very broadly includes the contributions of all parameters resisting shear in a beam with no web reinforcing. These parameters include the shear in the compression zone of the concrete, aggregate interlock at an inclined shear crack, and dowel action of the longitudinal reinforcing. ACI318M-02 limits the shear resistance contribution from the aforementioned parameters to a maximum stress of:

$$v_c = \frac{V_c}{bd} = 0.167\sqrt{f'_c} \quad \text{(MPa)} \quad \text{(E 3-2)}$$

Where b is the section thickness (0.6 m) and d is the effective depth to the longitudinal reinforcement. The clear cover is assumed to be 50 mm, and the effective depth, d is taken as 1.45 m.

ACI 318M-02 dictates that a minimum area of shear reinforcement, $A_{v,\,min}$, shall be provided in all reinforce concrete flexural members where V_u exceeds 50% of the concrete resistance contribution (i.e.$0.5\emptyset_v V_{c)}$. Typically, the spacing of shear reinforcement, s, is an unknown. Therefore, $A_{v,\,min}$ can be described as a function of s per ACI 318M-02 by the following equation:

$$\frac{A_{v,\ min}}{s} = 0.062\sqrt{f'_c}\frac{b}{f_y} \ (m^2/m) \qquad \text{(E 3-3)}$$

Where, f_y is the yield strength of the shear reinforcement, which will be taken as 414 MPa throughout the case study. ACI 318M-02 limits the ratio of $\frac{A_{v,\ min}}{s}$ to a maximum of $0.35b/f_y$.

It is important to note the nomenclature criteria in Part II of this report: all small letters indicate stresses, while all capital letters indicate forces or moments.

The following tables present the final design in amounts of reinforcing, expressed as a percentage ratio using the Greek letter ρ. A sample calculation for shear and flexural reinforcement will follow each table.

Table 3.2: Shear reinforcement code requirements in the six link beams

FULL MODEL - LINEAR ELASTIC RESPONSE							
Link Beam	Shear Reinforcement per ACI 318M						
	v_u (MPa)	V_u (MN)	V_s Req'd?	V_n (MN)	v_n (MPa)	v_s (MPa)	ρ_v (%)
6	4.636	4.033	YES	5.378	6.181	5.195	**1.25**
5	3.949	3.436	YES	4.581	5.266	4.280	**1.03**
4	2.849	2.479	YES	3.305	3.799	2.813	**0.68**
3	2.008	1.747	YES	2.329	2.677	1.691	**0.41**
2	1.366	1.188	YES	1.584	1.821	0.835	**0.20**
1	0.861	0.749	YES	0.999	1.148	0.162	**0.09**

The following is a sample calculation for link beam 4 in Table 3.2.

Concrete contribution to shear force resistance:

$V_c = 0.167\sqrt{f'_c}bd$

$= 0.167\sqrt{35\ \text{MPa}}\ (0.6\text{m})(1.45\text{m}) =$ **0.859 MN**

$v_c = \frac{V_c}{bd}$ = **0.986 MPa**

Shear reinforcement requirement check:

$0.5\emptyset_v V_c = 0.5(0.75)(0.86MN)$ = **0.322 kN**

Since $V_u > 0.5\emptyset_v V_c$, **shear reinforcement is needed.**

Minimum area of steel to spacing ratio:

$$\frac{A_{v,\ min}}{s} = 0.062\sqrt{f'_c}\frac{b}{f_y}$$

$$= 0.062\sqrt{35\ MPa}\frac{0.6\ m}{414\ MPa} = \mathbf{5.36\ x\ 10^{-4}\ m^2/m}$$

Required area of steel:

$V_s = V_n - V_c$

$V_n = V_u/\emptyset_v$

$= 2.479\ MN/0.75 =$ **3.305 MN**

Therefore,

$V_s = 3.305\ MN - 0.86\ MN =$ **2.446 MN**

Or,

$v_s =$ **2.81 MPa**

Minimum shear reinforcement ratio required (for temperature, shrinkage, and crack control):

$$\rho_{v,\ min} = \frac{v_{s,\ min}}{f_y} = \frac{A_{v,\ min}}{(b)(s)}$$

$$= \frac{5.36 \times 10^{-4}\ m^2/m}{0.6\ m} \times 100 = \mathbf{0.089\%}$$

Required shear reinforcement ratio:

$$\rho_v = \frac{v_s}{f_y} =$$

$$= (2.81 / 414) \times 100 = \underline{\mathbf{0.68\%}} > \rho_{v,\,min}\ \mathbf{(O.K.)}$$

Design for Flexure:

ACI 318M-02 [2] design requirements for flexural reinforcement in Chapter 10 of the code prescribe that the factored nominal moment strength or capacity, $\emptyset_f M_n$, must be greater than or equal to the factored moment demand, M_u, where $\emptyset_f$ is the flexural strength reduction factor, taken as 0.9, the section being analyzed is tension controlled. Sections are tension controlled if the net tensile strain in the extreme tension steel, ε_t, is equal to or greater than 0.005 when the concrete un compression reaches its assumed strain limit of 0.003. The tensile strain ε_t is a function of the depth of the compressive stress block and the flexural lever arm, known as jd, of the section.

Since the depth of the compressive stress block is usually an unknown, a typical flexural lever arm assumption is used in this chapter. 85% of the effective depth, d, is taken is the flexural lever arm, jd, for all flexural reinforcement in Table 3.3.

It can be shown that the analysis of a concrete section yields the following relationships:

$$\emptyset_f M_n = \emptyset_f [A_s f_y (d - \frac{a}{2})] = \emptyset_f [A_s f_y (jd)] \qquad \text{(MN-m)} \qquad \text{(E 3-4)}$$

$$A_s = \frac{M_u}{\emptyset_f f_y (jd)} \qquad (m^2) \qquad \text{(E 3-5)}$$

Where As is the area of flexural steel reinforcement. The minimum area of steel required by ACI 318M-02 is the greater of the following:

$$A_{s,\,min} = \frac{0.25\sqrt{f'_c}}{f_y} bd \qquad (m^2) \qquad \text{(E 3-6)}$$

$$A_{s,\,min} = 1.4bd/f_y \qquad (m^2) \qquad \text{(E 3-7)}$$

Table 3.3: Flexure reinforcement code requirements in the six link beams

FULL MODEL - LINEAR ELASTIC RESPONSE				
Link Beam	Flexure Reinforcement per ACI 318M			
	M_u (MN-m)	M_n (MN-m)	$A_{s,\,req'd}$ (m^2)	$\rho_{l,\,req'd}$ (%)
6	7.105	7.895	0.015472	**1.77**
5	5.426	6.029	0.011815	**1.35**
4	3.898	4.331	0.008489	**0.98**
3	2.759	3.065	0.006008	**0.69**
2	1.905	2.117	0.004148	**0.47**
1	1.227	1.363	0.002672	**0.35**

The following is a sample calculation for link beam 4 in Table 3.3.

Minimum area of steel required:

$$A_{s,\,min} = \frac{0.25\sqrt{f'_c}}{f_y} bd$$

$$= \frac{0.25\sqrt{35\ MPa}}{414\ MPa} (0.6\ m)(1.45\ m) = 3.11 \times 10^{-3}\ m^2$$

$$A_{s,\,min} = 1.4bd/f_y$$

$= 1.4(0.6\text{ m})(1.45\text{ m})/(414\text{ MPa}) = 2.94 \times 10^{-3}\text{ m}^2$

$A_{s,\,min}$ = **3.11×10^{-3} m^2 governs**

Minimum shear reinforcement ratio required:

$$\rho_{l,\,min} = \frac{A_{s,\ min}}{bd} =$$

$$= \frac{3.11 \times 10^{-3}\text{ m}^2}{(0.6\text{ m})(1.45\text{ m})} \times 100 = \mathbf{0.357\%}$$

Required area of steel:

$$A_s = \frac{M_u}{\phi_f f_y (jd)}$$

$$= \frac{3.898\text{ MN–m}}{0.9(414\text{ MPa})(0.85 \times 1.45\text{ m})} = \mathbf{8.49 \times 10^{-3}\text{ m}^2}$$

Required flexural reinforcement ratio:

$$\rho_l = \frac{A_s}{bd}$$

$$= \frac{8.49 \times 10^{-3}\text{ m}^2}{(0.6\text{ m})(1.45\text{ m})} \times 100 = \mathbf{0.98\%} > \rho_{l,\,min}\ \mathbf{(O.K.)}$$

The reinforcement ratios presented in Tables 3.2 and 3.3 are schematically visualized in elevation and section view in Figures 3.4 and 3.5, respectively, on the next page. It is worth noting that the link beams in the case study are considered “deep” beams per ACI 318M-02 [2]. As a result, “skin” reinforcement should be added to the side faces of the link beams in order to control cracking

and improve general performance. Skin reinforcement is also shown in the referenced figures.

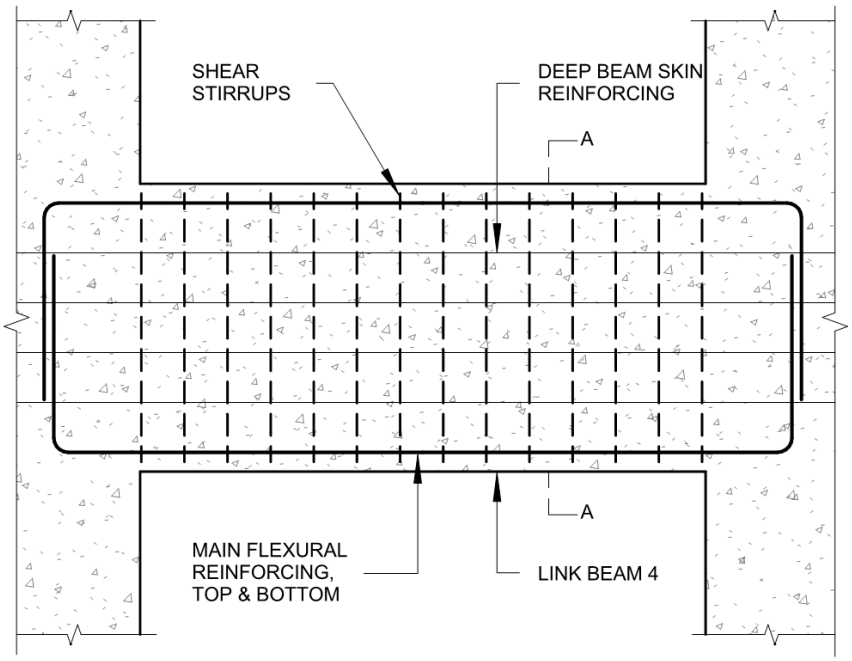

Figure 3.4: Elevation view of link beam 4, showing traditional layout of reinforcing.

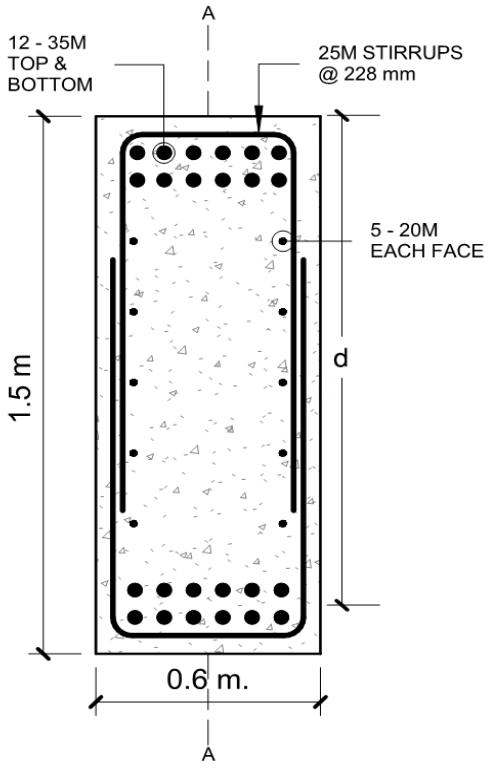

Figure 3.5: Section view Figure 3.4, showing details of the reinforcing.

Chapter 4: Inelastic Analysis of Single Link Beam

As discussed in earlier chapters, reinforced concrete structures are not linear elastic in reality. Reinforced concrete's response depends greatly on amounts of reinforcement and other parameters. Another shortcoming in traditional design practice is that provisions in codes-of-practice provisions often use "one size fits all" empirical expressions. These expressions are concerned primarily with strength, and provide no descriptions or guidance on performance based results.

It could be argued that since structural concrete is a composite material with non-orthotropic behavior and as a result inherently extremely complex to model, imposing limitations on practical design to relatively simple and idealized

empirical code provisions seems reasonable. However, the rapid evolution of technology in terms of computing power, mathematical techniques, and structural analysis have provided professional designers with tools for more accurate performance based designs while improving life safety and structural integrity.

In order to demonstrate both the advantages and simplicity of utilizing advanced computational tools in predicting the inelastic response of a concrete structure, this chapter provides an in-depth analysis of the response of a single link beam model in VecTor2, subjected to gravity loading as shown in Figure 4.1. The single link beam model is used to validate that nonlinear response is indeed very significant. It will also be used as the "benchmark" model to inform the amounts of longitudinal and transverse reinforcing for the full nonlinear model trials in Chapter 5 of this report.

In order to have the full model presented earlier in Figure 3.1, and later in Figure 5.1 experience nonlinear behavior as expected (for example: negligible axial stresses in the link beam), appropriate boundary conditions and reinforcement amounts were developed and calibrated in order to simulate the desired response. For instance, the pier walls at either ends of the link beams are expected to provide significant restraint against vertical expansion. This confines the concrete at either support, thereby increasing the compressive strength at those regions.

As discussed in section 2.6 of this report, the 5200 maximum node limitation of VecTor2 [22] compelled the full model to have a very coarse mesh in areas

relatively far away from the link beams, as shown in Figure 3.1. However, this was not an issue with the single link beam model studied in this chapter, which served as a major advantage in its optimization for use as a reinforcing benchmark model.

Figure 4.1 shows the single link beam finite element model with dimensions and boundary conditions. Its thickness matched that of the full model, as in Figure 3.1, and was thus taken as 0.6 m. Since the single link beam model required no mesh density transitions, VecTor2 had enough node capacity to accommodate fine plane stress rectangular elements for the entire finite element model. The boundary conditions were: (i) restricting the horizontal displacement of the western (left) wall pier and, (ii) restricting vertical displacement of the eastern (right) wall pier. The piers were widened to a degree enough to produce couple reactions at both boundary condition supports, thereby stabilizing the deformation and stresses of the overall model. Another advantage of widening the piers was to produce symmetrical stress concentrations, as will be demonstrated and discussed in this chapter.

Further, since symmetrical results are preferred for the validation of the single link beam model's capability of being used as a benchmark model (because they ensure the most efficient design and most stable model), the reinforcing pattern for the single link beam model was optimized. While the single link beam portion in the model was designed for its specific demands (demand criteria will be discussed later in this chapter), the remainder of the model was optimized with the necessary reinforcement amounts to produce the desired effects and conduct a

thorough and informative investigation of the analyses results. As noted in Chapter 2 of this report, steel reinforcement was modeled as smeared reinforcement for all elements in the case study.

As shown in Figure 4.1, deformation in the model was induced and controlled by applying displacement instead of force on the western pier. This was done in order to stabilize the analysis and results, and clearly locate the peak capacity of the single link beam, which will be demonstrated and discussed in the figures of this chapter.

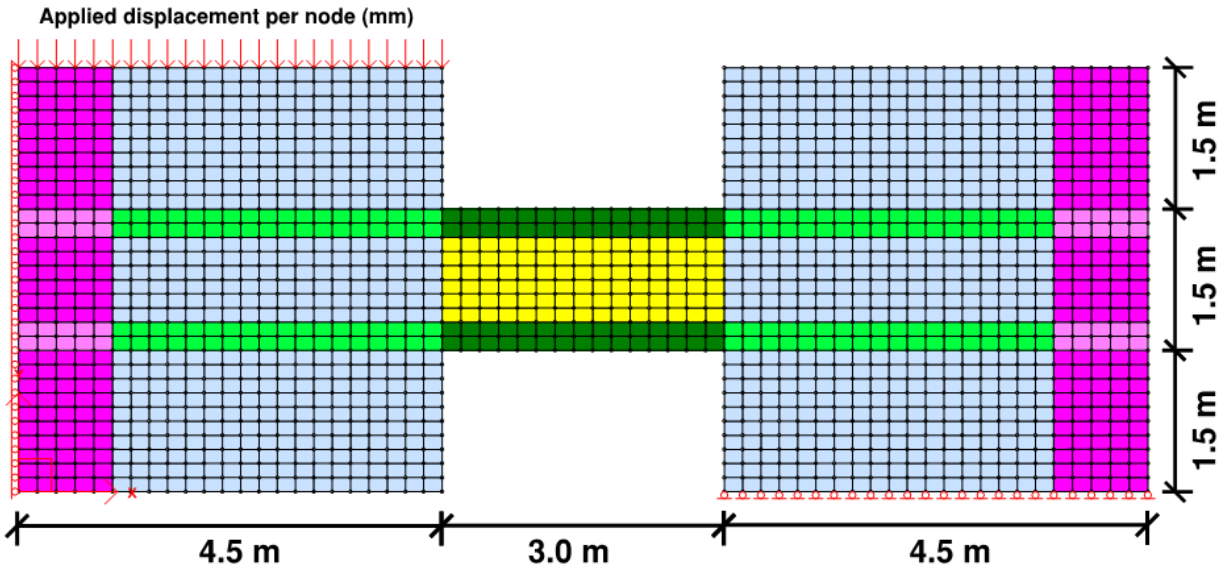

Figure 4.1: Finite element model of single link beam. Colors correspond to different smeared reinforcing ratios

In order to standardize the approach for using the single model as a benchmark for behavior, and by extension to inform reinforcement amounts in the full model nonlinear analysis in Chapter 5 of this report, a range of loading was

selected based on the ACI 318M-02 nominal shear stress capacity limits for beams to be used as the **factored** load case criteria. The stress values of the criteria ranged from of $v_u = 0.167\sqrt{f'_c}$ to $v_u = 1.167\sqrt{f'_c}$ in MPa, in increments of 0.167. As shown in Table 4.1, this yielded a total of seven factored load cases for the single link beam model. The lower end of the range was taken as per equation 3-2 in Chapter 3 of this report. Regarding the upper range of v_u, ACI 318M-02 [2] limits the nominal shear stress carried by steel reinforcement to $v_s = 0.667\sqrt{f'_c}$ MPa in order to control inclined cracking and, more importantly, diagonal compression. This yields a maximum total nominal shear capacity of $v_n = 0.833\sqrt{f'_c}$ However, in a real structure, a uniform diagonal compression field with no fanning at supports is expected. This would increase the diagonal compression capacity of the member to beyond ACI 318 limits. Therefore, it can be shown that the ACI 318M-02 limitation on nominal shear stress capacity is conservative if the nonlinear response of concrete were considered, and extending the v_u by up to 40% (to $v_u = 1.167\sqrt{f'_c}$) is considered a reasonable threshold for the link beams in this case study. In order to further accurately compare and discuss results, the v_u load criteria ratios will be divided by the shear load reduction factor, $\emptyset_v = 0.75$. This is because the capacities analyzed by VecTor2 will be the actual nominal capacity of the link beam. Therefore, it cannot be compared with the factored design load criteria, but rather the nominal design load criteria as shown in Table 4.3.

Table 4.1 presents the shear reinforcement design for the seven factored load cases based on the aforementioned v_u range. As shown in the sample calculations of Chapter 3 in this report, the reinforcement ratios were computed by taking the values in the second column of Table 4.1 as the factored demands for each case. Each case was then modeled and analyzed based on changing the reinforcement ratios in the single link beam model. The shear reinforcement ratio is changed in the dark green and yellow elements in Figure 4.1 (the elements that make up the link beam itself) for each load case. Those elements are not one color because flexural reinforcement is typically concentrated at the top and bottom portions of a beam in order to maximize the effective depth and the internal flexural lever arm. Therefore, the dark green elements at the top and bottom of the finite element model in Figure 4.1 are where the primary flexural reinforcement will be smeared, and the yellow elements would include smeared skin reinforcement for deep beams (typical ratio of 0.25% for skin reinforcement is used throughout case study). The steel reinforcement properties for the case study in this report are typical for linearly elastic perfectly plastic steel. The yield (and ultimate) strength of the steel is taken as f_y = 414 MPa, and the elastic modulus is taken as, E = 200,000 MPa.

Table 4.2 presents the flexural reinforcement design for the seven factored load cases. Since the factored moment demands are unknown as per the loading criteria presented for the single link beam, the factored moment demand was predicted based on an assumed point of contra-flexure occurring at mid-span of the link beam for every load case. An investigation and discussion on whether this

assumption is true will be made later in this chapter. The flexural reinforcement ratios shown in Table 4.2 are the requirements for the gross cross-section of the link beam, so the smeared reinforcement ratios in the top and bottom two layers of elements in the link were adjusted for this condition at every load case.

Table 4.1: Loading and shear reinforcing information for the single link beam.

SINGLE LINK BEAM MODEL							
Shear Reinforcement Criteria							
Case #	$v_u/\sqrt{f'_c}$	v_u (MPa)	V_u (MN)	V_n (MN)	v_n (MPa)	v_s (MPa)	$\rho_{v,\,req'd}$ (%)
1	**0.167**	0.986	0.858	1.144	1.315	0.329	**0.09**
2	**0.333**	1.950	1.697	2.262	2.600	1.614	**0.39**
3	**0.500**	2.925	2.545	3.393	3.900	2.914	**0.70**
4	**0.667**	3.900	3.393	4.524	5.200	4.214	**1.02**
5	**0.833**	4.875	4.242	5.655	6.500	5.514	**1.33**
6	**1.000**	5.850	5.090	6.786	7.801	6.815	**1.65**
7	**1.167**	6.825	5.938	7.918	9.101	8.115	**1.96**

Table 4.2: Loading and flexural reinforcing information for the single link beam.

SINGLE LINK BEAM MODEL					
Flexure Reinforcement Criteria					
Case #	$v_u/\sqrt{f'_c}$	*M_u (MN-m)	M_n (MN-m)	$A_{s,\,req'd}$ (mm^2)	$\rho_{l,\,req'd}$ (%)
1	**0.167**	1.287	1.430	2802	**0.357**
2	**0.333**	2.545	2.828	5542	**0.637**
3	**0.500**	3.817	4.242	8313	**0.955**
4	**0.667**	5.090	5.655	11083	**1.274**
5	**0.833**	6.362	7.069	13854	**1.592**
6	**1.000**	7.635	8.483	16625	**1.911**
7	**1.167**	8.907	9.897	19396	**2.229**

Point of contra-flexure assumed @ mid-span

Table 4.3: Ultimate capacities from VecTor2 response for each load case.

SINGLE LINK BEAM MODEL					
Nominal Design Forces per Tables 4.1 & 4.2 and VecTor2 Capacities					
Case #	$v_u/\phi\sqrt{f'c}$	V_u/ϕ (KN)	$V_{VecTor2}$ (KN)	M_u/ϕ (KN-m)	$M_{VecTor2}$ (KN-m)
1	**0.222**	1144	**1636**	1716	**2045**
2	**0.444**	2262	**2711**	3393	**3533**
3	**0.667**	3393	**3666**	5090	**4868**
4	**0.889**	4524	**4593**	6786	**6161**
5	**1.111**	5655	**5273**	8483	**7195**
6	**1.333**	6786	**5726**	10180	**7890**
7	**1.556**	7918	**6093**	11876	**8475**

The advantages of nonlinear analysis can be immediately observed from the results in Table 4.3. Taking load case #1 as an example, the nominal capacities from VecTor2 in shear and flexure are almost 1.5 times the nominal capacity of what they were designed for. This trend holds until load case #4, which coincidentally, is the nominal shear capacity limit imposed by ACI 318M-02. Moreover, it was observed that the primary mode of failure for load cases 5 through 7 was diagonal compression, which is the very reason the ACI code imposes the nominal shear capacity limitation. However, this can be the case due to the abnormally high shear demands and the stockiness of the link beam. Another reason is the effect of nonlinear concrete properties, mainly compression softening. Diagonal compression failure happens when the flexural steel yields and imposes large tensile strains on the concrete. These strains increase the principal tensile stresses in those concrete elements, thereby softening the concrete and increasing the diagonal compression in the beam. Due to the increase compression, the stirrups begin to experience yielding as they are picking up the diagonal compressive strut forces in tension. When the stirrups yield, they

also induce large strains on the concrete, especially at their extreme fibers, which would yield first since they are the most developed in terms of length. Recall that structural steel is assumed to behave in a linear elastic perfectly plastic fashion for this case study. As a result, the steel is able to sustain loading that is several times its yield capacity due to its yield plateau on the perfectly plastic portion of its stress-strain curve. These rather large strains increase the principal tensile strains in the concrete even further, thereby softening the concrete in those regions even further. The concrete compressive stress capacity gets softened to appoint where the principal compressive stresses take over, inducing crushing in the concrete in the direction of the principal compression stresses.

Figures 4.2 through 4.16 present investigations and discussions on the nonlinear effects of the single link beam response under load case #4.

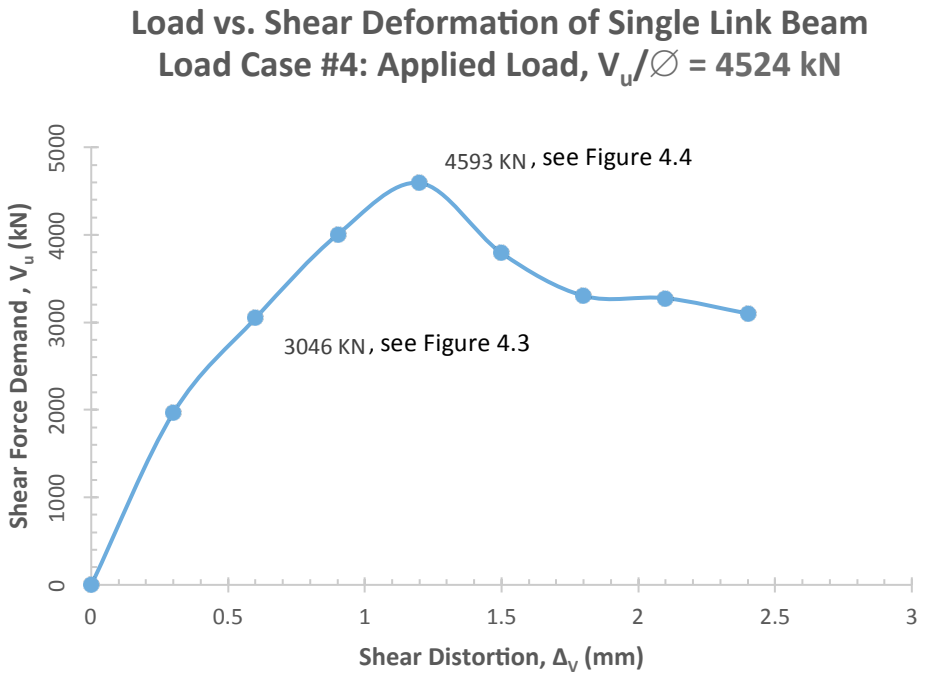

Figure 4.2: Load-Deformation response of the single link beam under load case #4.

The load-deformation response shown in Figure 4.2 clearly shows the post- peak response of the link beam, which is one of the primary advantages of applying displacements rather than forces to distort and induce stresses in the single link beam model. For every load case in Table 4.3, nine monotonic load steps were applied were applied to the link beam: from 0.0 to 1.6, in increments of 0.2. The response for load case #4 peaked at a shear force of 4593 kN, which equates a shear stress value of just over 5 MPa (talk about what is typically expected as a limit). This peak shear force demand is the nominal moment capacity of the link beam. Further, the ductility of the response is in line with what is expected of reinforced concrete beam sections subjected to shear and flexure. Up until the first load step of 0.2 in the response, the link beam experiences linear elastic behavior and large stiffness as expected. Between load steps 0.4 and the peak at load step 0.8, the response experiences less stiffness but appears to be somewhat linear in that portion. This is due to the coarseness of the load steps, because the behavior between in that portion of the response is indeed inelastic.

Figure 4.3 shows a graphical representation of the shear distortion, Δ_v, and cracking (red lines) for the single link beam at load step 0.4 for load case #4, marked on the response of Figure 4.2. It is clear that the response appears to be symmetrical in both cracking and shear distortion. As expected, no crack patterns

appear on the top left and bottom right corners of the link beam, since they are experiencing compressive stresses. The top right and bottom left corners of the link beam indicate tensile stress concentrations, also as expected. The crack patterns at those locations appear to be less inclined than those along the middle of the link beam, which indicates a combination of both flexural and shear cracking. Along the middle of the beam, specifically from the top compression corner to the bottom one, the crack pattern clearly indicates a diagonal compression field. Figure 4.4 shows the link beam at its ultimate nominal capacity at load step 0.8 as shown in Figure 4.2. The shear distortion and cracking have increased significantly as expected. The stability of the model in relation to the width of the wall piers indicates that no significant distortion or rotation occurred at the wall piers, which is why the response is virtually symmetrical.

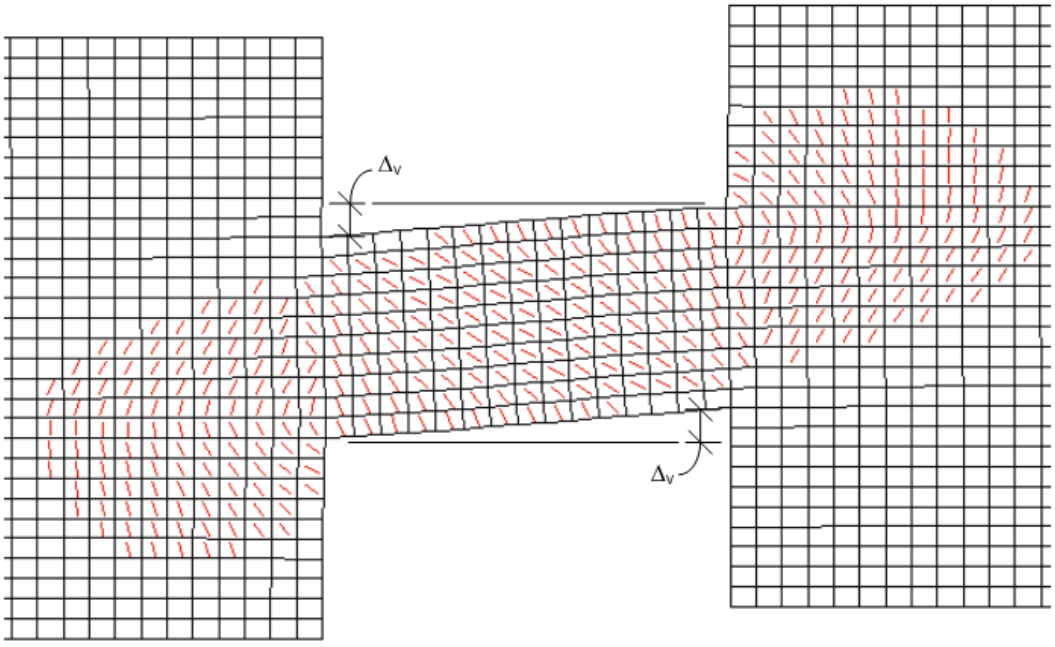

Figure 4.3: Shear distortion and cracking patterns in the single link beam under load case #4 and load step 0.4, V_u = 3046 KN.

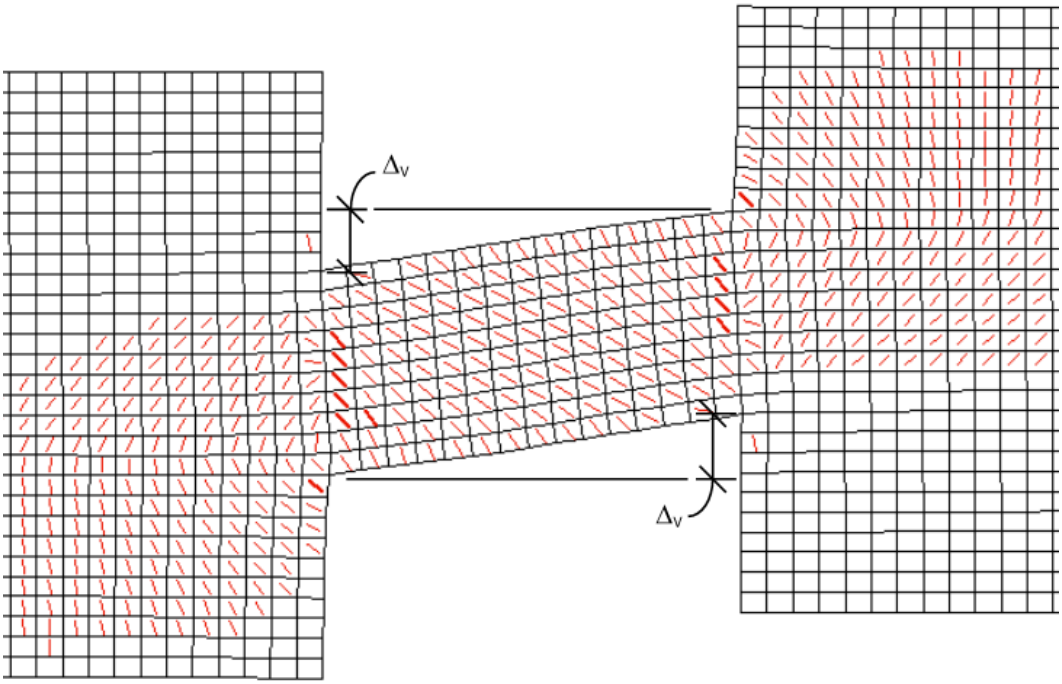

Figure 4.4: Shear distortion and cracking patterns in the single link beam under load case #4 and at the ultimate capacity (load step 0.8), V_u = 4593 KN.

In order to more accurately assess the response and its stability, a more in depth investigation of individual element and sectional strains and stresses is shown in Figure 4.5 to Figure 4.16. Figures 4.5 and 4.6 show a contour elevation of the diagonal compression field at load steps 0.4 and 0.8, respectively. The contours show the average concrete compressive stress per element at the load step as a function of the maximum concrete stress capacity, $f'_{c,\ max}$, of the link beam. These stress ratios include nonlinear effects, namely compression softening, which means that the value of $f'_{c,max}$ is not constant within the link beam. Individual element investigations in Figures 4.11 to 4.16 will clearly indicate the variations in $f'_{c,\ max}$. In Figure 4.5, no elements experienced concrete crushing. The largest stresses, approximately 75% of $f'_{c,\ max}$, were at the

compression corners as expected. Along the compression field, the stresses were between 40% and 60% of the concrete capacity. The contours also indicate that there is relatively considerable concrete compression at the tension corner elemtns of the link beam. It will be shown in the upcoming figures that this is due to extreme compression softening in those areas. This is expected since the average principal tensile strains from the main longitudinal reinforcement are very significant primarily because of the linear elastic perfectly plastic behavior of the steel. The relatively long yield plateau allows for significantly large strain capacities.

Figure 4.6 shows the limit state on the single link beam's capacity to be diagonal compression failure, with concrete crushing at the compression corners. However, in order to determine the principal cause of failure and limiting the capacity, the yielding in the steel reinforcing is investigated in Figures 4.7 to 4.9.

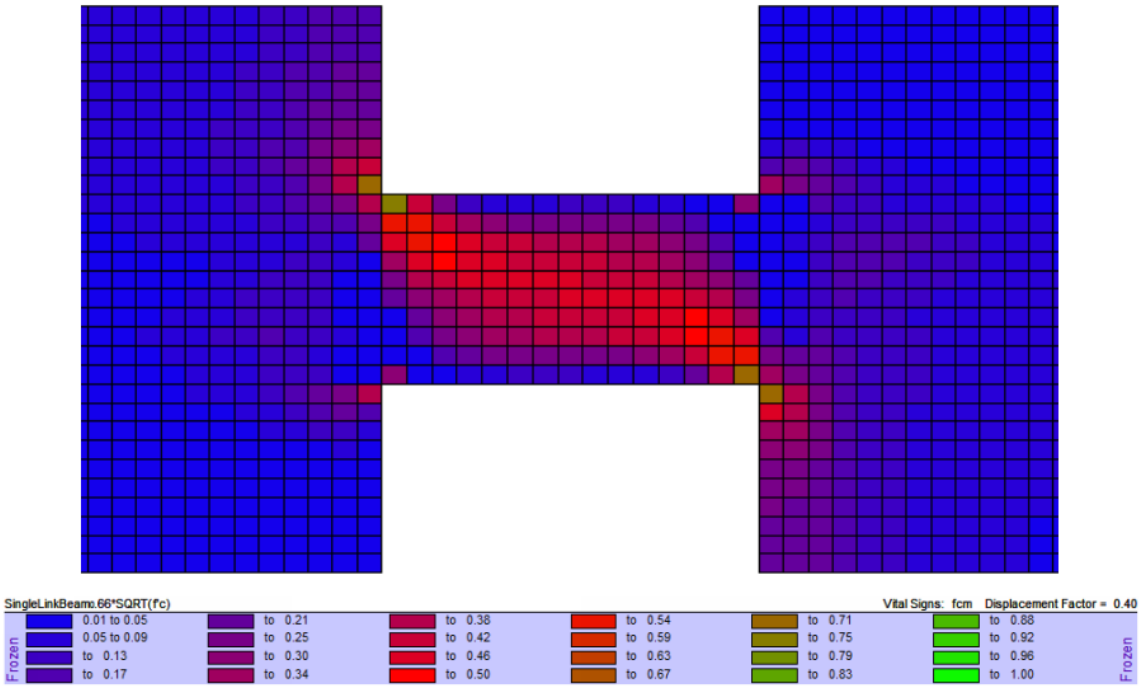

Figure 4.5: Diagonal compression field in the single link beam under load case #4 and load step 0.4, V_u = 3046 KN.

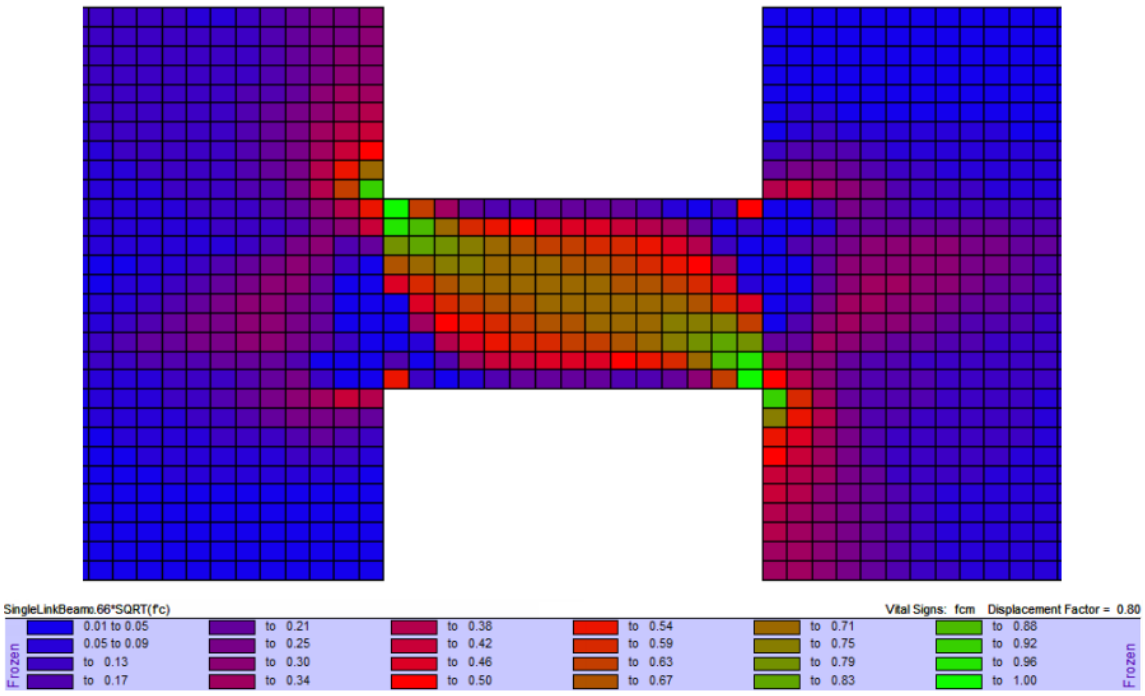

Figure 4.6: Diagonal compression field in the single link beam under load case #4 and at the ultimate capacity (load step 0.8), V_u = 4593 KN.

Figure 4.7 shows the flexural steel reinforcing average yield strain per element as a function of the yield strain capacity, which is ε_y = 0.2% for the linearly elastic perfectly plastic steel used in this case study. It appears that the strain in the tension corners of the link beam are already within the yield plateau of the steel stress-strain curve. The middle elements that are reinforced with less steel (skin reinforcement) appear to have the highest amount of strain at this load step, which is logical. The compressive strain in the steel at the compression corners appears to not have yielded yet. Figure 4.8 shows the same information but at the ultimate capacity at load step 0.8. It shows a very significant increase in the tensile strains

in the aforementioned locations, and no considerable increase in the compressive strains, which matches the crack patterns shown in Figure 4.4. This informs where the greatest compression softening effects occur. As discussed in the paragraph under Table 4.3, the strains from the stirrups yielding induces rather large strains on the concrete, increases the principal tensile stresses in the concrete elements at the extremes of the stirrups, and softens the concrete as a result. Since the highest principal compressive stresses are oriented at approximately 45 degrees near the supports under typical beam action, it is expected for the concrete to crush at those locations once the concrete compressive stress capacity is softened to a small enough value. Further, the diagonal compression field in Figures 4.5 and 4.6 clearly indicates orientation of the principal compressive and tensile stresses.

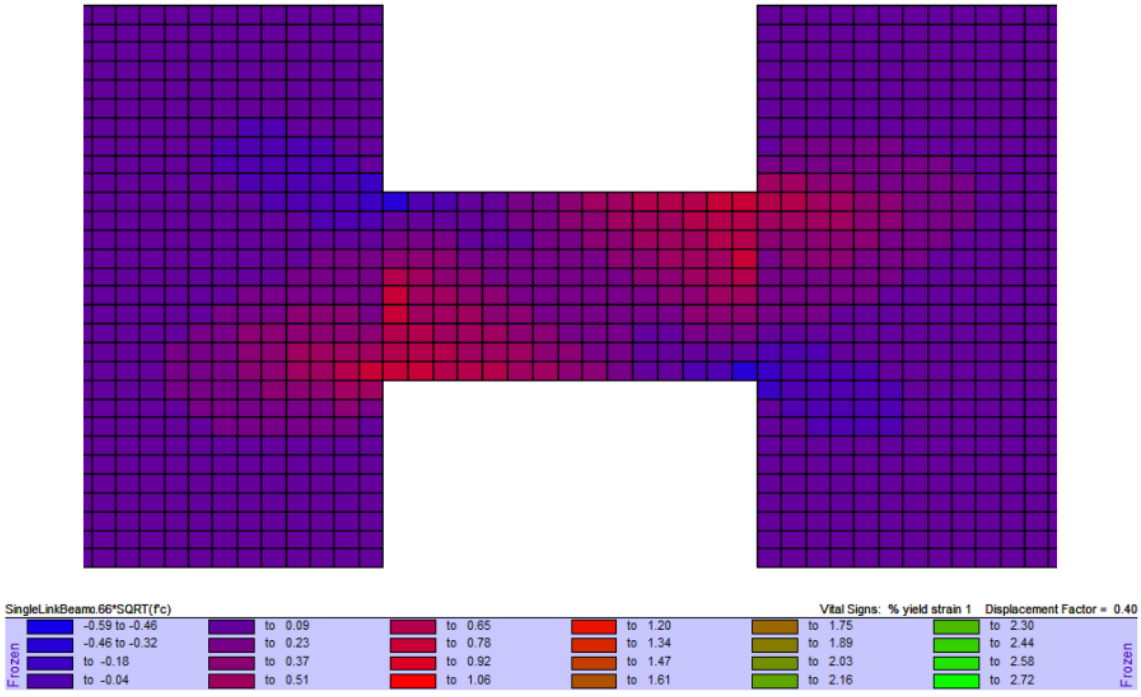

Figure 4.7: Longitudinal steel reinforcing yield strain ratio in the single link beam under load case #4 and load step 0.4, V_u = 3046 KN.

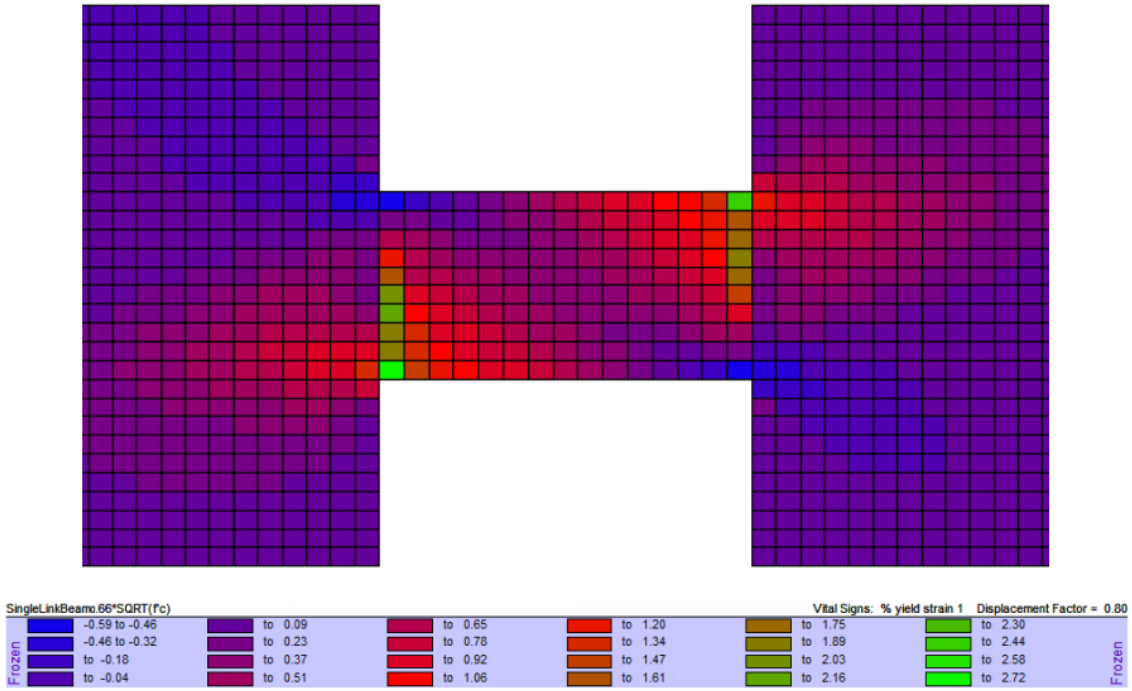

Figure 4.8: Longitudinal steel reinforcing yield strain ratio in the single link beam under load case #4 and at the ultimate capacity (load step 0.8), V_u = 4593 KN.

Figure 4.9 shows the transverse steel reinforcing yield strain as a function of the yield strain capacity. It appears that the strain in the elements within the middle of the link beam are still within the linear elastic range on the steel stress strain curve. This is expected since the stirrups in this portion of a typically reinforced beam would be resisting the inclined crack stresses of the diagonal compression field. Figure 4.10 shows the same information but at the ultimate capacity at load step 0.8. With the exception of the high strain in the elements just outside the link beam boundaries, the figure shows that the steel within the middle of the link beam has just entered the yield plateau of the steel stress-strain curve. This backs up the aforementioned discussions about the reasons for diagonal

compression failure for load case #4. It also informs about the reasons for the reduction in capacity in the last three load cases of Table 4.3. The more flexural demand, the sooner the steel yields. Also, the higher the shear demand, the larger the diagonal compressive strut that has to be transferred to the support by stirrups. When these parameters are amplified, the onset of compression softening followed by diagonal compressive crushing occurs much more quickly. This effect can be mitigated by adding larger amounts of flexural steel, in order to delay the yielding of the flexural steel, and the softening of the concrete as a result.

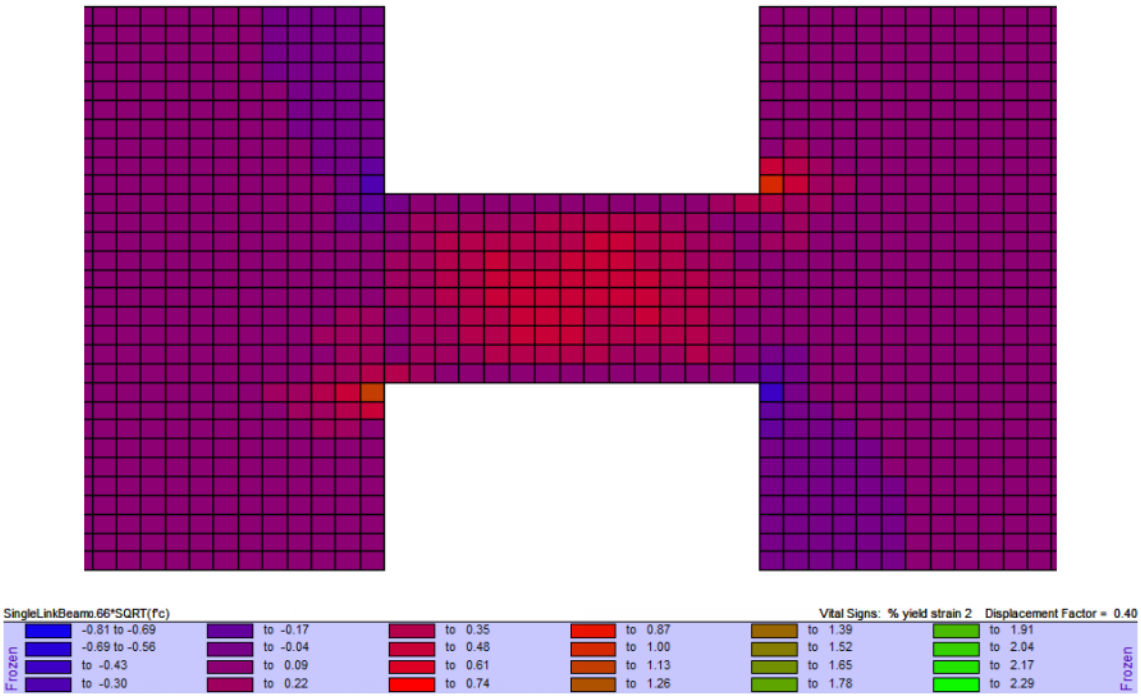

Figure 4.9: Transverse steel reinforcing strain as a function of yield strain at strain at load factor 0.4, V_u = 3046 KN.

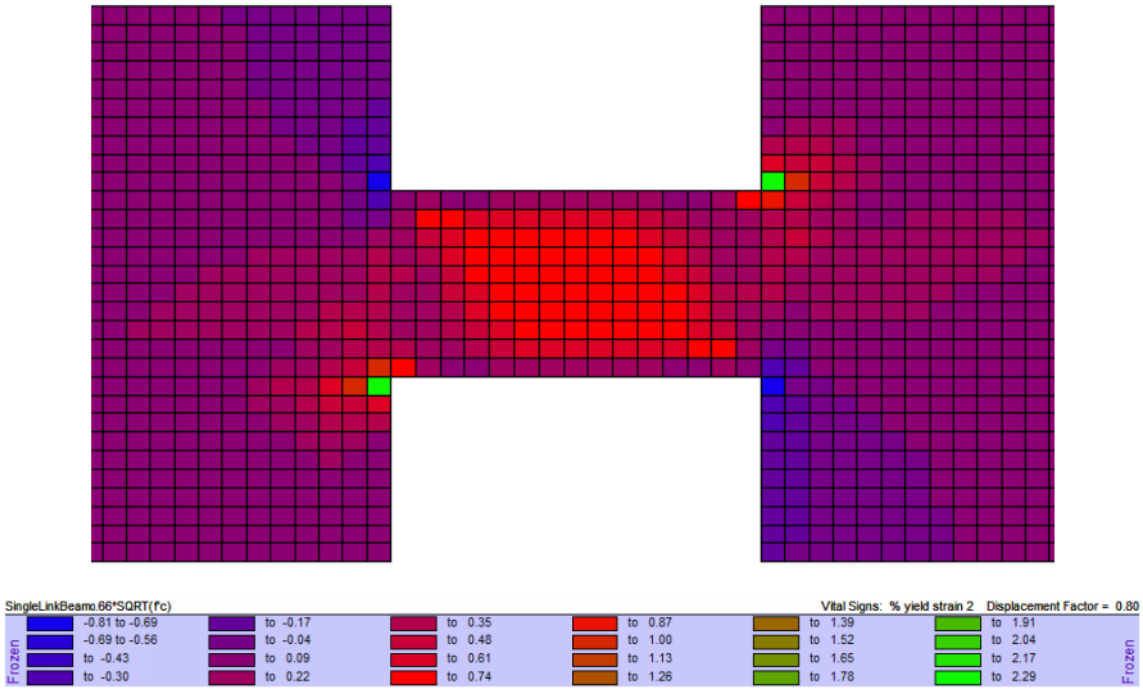

Figure 4.10: Transverse steel reinforcing strain as a function of yield strain at the ultimate capacity (load factor 0.8), V_u = 4593 KN.

Figures 4.11 to 4.13 show the graphical interface of the VecTor2 post-processor, Augustus, for making section cuts at desired locations within the model. This tool is the source for the values shown in Table 4.3. The sections were all taken at the ultimate capacity for load case #4 at load step 0.8. The cut is the dark red marked area on the link beam model in the figures. The ε_s plot shows the total longitudinal strain in the section at the cut, which show a logical transition from compression into tension. The vertical axis indicates the length from the bottom of the bottom link beam element to the top of the top link beam element. Similarly, the total longitudinal stress, f_x, the total shear stress, and steel yield stress are plotted against the vertical elements across the section. The figures also show approximate curvature values and average shear strain. A more

accurate investigation on inelastic flexural and shear stiffness values will be discussed later in this chapter.

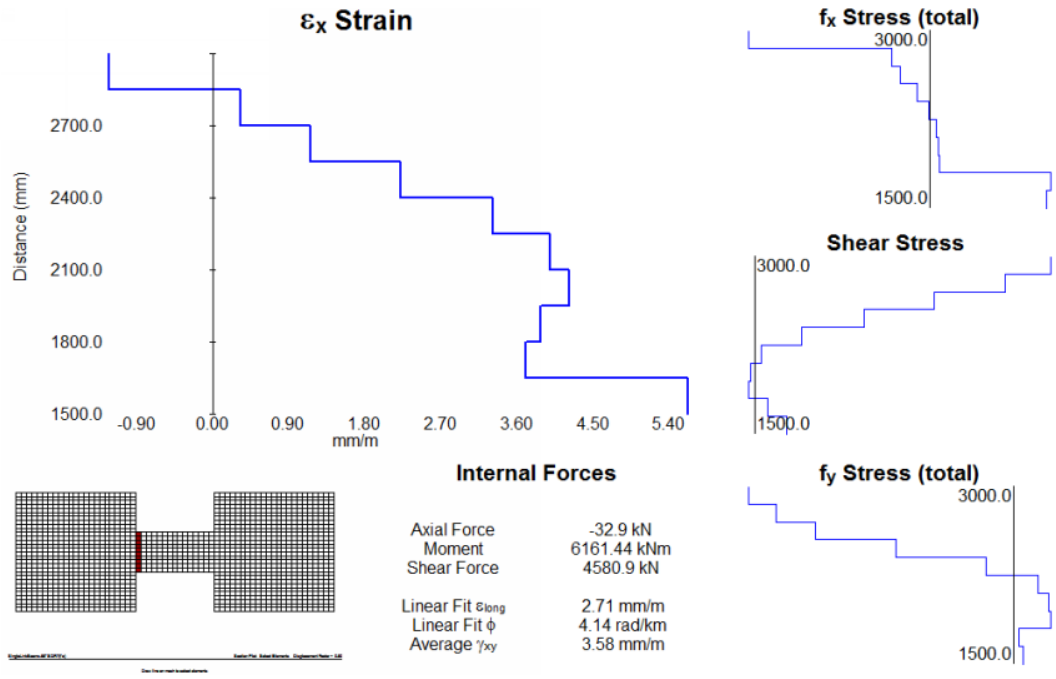

Figure 4.11: Snapshot from Augustus showing a section cut at the left face of the link beam at the ultimate capacity (load factor 0.8), V_u = 4593 KN.

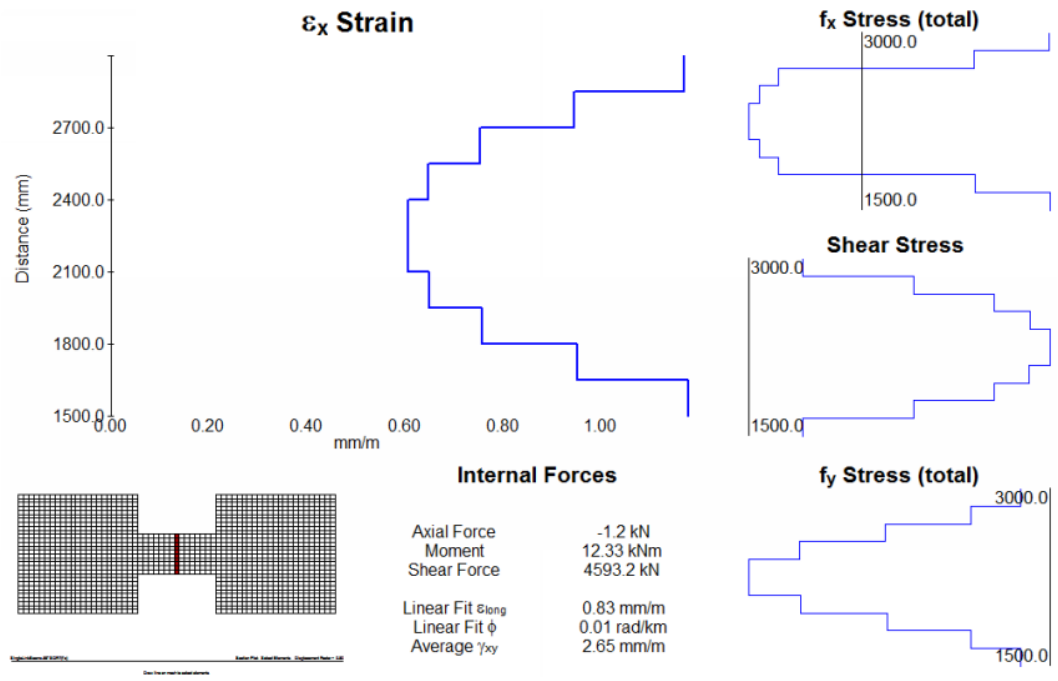

Figure 4.12: Snapshot from Augustus showing a section cut at mid-span of the link beam at the ultimate capacity (load factor 0.8), V_u = 4593 KN.

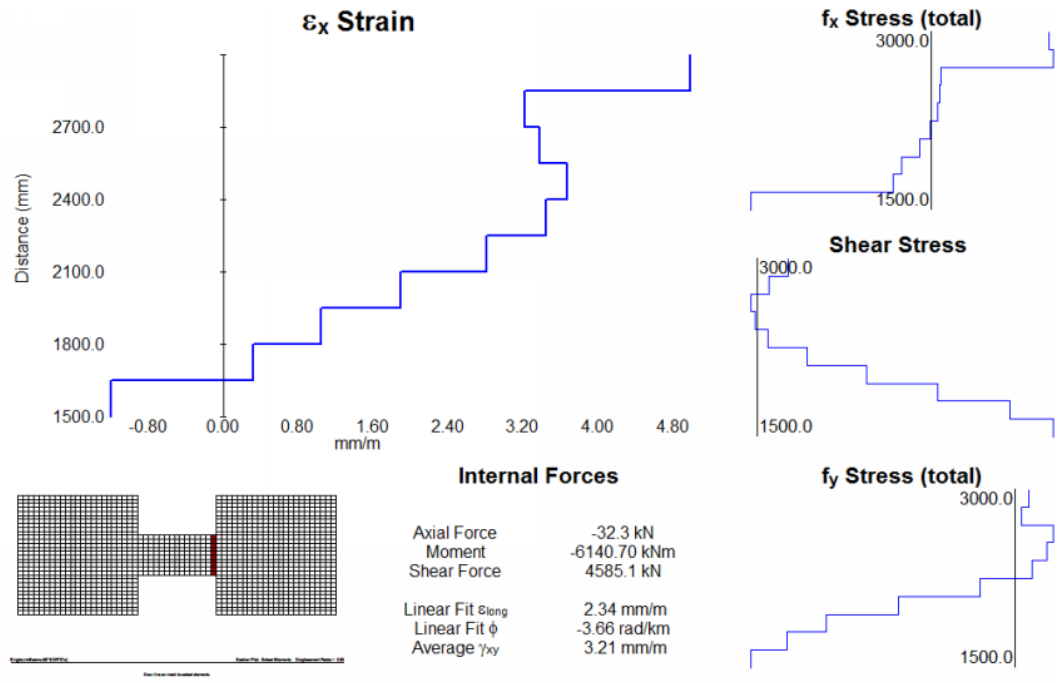

Figure 4.13: Snapshot from Augustus showing a section cut at the right face of the link beam at the ultimate capacity (load factor 0.8), V_u = 4593 KN.

Figures 4.14 to 4.16 show element specific details of stress and strain. It plots the parameter of choice, ε_s in the figures which is the average longitudinal strain in the element, against the vertical elements. It also plots the very informative Mohr's circle of average stress and strain for the element. The subscripts 1 and 2 refer to principal tension and principal compression, respectively.

The element selected in Figure 4.14 is the element experiencing the largest amount of diagonal compressive stress as evident in the previously discussed figures. It is apparent from Mohr's circle of stress that the concrete in that element is actually "hardened" rather than softened as evident by f_{2max}, because it shows confinement due to the compressive direction of f_1, which also explains why it is uncracked. This can be attributed to the boundary conditions from the wall piers imposing vertical restraints on the element. Although the degree of confinement is very small, it did delay the crushing of the concrete in that element by almost 2 MPa (approximately 6% of f'_c).

Figure 4.15 shows the element at middle of the mid-span section of the link beam. It is evident that the strains and stresses shown are compatible with the previously discussed figures. Although this element is experiencing less principal compression, it is experiencing significant compression softening as evident by f_{2max}. This is due to the relatively large tensile strain value, ε_1. Inputting the values corresponding to the MCFT compression softening equation (E 2-1):

$$f_{c2} = \frac{f'_c\left[\left(2(\varepsilon_{c2}/\varepsilon'_c)\right) - (\varepsilon_{c2}/\varepsilon'_c)^2\right]}{0.8 - 0.34(\varepsilon_{c1}/\varepsilon'_c)}$$

$$f_{c2} = \frac{35\ \text{MPa}\left[\left(2\left(\frac{-0.51}{-2.06}\right)\right) - \left(\frac{-0.51}{-2.06}\right)^2\right]}{0.8 - 0.34\left(\frac{2.59}{-2.06}\right)}$$

$f_{c2} =$ **12.4 MPa**

The value is off from the f_2 value shown in Figure 4.15 by approximately 15% because the principal tensile strain ε_1 includes the average smeared reinforcing strain as well, which would translate to less principal compressive stress than from the concrete principal tensile strains alone.

Further, linear elastic analysis of reinforced concrete assumes that the concrete has negligible stiffness post-cracking. However, as discussed in chapter 2, the tension stiffening and tension softening effects can predict the post-cracking stiffness of reinforced concrete. A brief comparison is shown in the following sample calculations:

Recalling that the relationship between flexural stiffness and curvature is:

$$\emptyset = \frac{M}{EI} \qquad \text{(E 4-1)}$$

Recalling that curvature can be defined as the strain differential of a section over the height of the section:

$$\frac{\varepsilon_{top}-\varepsilon_{bot}}{h} = \frac{M}{EI} \quad \text{(E 4-2)}$$

$$EI_{inelastic} = \frac{Mh}{\varepsilon_{top}-\varepsilon_{bot}} \quad \text{(E 4-3)}$$

Therefore, the curvature of the single link beam for load case #4 at its ultimate capacity can be determined from Figure 4.14 and 4.16.

$$EI_{inelastic} = \frac{6161\ \text{kNm} \times 1.5\text{m}}{-1.39-(+5.22)} = \mathbf{1398\ MN\text{-}m^2}$$

Comparing the $EI_{inelastic}$ value above to the $EI_{elastic}$ value shows a direct comparison of inelastic versus elastic flexural stiffness:

$$I_{elastic} = \frac{bh^3}{12} = \frac{0.6\ m \times 1.5\ m^3}{12} = 0.16875\ m^4$$

$E_{elastic}$ for normal weight concrete per ACI 318M-02 is:

$$E_c = 4{,}700\sqrt{f'_c} = 4{,}700\sqrt{35\ MPa} = 27806\ MPa$$

Therefore,

$EI_{elastic} = \mathbf{4692\ MN\text{-}m^2}$

The ratio of $EI_{inelastic}$ to $EI_{elastic}$ is approximately 30%, indicating significant post-cracking flexural stiffness in the member. In order to compare the shear stiffness, $GA_{inelastic}$ to $GA_{elastic}$, the following relationships can be used:

Recalling that the shear modulus of a beam section can be defined as:

$$G = \frac{E}{2(1+\upsilon)} \quad \text{(E 4-4)}$$

Where, υ is Poisson's ratio, which is taken as 0.15 in the default VecTor2 parameters.

Therefore, $G_{elastic}$ can be predicted by:

$$G = \frac{E_c}{2(1+\upsilon)} = \frac{27806 \text{ MPa}}{2(1+0.15)} = 12090 \text{ MPa}$$

Thus, the inelastic shear flexural stiffness, $GA_{elastic}$, is predicted as:

$GA_{elastic}$ = 12090 MPa (0.6 m)(1.5 m) = **10881 MN**

From the shear force, $V_{VecTor2}$, and average sectional shear strain, γ_{xy}, in Figure 4.12 (Figures 4.11 and 4.13 would give similar results since shear is constant over the length of the link beam), the inelastic shear stiffness, $GA_{inelastic}$, can be found by Hook's law:

$GA_{inelastic} = V_{VecTor2} / \gamma_{xy}$ = 4593 KN / 2.65 (mm/m) = **1733 MN**

The ratio of $GA_{inelastic}$ to $GA_{elastic}$ is approximately 16%, which from fundamental solid mechanics principals, aligns with the typical expectation that a material's shear rigidity is between 0.5 to 0.6 times the flexural rigidity.

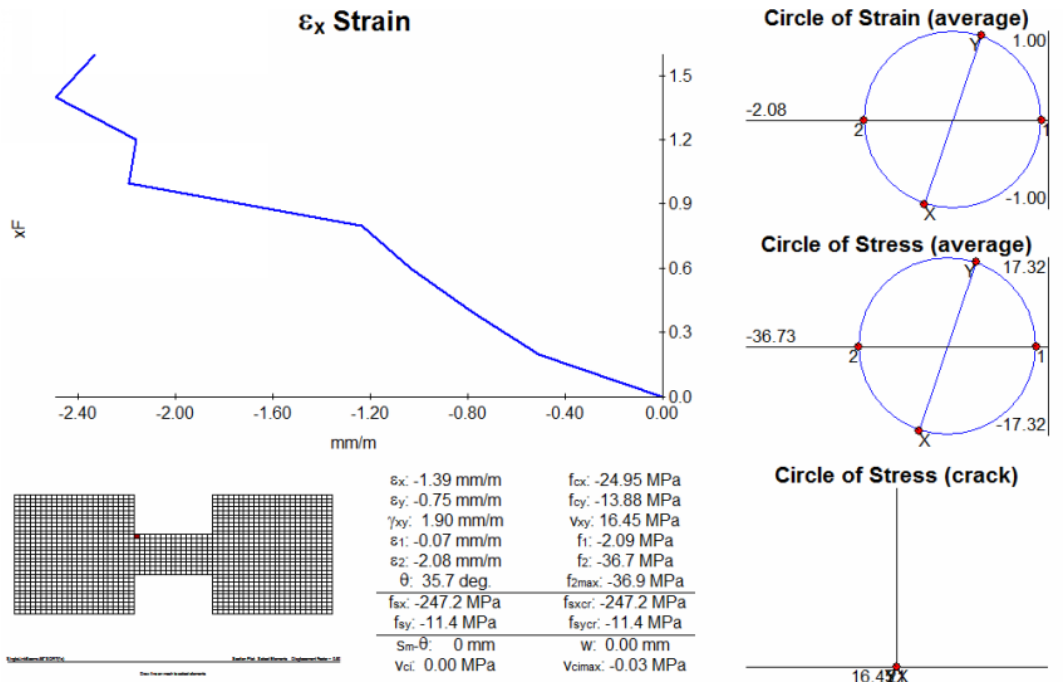

Figure 4.14: Stresses and strains from Augustus at the top left element of the link beam at the ultimate capacity (load factor 0.8), V_u = 4593 KN.

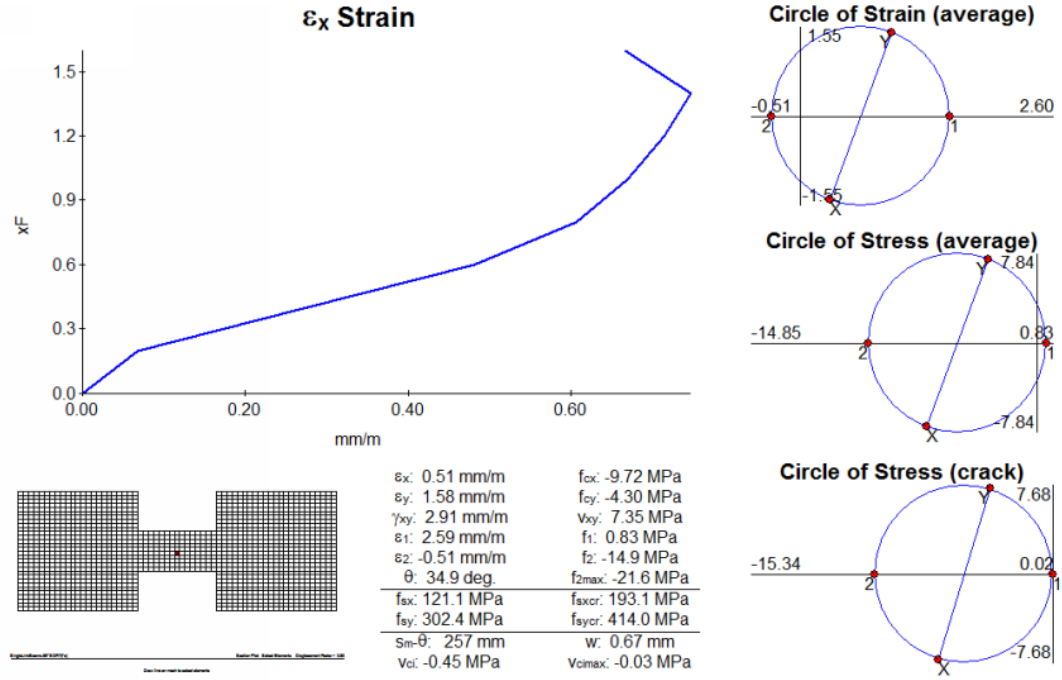

Figure 4.15: Stresses and strains from Augustus at the middle element of the link beam at the ultimate capacity (load factor 0.8), V_u = 4593 KN.

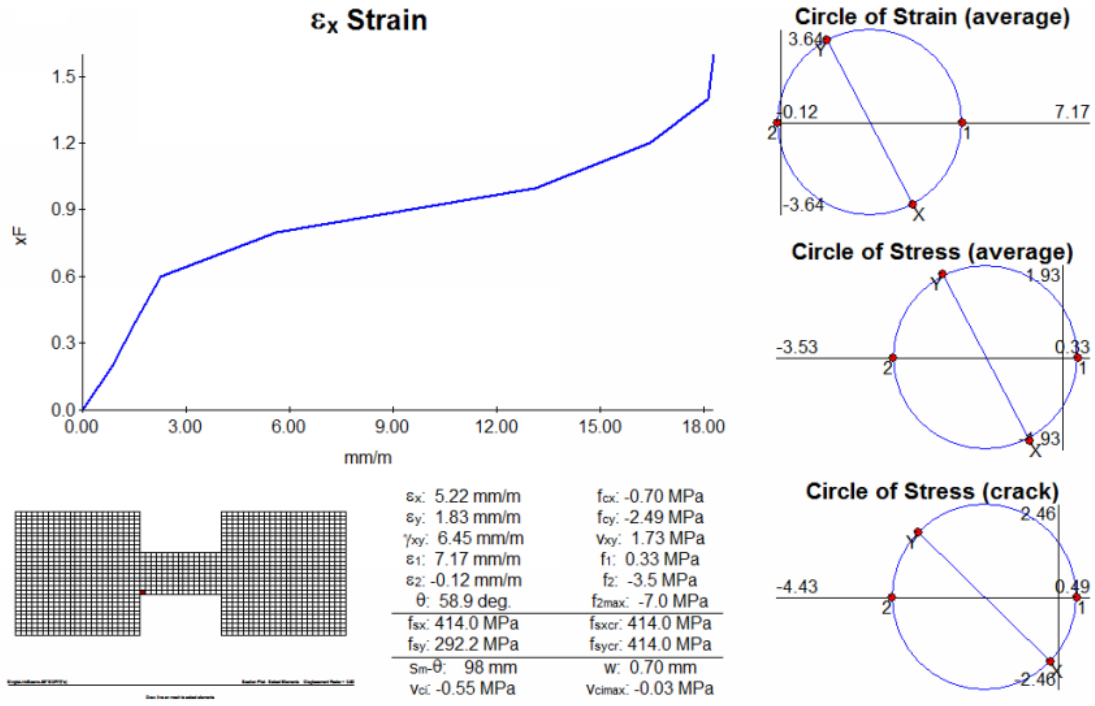

Figure 4.16: Stresses and strains from Augustus at the bottom left element of the link beam at the ultimate capacity (load factor 0.8), V_u = 4593 KN.

Chapter 5: Iterative Design and Analysis for Case Study

As evident in the discussion of chapter 4, the link beams for the case study of this thesis experience very significant nonlinear behavior. This chapter will demonstrate an example of designing the same structure in Chapter 3, as seen in Figure 5.1, but for nonlinear analysis using the default parameters of VecTor2. In order to optimize the design, trial and error analyses have to be performed, resulting in a few nonlinear iterations, until a final converged solution is selected. The solution converged after only three nonlinear trials for this case study. Further, in order to be able to directly compare the advantages of nonlinear analysis versus linear elastic analysis, the first trial for this chapter will be that presented in chapter 3. Thus, a linear elastic analysis on the structure will be

performed for plain concrete, and the loading criteria shown in Figure 5.1, which is the same loading criteria used in chapter 3, will be used in order to obtain demands to reinforce for. The selected reinforcement will be based on the nominal capacities for the load cases presented in Chapter 4. Tables 4.1 through 4.3 are summarized and combined in this chapter in Table 5.1. The nominal moment capacity reinforcing requirements are used as the benchmark criteria to inform the amount of shear and flexure reinforcement for every trial. This is because the capacities shown in Chapter 4 predict much more realistic and informative responses for the link beams, compared to the empirical code provisions in the ACI building code requirements.

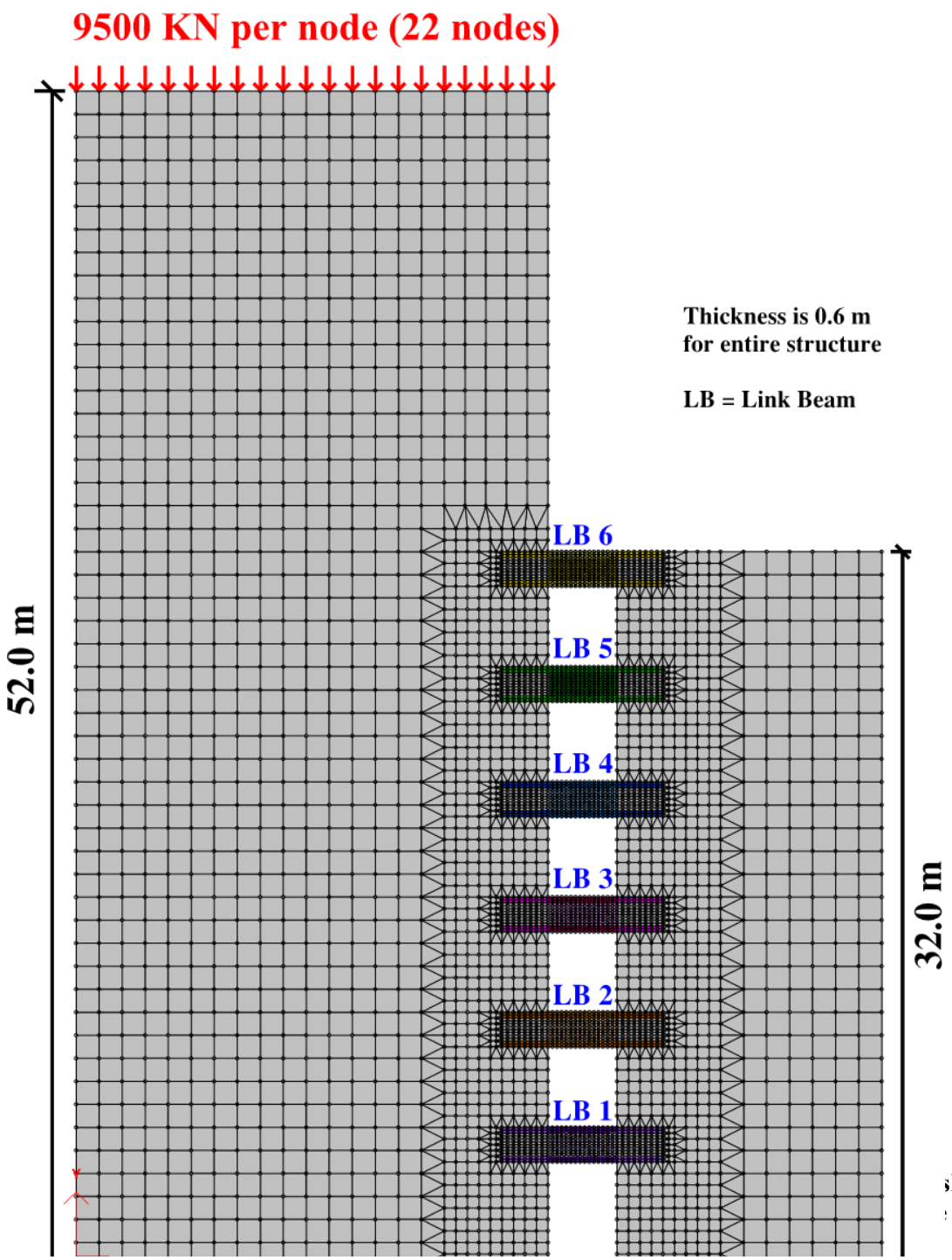
9500 KN per node (22 nodes)
Thickness is 0.6 m
for entire structure
LB = Link Beam
LB 6
LB 5
LB 4
LB 3
LB 2
LB 1
52.0 m
32.0 m
showing overall
six individually

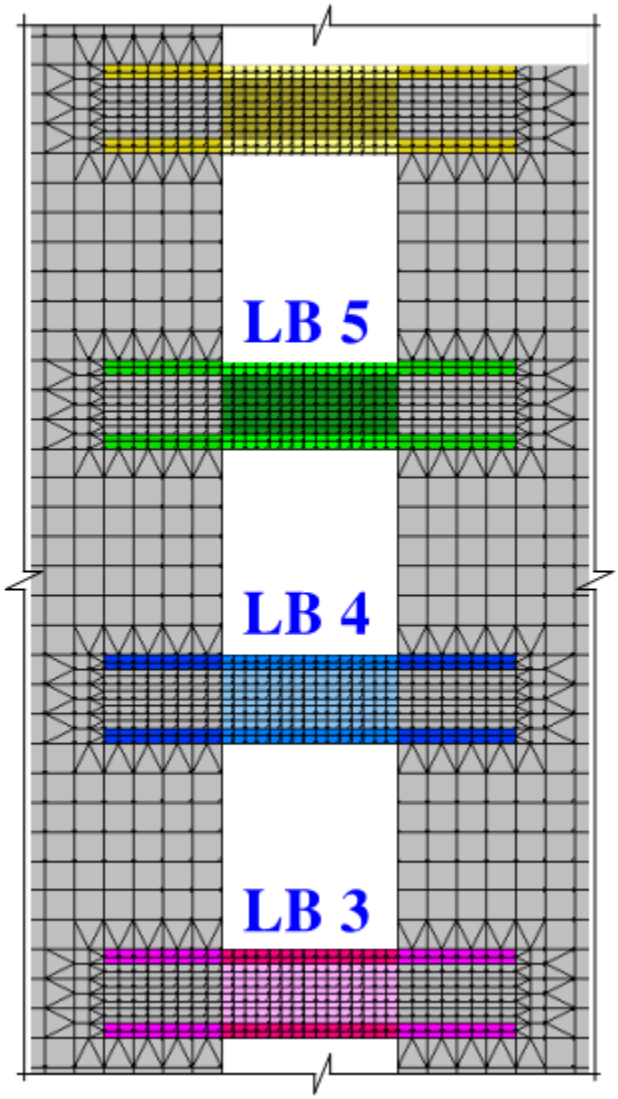

Figure 5.2: Close up on Figure 5.1, showing unique reinforcing patterns for each link beam. Specific reinforcement amounts are presented in Table 5.1.

The reinforcement patterns in Figure 5.2 are for flexural and shear reinforcing (all smeared). The remainder of the structure (the gray elements) was kept at a constant ratio of 1% for both directions. This ratio is considered negligible in terms of strength, especially as the elements get larger. However, the reasoning for adding them is to maintain continuity in the structure, limit

excessive cracking, and simulate an actual reinforced concrete structure, and because in reality a structure will have at least temperature and shrinkage reinforcement in most sections. The top and bottom bands of two-element layers are the primary flexural steel reinforcing. The bands extend in order to ensure adequate development of anchorage and to guard against abrupt stress differentials in an adjacent element as soon as the reinforcing is terminated at an element.

Figure 5.3 and 5.4 show a plot of the final results of the linear elastic trial plus the three nonlinear trials, which are tabulated in Tables 5.2 to 5.5. Although the plots should be discrete since there is no material from link beam to link beam, connecting the discrete points provides a more informative graphic to the discussion. It clearly indicates how linear elastic analysis overestimates the demands for the higher link beams, while underestimating the demands for the lower link beams. This is due to the predicted linear elastic response, which is based on a systematic stress redistribution due to the amount of shear distortion. In other words, since the top link beam is expected to distort the most, it will take the majority of the demand, fail, and distribute it to the lower link beam. While this approach is indeed correct, it ignores all of the nonlinear effects, especially those highlighted in chapter 4.

Under nonlinear analysis, the stress redistribution is very different and is not a uniform redistribution. This is evident in that the linear elastic plots in Figures 5.3 and 5.4 show a relatively constant slope compared to the varying

slopes of the nonlinear trials. It is also evident that the third trial converges very reasonably with the second trial, removing the need for a fourth trial. This makes for a very efficient iterative design procedure for nonlinear analysis on a reinforced concrete structure that behaves similar to this case study structure.

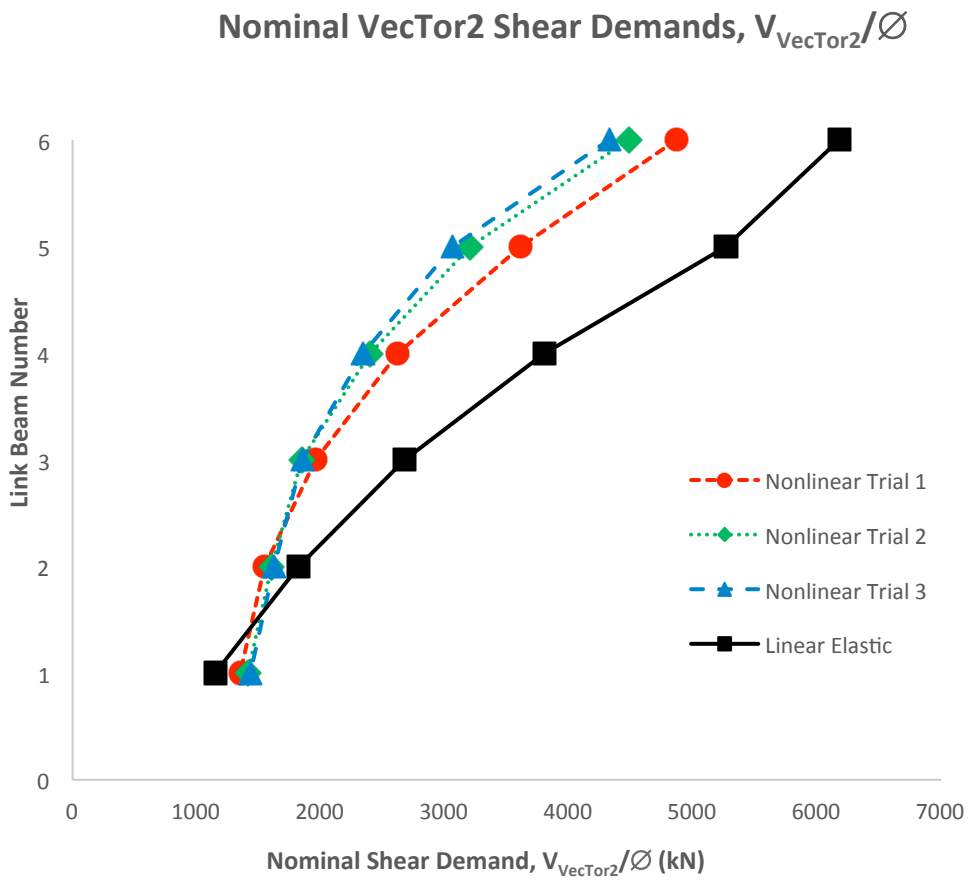

Figure 5.3: Nominal shear demands from VecTor2, comparing the linear elastic design with the nonlinear trials for the load case in Figure 5.1.

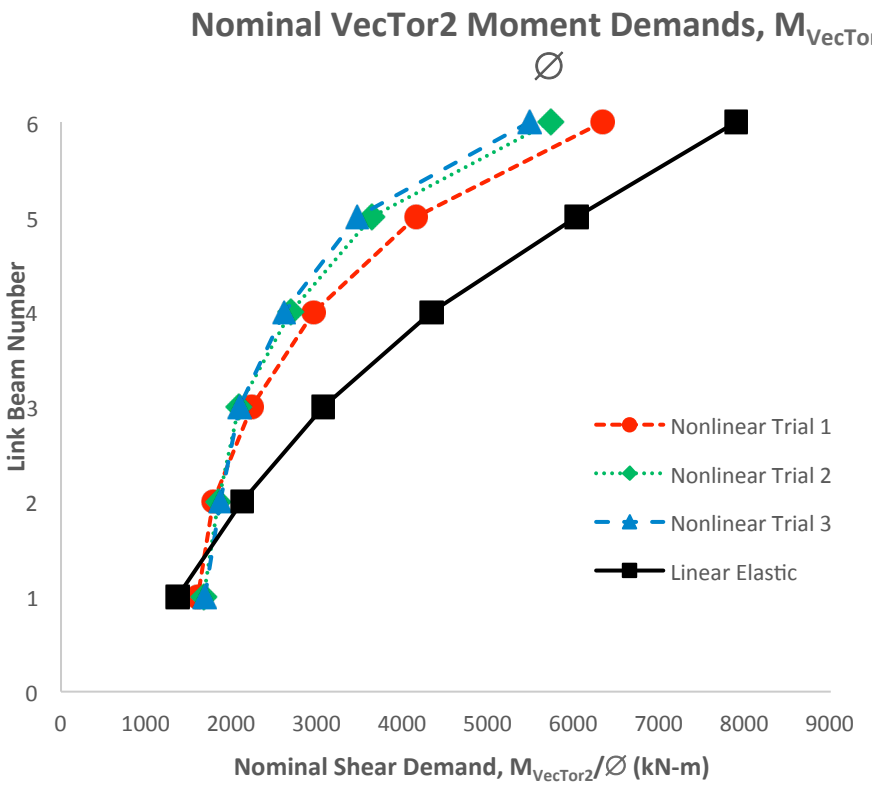

Figure 5.4: Nominal shear demands from VecTor2, comparing the linear elastic design with the nonlinear trials for the load case in Figure 5.1.

Table 5.1 on the next page is a summary of the tables in chapter 4. It shows the benchmark criteria that is used in order to clearly compare the progression of each trial. The reinforcement amounts for the trials were linearly interpolated based on the benchmark criteria. An outlined process shown below helps explain the interpolation process, taking link beam 4 in Table 5.3 as an example. Link beam 4 for nonlinear trial 1 must be reinforced for the factored demands from the linear elastic analysis. To simplify the linear interpolation process, everything was done in terms of nominal demands and capacities. This was accounted for when the reinforcement amounts were determined. To

determine the nominal shear demand required to reinforce link beam 4, a new value for the ration V_{LE} must be determined. This is due to the evidences presented in chapter 4 that shows the link beams have more capacity that what they were reinforced for. Therefore, link beam 4 in Table 5.3 will not require reinforcement for the full V_{LE}. The interpolation process is as follows:

1. Determine where V_{LE} lies within the range of V_B from Table 5.1.
2. Determine which $v_u/\phi\sqrt{f'_c}$ corresponds to the lower value of the correct V_B range identified in step 1.
3. Recognize that $v_u/\phi\sqrt{f'_c}$ values are in $0.167/\emptyset_v$ increments, and interpolate as such.

The following is a sample calculation for link beam 4 in Table 5.3:

1. $V_{LE} = 0.738$ (from Table 5.2). It lies within the range of $V_B = 0.712$ and $V_B = 0.892$ (from Table 5.1). This corresponds to load case 4 from Table 5.1.
2. The lower end of the V_B range corresponds to load case 3 in Table 5.1, with $v_u/\phi\sqrt{f'_c} = 0.67$.
3. Determine the "Shear $[v_u/\phi\sqrt{f'_c}]_{req'd}$ per V_B" value in Table 5.3 by:

$$0.67 + \left\{\left[\frac{(0.738 - 0.712)}{(0.892 - 0.712)}\right]\left(\frac{0.167}{0.75}\right)\right\} = 0.69$$

Table 5.1: Benchmark reinforcing criteria for the full model nonlinear trials.

SINGLE LINK BEAM MODEL					
Design Forces and Reinforcing per and Tables 4.1 & 4.2					
Case #	$v_u/\sqrt{f'_c}$	V_u/ϕ (KN)	ρ_v (%)	M_u/ϕ (KN-m)	ρ_l (%)
1	0.167	1144	**0.09**	1716	**0.357**
2	0.33	2262	**0.39**	3393	**0.637**
3	0.50	3393	**0.70**	5090	**0.955**
4	0.67	4524	**1.02**	6786	**1.274**
5	0.83	5655	**1.33**	8483	**1.592**
6	1.00	6786	**1.65**	10180	**1.911**
7	1.17	7918	**1.96**	11876	**2.229**
Benchmark Reinforcing Criteria per VecTor2 Capacities					
Case #	$v_u/\phi\sqrt{f'c}$	$V_{VecTor2}$ (KN)	V_B: $v_{VecTor2}/\sqrt{f'_c}$	$M_{VecTor2}$ (KN-m)	M_B: $v_{VecTor2}/\sqrt{f'_c}$
1	**0.22**	1636	**0.318**	2045	**0.318**
2	**0.44**	2711	**0.527**	3533	**0.549**
3	**0.67**	3666	**0.712**	4868	**0.757**
4	**0.89**	4593	**0.892**	6161	**0.958**
5	**1.11**	5273	**1.024**	7195	**1.118**
6	**1.33**	5726	**1.112**	7890	**1.226**
7	**1.56**	6093	**1.184**	8475	**1.317**

Table 5.2: Nominal demands for linear elastic analysis on the full model.

FULL MODEL - LINEAR ELASTIC (LE)				
Plain Concrete, Factored Applied Load = 209,000 KN				
Link Beam	VecTor2 Nominal Demands			
	$V_{VecTor2}/\phi$ (KN)	V_{LE}: $v_{VecTor2}/\sqrt{f'_c}$	$M_{VecTor2}/\phi$ (KN-m)	M_{LE}: $v_{VecTor2}/\sqrt{f'_c}$
6	6181	**1.201**	7895	**1.227**
5	5266	**1.023**	6029	**0.937**
4	3799	**0.738**	4331	**0.673**
3	2677	**0.520**	3065	**0.476**
2	1821	**0.354**	2117	**0.329**
1	1148	**0.223**	1363	**0.212**

Table 5.3: Reinforcing and analysis for first nonlinear run on the full model.

FULL MODEL - NONLINEAR TRIAL 1 (NL1)						
Link Beam	Reinforcing per Benchmark for LE Nominal Demands					
	Shear $[v_u/\phi\sqrt{(f'_c)}]_{req'd}$ per V_B	Design $V_u/\phi_{,NL1}$ (KN)	$\rho_{v,\ req'd}$ (%)	Flexure $[v_u/\phi\sqrt{(f'_c)}]_{req'd}$ per V_B	Design $M_u/\phi_{,NL1}$ (KN-m)	$\rho_{l,\ req'd}$ (%)
6	**1.201**	6182	**1.478**	**1.320**	8495	**1.914**
5	**1.099**	5656	**1.332**	**0.859**	5525	**1.245**
4	**0.691**	3557	**0.749**	**0.572**	3683	**0.830**
3	**0.437**	2251	**0.387**	**0.375**	2410	**0.543**
2	**0.260**	1340	**0.134**	**0.233**	1498	**0.357**
1	**0.222**	1144	**0.089**	**0.222**	1430	**0.357**

Link Beam	VecTor2 Nominal Demands for NL1			
	$V_{VecTor2}$ (KN)	V_{NL1}: $v_{VecTor2}/\sqrt{(f'_c)}$	$M_{VecTor2}$ (KN-m)	M_{NL1}: $v_{VecTor2}/\sqrt{(f'_c)}$
6	4868	**0.946**	6334	**0.985**
5	3612	**0.702**	4151	**0.645**
4	2619	**0.509**	2958	**0.460**
3	1960	**0.381**	2227	**0.346**
2	1546	**0.300**	1780	**0.277**
1	1351	**0.263**	1598	**0.248**

Table 5.4: Reinforcing and analysis for second nonlinear run on the full model.

FULL MODEL - NONLINEAR TRIAL 2 (NL2)						
Link Beam	Reinforcing per Benchmark for NL1 Nominal Demands					
	Shear $[v_u/\emptyset\sqrt{(f'_c)}]_{req'd}$ per V_B	Design $V_u/\emptyset_{,NL1}$ (KN)	$\rho_{v,\ req'd}$ (%)	Flexure $[v_u/\emptyset\sqrt{(f'_c)}]_{req'd}$ per V_B	Design $M_u/\emptyset_{,NL1}$ (KN-m)	$\rho_{l,\ req'd}$ (%)
6	**0.969**	4987	**1.146**	**0.916**	5895	**1.328**
5	**0.649**	3342	**0.690**	**0.542**	3490	**0.786**
4	**0.426**	2190	**0.370**	**0.359**	2307	**0.520**
3	**0.289**	1489	**0.175**	**0.249**	1604	**0.361**
2	**0.222**	1144	**0.089**	**0.222**	1430	**0.357**
1	**0.222**	1144	**0.089**	**0.222**	1430	**0.357**

Link Beam	VecTor2 Nominal Demands for NL2			
	$V_{VecTor2}$ (KN)	V_{NL2}: $v_{VecTor2}/\sqrt{(f'_c)}$	$M_{VecTor2}$ (KN-m)	M_{NL2}: $v_{VecTor2}/\sqrt{(f'_c)}$
6	4483	**0.871**	5725	**0.890**
5	3203	**0.622**	3635	**0.565**
4	2398	**0.466**	2687	**0.418**
3	1846	**0.359**	2082	**0.324**
2	1603	**0.312**	1838	**0.286**
1	1414	**0.275**	1669	**0.259**

Table 5.5: Reinforcing and analysis for third nonlinear run on the full model.

FULL MODEL - NONLINEAR TRIAL 3 (NL3)						
Link Beam	Reinforcing per Benchmark for NL1 Nominal Demands					
	Shear $[v_u/\phi\sqrt{(f'_c)}]_{req'd}$ per V_B	Design $V_u/\phi_{,NL1}$ (KN)	$\rho_{v,\ req'd}$ (%)	Flexure $[v_u/\phi\sqrt{(f'_c)}]_{req'd}$ per V_B	Design $M_u/\phi_{,NL1}$ (KN-m)	$\rho_{l,\ req'd}$ (%)
6	**0.855**	4402	**0.984**	**0.807**	5189	**1.169**
5	**0.554**	2851	**0.553**	**0.457**	2937	**0.662**
4	**0.380**	1955	**0.305**	**0.318**	2046	**0.461**
3	**0.266**	1367	**0.141**	**0.228**	1466	**0.357**
2	**0.222**	1144	**0.089**	**0.222**	1430	**0.357**
1	**0.222**	1144	**0.089**	**0.222**	1430	**0.357**

Link Beam	VecTor2 Nominal Demands for NL2			
	$V_{VecTor2}$ (KN)	V_{NL3}: $v_{VecTor2}/\sqrt{(f'_c)}$	$M_{VecTor2}$ (KN-m)	M_{NL3}: $v_{VecTor2}/\sqrt{(f'_c)}$
6	4325	**0.840**	5479	**0.852**
5	3065	**0.595**	3462	**0.538**
4	2339	**0.454**	2612	**0.406**
3	1850	**0.359**	2086	**0.324**
2	1622	**0.315**	1858	**0.289**
1	1431	**0.278**	1686	**0.262**

It is evident at this point how much more effective is the design by the iterative nonlinear analyses than when the linear elastic analyses are used. For link beam 5, the shear demand by linear elastic analysis is approximately 72% more than what is required for nonlinear trial 3. Further, the moment demands by linear elastic analysis at link beam 5 were approximately 78% more than what is required for nonlinear trial 3. To add to the efficiency and optimization advantage of using the benchmark reinforcing criteria, link beam 3 in the linear elastic trial required almost 64% more shear reinforcement that what was required for the nonlinear trial 3 demands. However, link beam 1 demands for the linear elastic trial were underestimated; approximately 20% less than what was required for nonlinear trial 3.

Figures 5.4 and 5.5. show the shear distortion and crack patterns for the six link beams at the load case in Figure 5.1. The patterns for the top link beams clearly resemble very similar behavior to the single link beam response in chapter 4.

Further, Figures 5.6 through 5.11 compare the two extremes in terms of the response for nonlinear trial 3: link beam 6 and link beam 1. The diagonal compression field is evident and uniform, with the concrete well below its compressive stress capacity at the critical location in the top left and bottom right elements. The flexural steel appears to still be within the linear elastic range and not yielded, similarly with the transverse steel although it is much less stressed.

These performance-based parameters are very helpful if post-peak behavior is to be predicted.

For link beam 1, the stresses and strain ratios appear to be negligible. The top link beams had enough strength to share the load efficiently before link beam 1's contribution initiated. Figure 5.9 shows the onset of a uniform diagonal compression field. Figures 5.10 and 5.11 also resemble the onset of a response similar to link beam 6 and the single link beam model.

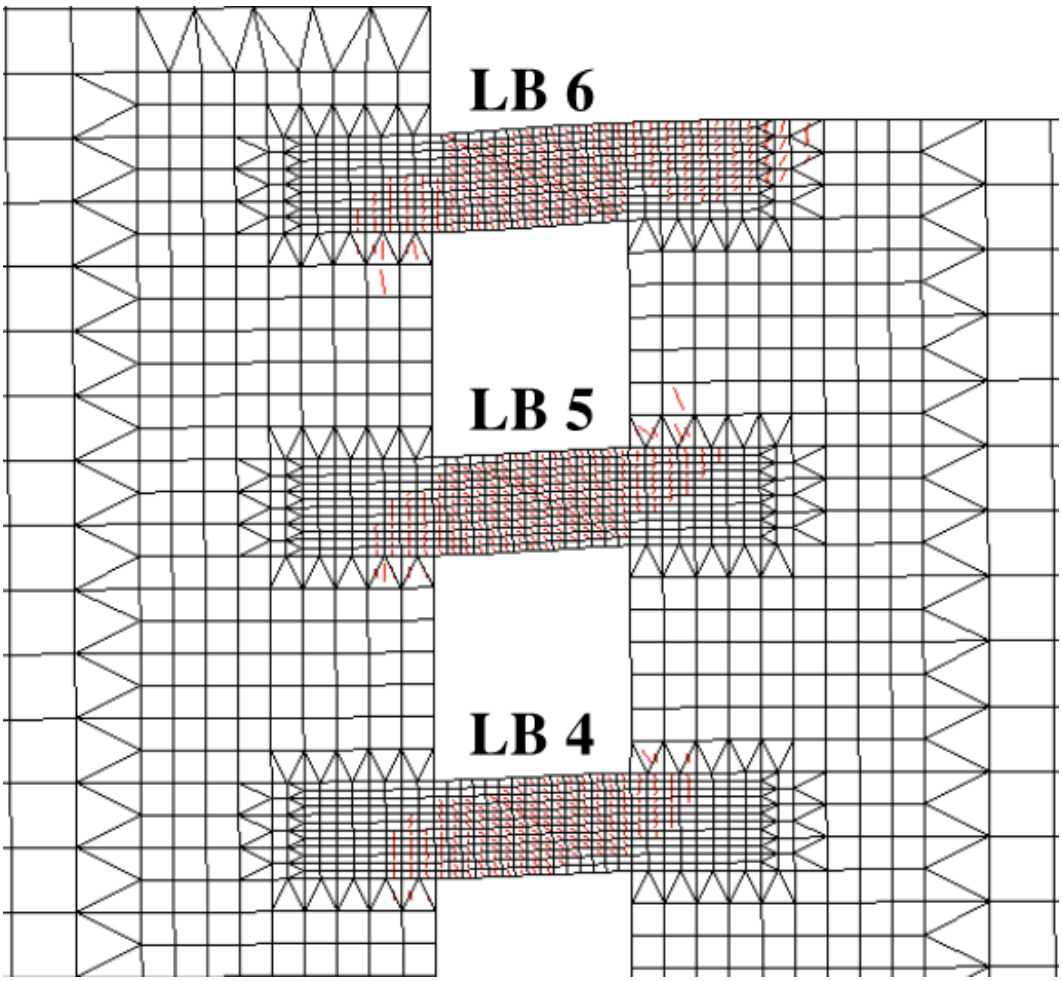

Figure 5.4: Shear distortion and cracking patterns in the top three link beams for the final converged trial (trial NL3)

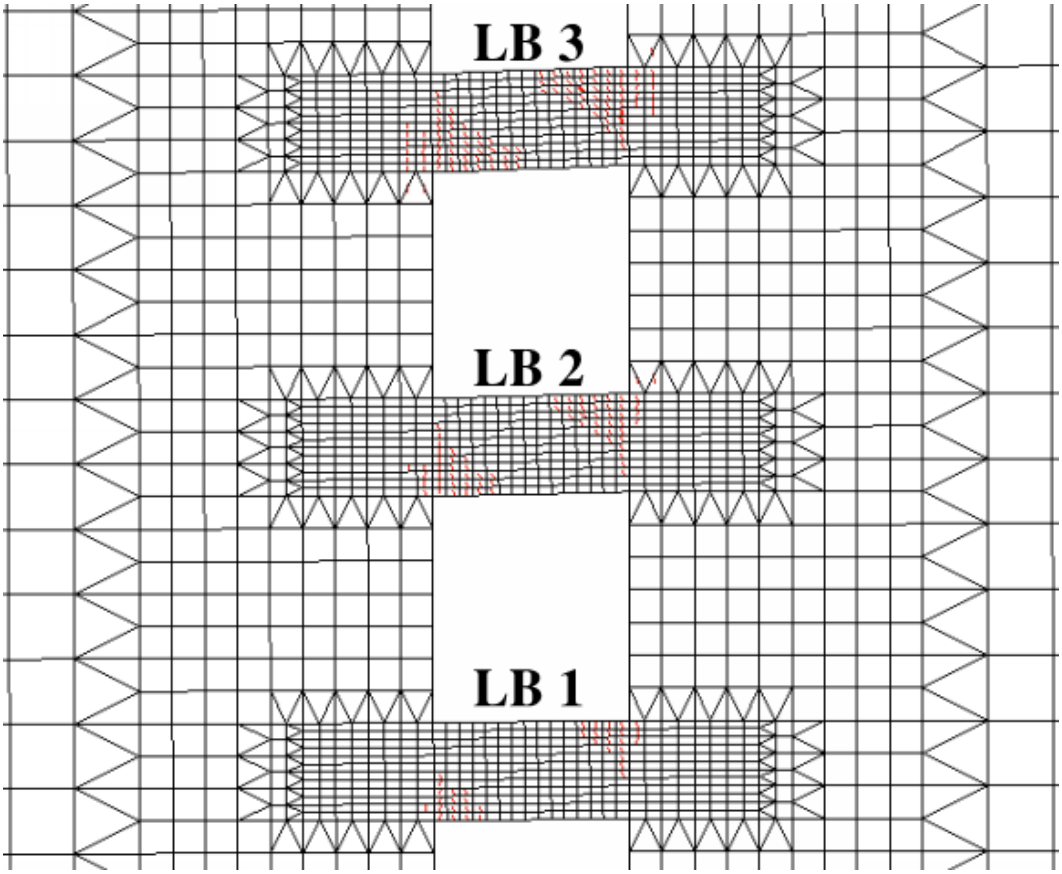

Figure 5.5: Shear distortion and cracking patterns in the bottom three link beams for the final converged trial (trial NL3)

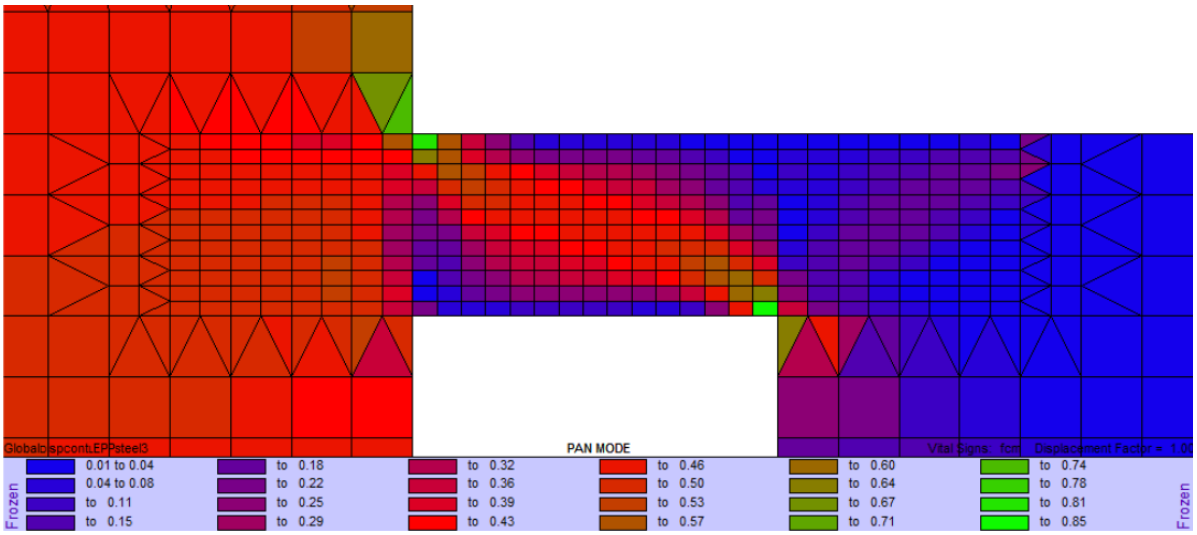

Figure 5.6: Diagonal compression field – concrete compressive stress as a function of compressive stress capacity – for LB6 in trial NL3

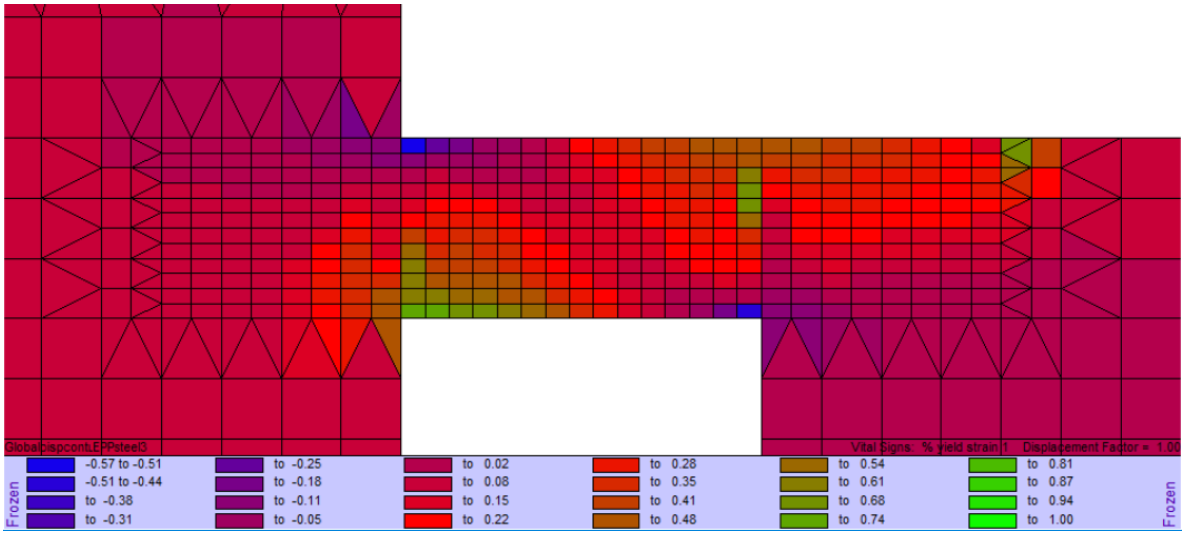

Figure 5.7: Longitudinal steel reinforcing strain as a function of yield strain at load factor for LB6 for trial NL3

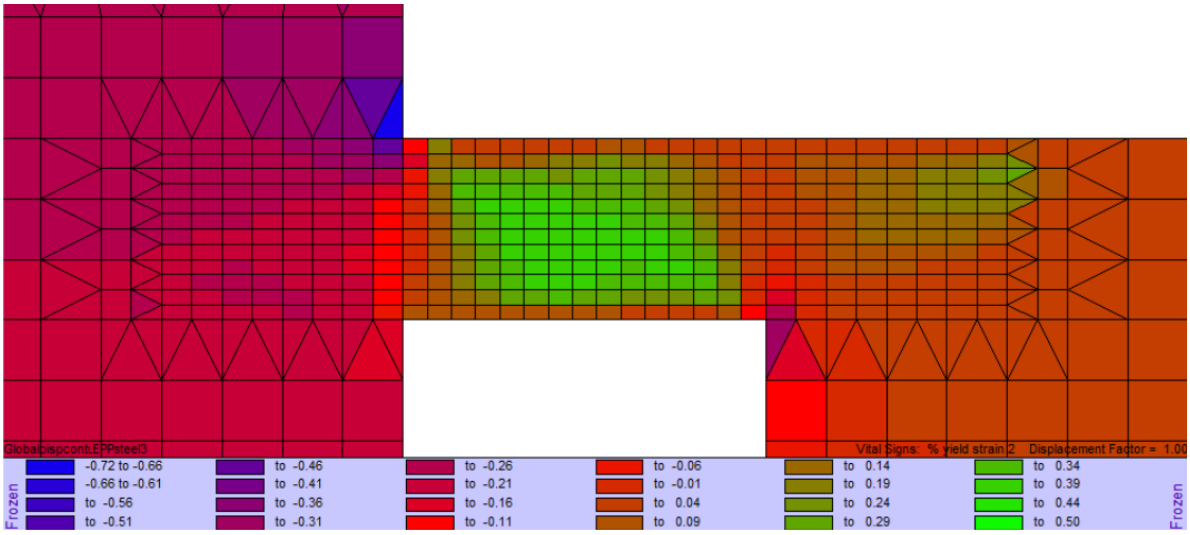

Figure 5.8: Transverse steel reinforcing strain as a function of yield strain at load factor for LB6 for trial NL3

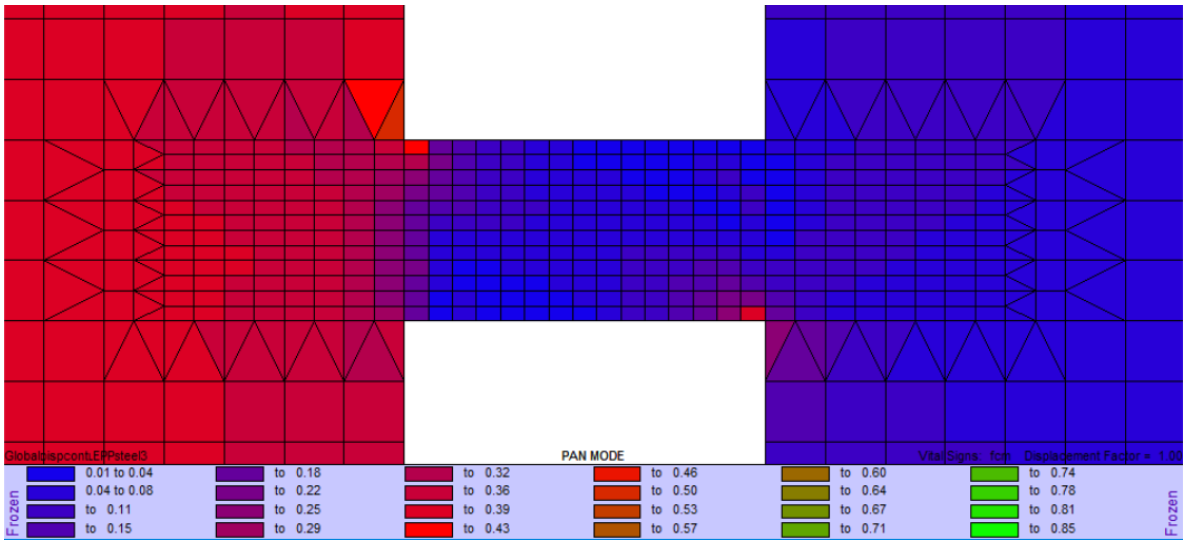

Figure 5.9: Diagonal compression field – concrete compressive stress as a function of compressive stress capacity – for LB1 in trial NL3

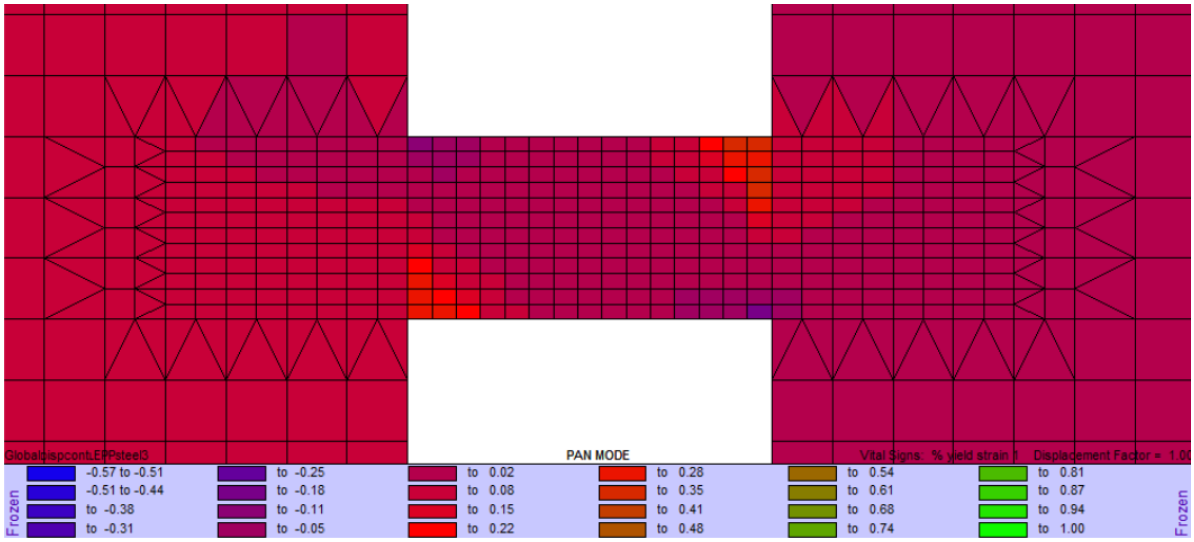

Figure 5.10: Longitudinal steel reinforcing strain as a function of yield strain at load factor for LB1 for trial NL3

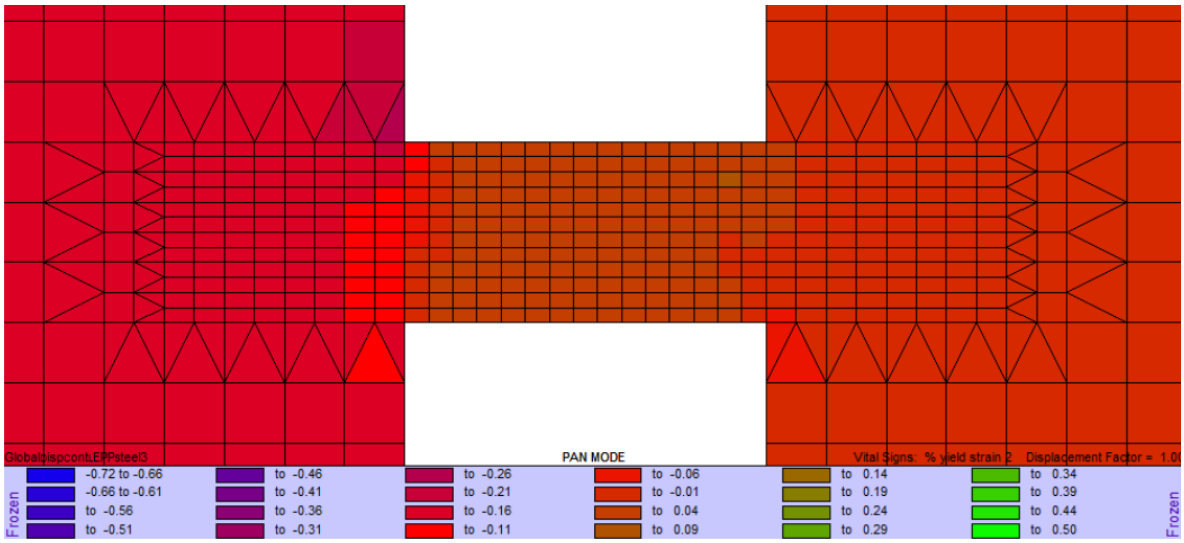

Figure 5.11: Transverse steel reinforcing strain as a function of yield strain at load factor for LB1 for trial NL3

Chapter 6: Findings and Conclusion

This thesis investigated the effects of inelasticity on the design and capacity of nonprestressed reinforced link beams under gravity loading. A case study of a typical high-rise building with link beams connecting the building's core to a large wall pier or "wing" was used. The investigation was performed using VecTor2, an open source specialized nonlinear finite element analysis software program for 2D continuum analysis. VecTor2 employs the constitutive relationships of the Modified Compression Field Theory (MCFT). An iterative trial-and-error procedure was used in order to optimize the design and provide reinforcement amounts that correspond to the nonlinear response expected. A single link beam model was constructed in VecTor2 in order to study the nonlinear response characteristics, predict realistic nominal load carrying capacities, and inform the amounts of reinforcing required for the full model. The major findings of the case study are summarized in the following points:

1. For the purpose of structural analysis, it is common practice to consider reinforced concrete to be a linear elastic material. This leads to inaccuracies in design values, such as sectional shears and bending moments. Aspects of nonlinear response of concrete include cracking, compression softening, tension softening, and tension stiffening. Reinforced concrete should be considered to be an orthotropic composite material, where its stiffness characteristics are continuously changing with

increased loadings. In this case study, the shear demand for a link beam by linear elastic analysis could be approximately 72% more than what was required by nonlinear analysis, and the moment demand could be approximately 78% more. To further add to the efficiency and optimization advantage of using the benchmark reinforcing criteria, link beam 3 in trial 3 required almost 174% less shear reinforcement than what was required based on the linear elastic shear demands. However, the link beam 1 demands by linear elastic analysis were underestimated by approximately 20% in comparison to the nonlinear analysis. This was due to the inaccurate force transfer predicted by linear elastic analysis across the link beams, thereby predicting a nonrealistic failure mode and capacity criteria.

2. The capacity limit prediction, compared in Table 5-1, shows that VecTor2 can predict capacity limits up to 43% more than what is prescribed by ACI 318 provisions. However, just beyond the ACI shear stress limitation provided by transverse steel, $v_s = 0.667\sqrt{f'_c}$ (MPa) ($v_s = 8\sqrt{f'_c}$ (psi)), which is case #4 in Table 5-1, the VecTor2 capacities reach down to 23% less than ACI 318 limits, were the shear stress limit criteria were taken at linear increments of $0.167\sqrt{f'_c}$ ($2\sqrt{f'_c}$ (psi)) until $v_u = 1.167\sqrt{f'_c}$ ($v_u = 14\sqrt{f'_c}$ (psi)). This indicates that shear force resistance due to the plain concrete in compression, aggregate interlock, and dowel action are

underestimated by ACI 318, up until the limit of $v_u = 0.833\sqrt{f'_c}$ ($v_u = 10\sqrt{f'_c}$ (psi)).

3. The effects of significant restraint against vertical expansion by the pier walls on either end of the link beam are clearly highlighted with compression softening. The concrete will be confined near the link beam supports, resulting in compressive stresses larger than the cylinder compressive strength.

4. VecTor2 provides greater uniformity in maximum reinforcement stress ratios, for instance f_2/f_{2max}, in all of the link beams under the different load levels than when a traditional design criterion is used.

5. VecTor2 provides a relatively simple and straightforward platform for the design engineer to perform a nonlinear analysis for a reinforced concrete structure subjected to membrane action and undergoing stress and strain response characteristics for the presented case study. The iterative analysis and design process presents a method to reach a more optimal design within a few iterations. A primary advantage of a specialized software package for nonlinear finite element analysis for reinforced concrete, such as VecTor2, is that the user is not required to define reinforced concrete material inelasticity. Only basic parameters such as cylinder compressive

strength are required. The findings presented in this report demonstrated the viability of the default inelasticity models in predicting reasonable nonlinear behavior for the link beams.

6. The iterative design optimization process demonstrated in this report may prove invaluable for integrated design. The realistic load-capacity relationships predicted by nonlinear finite element analysis provide the design team with much greater flexibility.

References

1. AASHTO, “AASHTO LRFD Bridge Design Specifications,” third edition, Washington, DC, 2004, pp. 1450.

2. ACI Committee 318, "Building Code Requirements for Structural Concrete (318M-02) and Commentary-(318R-02)." ACI, Farmington Hills, Michigan, 2002.

3. ACI Committee 318, "Building Code Requirements for Structural Concrete (318-14) and Commentary-(318R-14)." ACI, Farmington Hills, Michigan, 2014.

4. Baker, W.; Novak, L.C.; Sinn, R.; and Viise, J., “Structural Optimization of 2000’ Tall 7 South Dearborn Building,” Proceedings of the 2000 ASCE Structures Congress, Track: 14th Analysis and Computational Conference, 2000.

5. Behfarnia, K., “The Effects of Tension Stiffening on the Behaviour of R/C Beams,” ASIAN JOURNAL OF CIVIL ENGINEERING (BUILDING AND HOUSING), V. 10, No. 3, 2009, pp. 243-255.

6. Bentz, E. C., and Collins, M. P., “Response 2000”, http://www.ecf.utoronto.ca/~bentz/r2k.htm, 2000.

7. Borosnyói, A., and Balázs, G.L., "Models for flexural cracking in concrete: the state of the art." Structural Concrete 6, no. 2 (2005): 53-62.

8. Clark, A. P., “Diagonal Tension in Reinforced Concrete Beams,” ACI JOURNAL, Proceedings V. 48, No. 2, Feb. 1951, pp. 145-156.

9. CSA Committee A23.3, “Design of Concrete Structures (CSA A23.3-04),” Rexdale, ON, Canada, 2004.

10. Guralnick, S. A., “High-Strength Deformed Steel Bars for Concrete Reinforcement,” ACI JOURNAL, Proceedings V. 57, No. 3, Mar. 1960, pp. 241-282.

11. Kagami, Y.; Mazuhara, H.; Takagi, H.; and Karino, Y., “Splitting Bond Failure of a Double Reinforced Concrete Beam, Part 1,” Summaries of Technical Papers of Annual Meeting, Architectural Institute of Japan, 1991, pp. 353 -354

12. Kaklauskas, G., and Šimkus, R., "Analysis of Parameters Affecting Tension Stiffening in Reinforced Concrete Beams," Statyba 4, No. 4, 1998, pp. 260-65.

13. Kim, M. S., and Lee, Y.H., "Comparison of Tension Stiffening Models for High Strength Concrete Beams," Proceedings of the World Congress on Civil, Structural, and Environmental Engineering, 2016.

14. Kuchma, D. A.; Lee, H. J.; Baker, W; and Novak, L.C., "Design and Analysis of Heavily Loaded Reinforced Concrete Link Beams for Burj Dubai." ACI Structural Journal, 43rd ser., 105, No. 4, 2008, pp. 451-59.

15. Lee, J.-Y., and Kim, U.-Y., “Effect of Longitudinal Tensile Reinforcement Ratio and Shear Span-to-Depth Ratio on Minimum Shear Reinforcement,” ACI Structural Journal, V. 105. No. 2, Mar.-Apr. 2008, pp. 134-144.

16. Lee, J-Y, and Hwang, H-B., "Maximum Shear Reinforcement of Reinforced Concrete Beams." ACI Structural Journal, 57th ser., 107, No. 05 2010, pp. 580-88.

17. Pi, Y.l., M.A. Bradford, F. Tin-Loi, and R.I. Gilbert. "Geometric and Material Nonlinear Analyses of Elastically Restrained Arches." Proceedings of the Tenth International Conference on Civil, Structural and Environmental Engineering Computing, 2007, pp. 283-95.

18. Placas, A., and Regan, P. E., "Shear Failure of Reinforced Concrete Beams," ACI JOURNAL, Proceedings V. 68, No. 10, Oct. 1971, pp. 763-773.

19. Mikame, A., Uchida, K., and Noguchi, H. (1991), "A Study of Compressive Deterioration of Cracked Concrete." Proc. Int. Workshop on Finite Element Analysis of Reinforced Concrete, Colombia Univ., New York, N.Y.

20. The International Federation for Structural Concrete (*fib*), "Practitioners' Guide to Finite Element Modeling of Reinforced Concrete Structures", 2008, pp. 1-33

21. Vecchio, F. J., and Collins, M. P., "The Modified Compression Field Theory for Reinforced Concrete Elements Subjected to Shear," ACI JOURNAL, Proceedings V. 83, No. 2, Feb. 1986, pp. 219-231.

22. Wong, P.S. and Vecchio, F. J., "VecTor2 and FormWorks User's Manual", August 2002, pp. 1-307.